



FINAL REPORT
DTPH56-14-H-00002
"Full Scale Testing of Interactive Features for Improved Models"

SUBMITTED BY: Team Project Manager

Deborah Jelen
Electricore, Inc.
27943 Smyth Drive, Suite 108
Valencia, CA 91355
Telephone: (661) 607-0260
E-mail: jelen@electricore.org

TEAM TECHNICAL AUTHORS: BMT Fleet Technology

Sanjay Tiku, Amin Eshraghi, Binoy John, and Aaron Dinovitzer
311 Legget Drive
Kanata, Ontario K2K 1Z8 Canada
Telephone: (613) 592-2830

ENGIE, R&I Department

Mures Zarea, Charles Fernandez, Maxime Bertin
361 Ave du President Wilson
B.P. 33, 93211 Saint-Denis, France
Telephone: +3 (366) 413.5637

TEAM PARTICIPANTS: Electricore, Inc.
BMT Fleet Technology
ENGIE
Pipeline Research Council International (PRCI)

SUBMITTED TO: U. S. Department of Transportation
Pipeline and Hazardous Materials Safety Administration
Mr. Warren D. Osterberg
Agreement Officer
warren.osterberg@dot.gov

REPORTING PERIOD: 12/30/2013 – 9/30/2017

SUBMITTED ON: September 30, 2017

Table of Contents

1 **Executive Summary** 7

2 **Next Steps**..... 9

2.1 Full Scale Testing of Complex Dents & Finite Element Analysis of Longitudinal Strain 9

2.2 Full Scale Testing of Dent and Gouge Defects 9

2.3 Stress Corrosion Cracking Colonies and SDO Modeling Coordination 10

3 **Team Project Activities**..... 11

3.1 Task 1: Project Kick-Off Meeting..... 11

3.2 Task 2a-b: Material Selection, Acquisition and Characterization..... 11

3.3 Task 3a-b: Baseline existing features..... 11

3.4 Task 4: Full Scale Testing of Complex Dents 11

3.5 Task 5a,b,c: Full Scale Testing of Dent and Gouge Defects 11

3.6 Task 6a,b: Stress Corrosion Cracking Colonies and SDO Modeling Coordination 11

3.7 Task 7: Finite Element Analysis of Longitudinal Strain..... 11

3.8 Task 8: Dissemination of Results 12

3.9 Task 9: Reporting and Project Management..... 12

3.10 Deliverables..... 12

4 **Full Scale Testing of Complex Dents (Task 4)**..... 14

4.1 Background..... 14

 4.1.1 Test Matrix..... 14

 4.1.2 Test Set-Up 16

4.2 Baseline Existing Features (Task 3)..... 19

 4.2.1 Material Characterization..... 21

 4.2.2 Experimental Approach 23

4.3 Experimental Results 27

4.4 Concluding Remarks and Next Steps 36

5 **Full Scale Testing of Dent and Gouge Defects (Task 5)**..... 38

5.1 Background and plan of investigation..... 38

 5.1.1 Test Matrix..... 39

 5.1.2 Defect creation process 41

 5.1.3 Experimental Approach for Burst tests 44

5.2 Material Selection, Acquisition and Characterization (Task 2)..... 45

5.3 Test set-ups for Task 5..... 47

 5.3.1 Dent and Gouge Severity (Task 5a)..... 47

 5.3.2 Interaction between Dents with Severe Dent and Gouge defect profiles (Task 5b) 48

 5.3.3 Dent and Gouge Defects Removed from Service (Task 5c) 49

5.4 Results and Conclusions (Task 5) 49

 5.4.1 Burst tests..... 49

 5.4.2 Uncertainties related to some tests..... 52

 5.4.3 Observations 53

 5.4.4 Conclusions and Gap analysis..... 53

6 **Stress Corrosion Cracking (SCC) Colonies and Standard Development Organization (SDO) Modeling Coordination (Task 6)** 55

6.1 Background..... 55

6.2 Material Selection, Acquisition and Characterization (Task 2)..... 55

6.3 Baseline Existing Features (Task 3)..... 56

6.4 Results 59

 6.4.1 Experimental approach 59

 6.4.2 Oil Condition Test..... 60

 6.4.3 Gas Transmission Pipeline Condition Test 71

6.5 Conclusions 76

7	Finite Element Analysis of Longitudinal Strain (Task 7)	78
	7.1 Background	78
	7.1.1 Axial Load and Bending Moment Capacity of Pipes.....	78
	7.1.2 Task Objective	78
	7.2 Finite Element Modeling	78
	7.3 Results	80
	7.3.1 Dent under compressive or tensile axial load	80
	7.3.2 Dent under applied bending	81
	7.3.3 Effect of axial load on Fatigue life.....	82
	7.3.4 Effect of bending load on fatigue life	85
	7.3.5 Effect on other Limit States	86
	7.3.6 Preliminary Understanding of the Axial Load Capacity of Dented Pipes	88
	7.4 Conclusions	91
8	Lessons learned	92
	8.1 Full Scale Testing of Dents	92
	8.2 Dent and Gouge	92
	8.3 Stress Corrosion Cracking (SCC) Colonies	93
	8.4 Finite Element Analysis of Longitudinal Strain	93
	8.4.1 Other Recommendations.....	94
9	Dissemination of Results	96
10	Annex	97

List of Tables

Table 1: Linepipe Details Used in the Current Test Program	14
Table 2: Listing of Indenters Used in the Current Test Program	14
Table 3: Dent Shape and Dent Interaction Test Matrix	15
Table 4: Dent Fatigue Test Matrix.....	16
Table 5: Corrosion Feature Dimensions Used in the Current Test Program	21
Table 6: Chemical Composition for Pipe D and Pipe F.....	21
Table 7: Tensile Properties for Pipe D and Pipe F.....	22
Table 8: Charpy Impact Test Results (a) Pipe D (b) Pipe F.....	22
Table 9: Vickers Hardness (10 kg) values for Pipe D and F.....	23
Table 10: CTOD Fracture Toughness Results for Pipe D.....	23
Table 11: Full Scale Dent Fatigue Test Results	28
Table 12: Dent and gouge defect test matrix, covering one task, three sub-tasks, four pipes, eighteen Dent and Gouge defects.....	40
Table 13: Dent and Gouge defect test matrix.....	42
Table 14: Overview of the four materials used in Task 5	45
Table 15: Pipe materials transverse tensile properties	46
Table 16: Pipe materials longitudinal tensile properties	46
Table 17: Pipe materials transverse Charpy impact properties	46
Table 18: Pipe materials longitudinal Charpy impact properties.....	46
Table 19: Pipe materials chemical composition.....	46
Table 20: Results of burst tests for Task 5 pipes	50
Table 21: Results of fatigue tests for Task 5 pipes	51
Table 22 : Overview of the two materials used in Task 6.....	55
Table 23: Task 6 pipe materials transverse tensile properties.....	56
Table 24: Task 6 pipe materials longitudinal tensile properties.....	56
Table 25: Task 6 pipe materials transverse Charpy impact properties	56
Table 26: Task 6 pipe materials longitudinal Charpy impact properties	56
Table 27: Task 6 pipe materials chemical composition	56

Table 28: Main characteristics of SCC colonies on pipe SCC-1 according to sizing by MWM FA214 Jentek Sensor.	58
Table 29: Composition of simulation NNPHSCC soil solutions (C2). Concentrations are in g/liter.	63
Table 30: Oil Condition Test Step 0: Fatigue in air	63
Table 31: Oil Condition Test Step 1: Effect of underloading on the SCC growth rate.....	63
Table 32: Oil Condition Test Step 2: SCC growth rates along constant loading conditions	64
Table 33: Oil Condition Test Step 3: Effect of overloading on the SCC growth rate	64
Table 34: Crack depths and crack growth rates	70
Table 35: Composition of simulation NNPHSCC soil solutions (C2) used for gas condition test. Concentrations are in g/liter.....	72
Table 36: Conditions of loading for one cyclic block as defined in Figure 59	74
Table 37: Crack depth measurements after gas pipeline condition test	75
Table 35: The FE Modeling Matrix	79
Table 36: FE Data Used for Developing and Testing the Unrestrained Dent Regression Equation.....	89

List of Figures

Figure 1: (a) Dent Rig with 24 inch Pipe (b) Pump & Motor Assembly and Water Reservoir	17
Figure 2: (a) Control System for Cyclic Pressure Fatigue Test (b) Control Panel enlarged view	17
Figure 3: Elliptical Indenters (a) 12in Indenter (b) 24 in Indenter.....	18
Figure 4: Cylindrical Bar Indenters (a) 10in short Axial Bar Indenter (b) 20in Long Transverse Bar Indenter	18
Figure 5: 20in Long Bar Indenter at 45 degree to Pipe longitudinal Axis (a) View 1 (b) View 2.....	18
Figure 6: Dent Interacting with (a) Girth Weld (b) Corrosion.....	19
Figure 7: 39% Corrosion Selection Procedure.....	20
Figure 8: 39% Corrosion Feature (a) Scan plot (b) Feature.....	20
Figure 9: Pipe D Characteristic curves (a) Strain life fatigue curve (b) Cyclic stress-strain curve	23
Figure 10: Test 14 – Gauge Schematic	24
Figure 11: (a) Pipe Test Specimen with End Caps (b) Close up of the Strain Gauges Installed on a Test Specimen.....	24
Figure 12: Dent Shape with (a) Transverse Bar (b) Axial Bar.....	25
Figure 13: Dent Shape with (a) 12 in Indenter (b) 24 in Indenter.....	25
Figure 14: Experiment vs FEA (a) Axial Dent Profile (b) Force vs LVDT Displacement.....	26
Figure 15: Test 15 Indentation Strains – 120mm Longitudinal Gauge (a) Hoop (b) Axial	26
Figure 16: Test 15 Cyclic Strains (a) Hoop (b) Axial OD Strain Ranges on Axial Path from 5% to 55% PSMYS Cycles.....	26
Figure 17: Plain Pipe Unrestrained Dent MPI (a) OD MPI - Axial OD Cracks (b) ID MPI - Axial OD Crack.....	29
Figure 18: Plain pipe Restrained Dent MPI (a) OD MPI - Circumferential ID Crack (b) ID MPI - Circumferential ID Crack	30
Figure 19: Corroded Pipe (a) OD MPI - Axial OD Cracks (b) ID MPI - Axial OD Cracks.....	30
Figure 20: Cross-Section Metallograph of Fatigue Crack in Test Specimen 13.....	31
Figure 21: Test # 17 Fracture Photograph	32
Figure 22: Pipe D & F Plain Dents - Stress Range vs Experimental Life.....	32
Figure 23: All Plain Dents - Stress range vs Experimental Life	33
Figure 24: Unrestrained Dents - Stress range vs Experimental Life.....	34
Figure 25: Restrained Dents - Stress range vs Experimental Life	34
Figure 26: Fatigue Life Reduction due to Long Seam and Girth Welds (a) Current Test Program (b) Previous and Current Test Program	35
Figure 27: Fatigue Life Reduction due to Corrosion interaction (a) Unrestrained Dent with 24 in Indenter and 10% Travel (b) Unrestrained Dent with 12 in Indenter and 10% Travel	35

Figure 28: Fatigue Life Reduction Due to Corrosion Interaction with Restrained Dent (a) Restrained Dent with 24 in Indenter with 6% Travel (b) Restrained Dent with 20in Long Bar Indenter with 6% Travel ...	36
Figure 29: State of the art of Dent and Gouge defect database and possible field of investigation at the beginning of the project t; some results are provided by the European Pipeline Research Group (EPRG)	38
Figure 30: State of the art of Dent and Gouge defect database and defects created during the project. Pipe 7 is not represented because gouge depth measurement had too high uncertainties due to defect configuration.....	39
Figure 31: Energy spent to create defect 6.6.1 by slow dynamic aggression (5,267 Joules).....	43
Figure 32: Seikowave measure for defect 7.ext2.2 dimensions (left); MPI on defect 8.ext2.3cp (right); ..	43
Figure 33: Dent pop-up of Dent and Gouge 6.6.2 followed by significant dent bulging for pressure increase at 67 bar when the four-point bending load was imposed.	44
Figure 34: Opening displacement clip gauge for burst test of Dent and Gouge defect 6.6.2	45
Figure 35: Test set-up for Dent and Gouge defect 5.4.1 (Task 5a).....	47
Figure 36: Test set-up for Dent and Gouge defect 5.5.3cp (Task 5a).....	47
Figure 37: Test set-up for Dent and Gouge defect 6.6.2a burst test with axial load by means of a 4-points-bending loading (Task 5a)	48
Figure 38: Test set-up for Interacting Dent and Gouge defects 5.5.3i2 and 5.5.3i2' (Task 5b)	48
Figure 39: Test set-ups for Dent and Gouge defects 7.ext1.2 (burst test, <i>top</i>) and 8.ext2.3cp (fatigue test under over cathodic protection, <i>bottom</i>) retrieved from service (Task 5c).	49
Figure 40: Air-tight electrochemical cell for full scale near neutral SCC crack propagation tests.....	55
Figure 41: View of the defect C8 after Magnetic Particle Inspection in which the location of the deepest cracks according to sizing with MWM FA214 Jentek Sensor is highlighted.	57
Figure 42: C-SCAN of magnetic relative permeability for colonies C9-C8-N2 colonies, as measured by MWM FA214 Jentek Sensor.....	57
Figure 43: C-SCAN of crack depths in C9-C8-N2 colonies as measured with MWM FA214 Jentek Sensor.....	58
Figure 44: Crack colony R156-im1	59
Figure 45: EDM notches + real SCC colony map for pipe SCC1a.....	61
Figure 46: EDM notches map for pipe SCC1b	62
Figure 47: EDM notches map for pipe SCC1c	62
Figure 48: Oil pipe loading profile	65
Figure 49: Crack depth propagation during phase 0 (fatigue in air)	65
Figure 50: SCC1a, SCC1b and SCC1c pipes with electrochemical cells	66
Figure 51: Modified oil test conditions for step 1 - 1 underload each 205 cycles	66
Figure 52 : Magnetic particle inspection of real SCC colony before step 1 of oil condition test	67
Figure 53 : Magnetic particle control of real SCC colony after 9792 cycles of step 1 of oil condition test	67
Figure 54: Crack depth measurements during oil conditions test	68
Figure 55: 7 EDM notches chosen for destructive observation.	69
Figure 56: Microscopic observation of SCC1b-12-15 defect after oil conditions test.....	70
Figure 57: Comparison of oil condition test results and University of Alberta summary of results (paper # IPC2008-64475).....	71
Figure 58: EDM notches map for pipe SCC1b during gas pipeline test condition	72
Figure 59: O ₂ concentration during the gas pipeline condition test	73
Figure 60: Loading conditions for gas pipeline condition test.....	73
Figure 61: Comparison between crack size at the tip of notches located under or out of the electrochemical cell	76
Figure 58: Typical FE Model of the Dent with Axial End Load (a) Side View of the Whole FE Model (b) Close up of the Dent Area.....	80
Figure 59: Buckling of a Restrained Dent due to Compression (a) Before Buckling (b) After Buckling..	81
Figure 60: Restrained Dent Under a 1350 kips Tensile Force (a) Before Thinning (b) After Thinning.....	81
Figure 61: A Typical Restrained Dent Prior to the Application of Bending – True Scale	82

Figure 62: A Typical Restrained Dent under Bending, Before Reaching the Buckling Point – True Scale	82
Figure 63: A Typical Restrained Dent under Bending, Beyond the Buckling Point – True Scale	82
Figure 64: Stress Magnification Factor of Unrestrained Dents with Axial Force	83
Figure 65: Stress Magnification Factor of Unrestrained Dents with Axial Displacement.....	84
Figure 66: Stress Magnification Factor of Restrained Dents under bending	85
Figure 67: Stress Magnification Factor of Unrestrained Dents under bending.....	86
Figure 68: Variation of Axial Force Capacity with Internal Pressure: (a) Unrestrained Dents (b) Restrained Dents	87
Figure 69: (a) Schematic of a dent under internal pressure and axial load, (b) buckling of dent with zero internal pressure, (c) buckling of dent with 70% PSMYS internal pressure.....	88
Figure 70: Effect of various parameters on the axial load capacity, (a) and (b) unrestrained dents, (c) and (d) restrained dents.....	89
Figure 71: Unity Plot for the Unrestrained Dents Buckling Equation	90
Figure 72: Unity Plot for the Restrained Dents Buckling Equation.....	91

1 Executive Summary

This is the Final Report for work completed under U.S. Department of Transportation Pipeline and Hazardous Materials Safety Administration (PHMSA) Other Transaction Agreement (OTA) DTPH56-14-H-00002, "Full Scale Testing of Interactive Features for Improved Models." The project was implemented to develop an experimental database on how pipelines respond when affected by mechanical damage, caused by both external interference and rock dents. This full-scale testing program produced detailed experimental data to support the development and validation of improved burst and fatigue strength models to assess:

1. Dents interacting with secondary features (gouges, close defects interacting between each other) under
 - a. normal operating conditions,
 - b. cathodic overprotection, and
 - c. with secondary loads (to simulate a quasi-static ground movement for example)
2. Stress Corrosion Cracks (SCC) defects

These very detailed and well documented reference data are a long term effort to support PHMSA and the pipeline industry to ensure safe operation of pipeline systems and to promote continuous improvements which will improve public safety and protect the environment.

The Final Report presents the activities completed to develop the database of mechanical damage and SCC defects and evaluating the impact of those defects on the structural significance of operating pipelines. Mechanical damage models (based on Failure Assessment Diagram, Paris Law, Ductile Flaw Battelle Growth Model, etc.), were previously developed to predict the conditions that lead to immediate (burst under constant loading conditions) or delayed failure (under fluctuating pressure loading (fatigue)). The engineering tools and empirical/mechanistic (numeric) models currently used for assessing the significance of mechanical damage with secondary features are based on a number of assumptions rather than detailed experimental data. This project provides additional data which the models need to avoid overly conservative assessments, promoting unnecessary maintenance, or the lack of required maintenance that could result in unexpected failures, which represent a significant environmental and safety concern for operating pipelines.

The project included the creation and full-scale testing of realistic Dent and Gouge and Dents/Dents with secondary features using modern and vintage steels. The test samples fabricated for the full-scale testing program were created to represent the types of damage encountered in the field on operating pipelines based on available data from previous PHMSA¹ and Pipeline Research Council International, Inc. (PRCI)² research projects and that compiled an inventory of mechanical damage data. The vintage steel samples were acquired from former in-service pipelines. The full-scale tests were highly instrumented to capture the level of detail needed for a range of parameters that are important to the development and validation of mechanical damage assessment models. The data will be used to develop or improve models that will be used by the industry for pipeline integrity management.

Preliminary investigation was carried out to evaluate the effect of longitudinal strains on the fatigue life of the dents. The analysis demonstrated that when the axial loading (i.e. axial force, bending, axial displacement or rotation) causes the dented pipe segment to buckle or yield, the fatigue response of the dented and buckled pipe segment is lower than the dented pipe segment.

The data collected was analyzed by the research team, including a broad group of more than fifty pipeline industry representatives, PHMSA representatives, and Subject Matter Experts (SMEs) in mechanical

¹ U.S. Department of Transportation Pipeline and Hazardous Materials Safety Administration "Structural Significance of Mechanical Damage #339 (Agreement DTPH56-08-T-000011)

² PRCI Projects Mechanical Damage (MD) -4-1 and MD-4-6

damage inspection, assessment, and modeling. There were multiple teleconferences and meetings to review the results of research. The detailed test reports and test database will reside upon PRCI's server and be made available to their member companies.

2 Next Steps

2.1 *Full Scale Testing of Complex Dents & Finite Element Analysis of Longitudinal Strain*

Having completed a broad range of pipe mechanical damage full scale testing and simulation research, as well as, drawing from observations of industry practice, the project team has identified several opportunities for improvement in mechanical damage integrity management including the following.

Natural Dent Evaluation - To date, all the dents for the dent fatigue test program have been created in the laboratory using artificial indenters. It is recommended to carry out full scale fatigue tests on dents removed from the field and obtain fatigue life data on realistic dent shapes. The fatigue lives of field dents can then be compared against laboratory created dents and the applicability of the current standardized curve (BS7608 Class D) can be further validated.

Dent Axial Loading - Axial loading was shown to not have a significant impact on the fatigue life of the dents, however, axial loading of dents affected other modes of failure, i.e. buckling. Preliminary results shown in the current program demonstrated that an analytical solution can be developed to predict the buckling capacity of the dented pipeline. It is recommended to carry out detailed finite element (FE) modeling incorporating different dent sizes and shapes, pipe geometry, axial and bending load condition and mean pressure to investigate the effect of axial loading and bending on other limit states such as buckling for dented pipes.

Field Dent Shape Validation - Dent depths are not good indicators of their fatigue life performance. Under PRCI research programs, dent shape parameters were developed and correlated with their fatigue life performance. The dent shape parameters were developed using FE modelling, validated using full scale dent fatigue test data, based on the hypothetical dent shapes created using different shape and size indenters. It is recommended to incorporate realistic dent shapes using field dent data in the dent shape parameter fatigue life calculations. In line inspection (ILI) data of field dents will be used for detailed FE modeling, as well as, to calculate dent shape parameters. The fatigue lives based on FE modeling will then be compared against the fatigue lives estimated based on the dent shape parameter. The analysis should be carried out for around 300-500 dents incorporating different depths and shapes, pipe geometry and pressure loading conditions.

2.2 *Full Scale Testing of Dent and Gouge Defects*

The analysis of test results evidenced the added value of the current work on Dent and Gouge defects, both realistically created, and retrieved from service. The experimental approach consisted in covering a wide range of threat interaction cases, each time trying to compare the baseline burst and fatigue resistance with corresponding burst and fatigue resistance of the combined threats.

The findings of this work show that based on defect geometry, the additional interacting threats, like cathodic overprotection or close geometric interaction, can play a significant role in bringing already severe defects closer to failure. However, the burst or fatigue resistance of less severe defects would not be significantly influenced by additional interacting threats.

This approach, therefore, requires additional investigation on better defining the Dent and Gouge severity limits for those defects that become sensitive to other interacting threats.

Based on current experimental findings, defect severity is a key factor when it comes to adding cathodic overprotection or close defect interaction. These aspects require clearly more work to define the key parameters that would make such defects more sensitive to these threat interactions. To perform this work, a combined experimental and FE modeling approach seems to be the most appropriate.

Concerning superimposed axial loads, the burst and fatigue strength of axially oriented defects are not significantly affected by axial loads generated with four-point bending. Circumferentially oriented Dent and Gouge defects or such defects oriented at an angle with the pipe axis may be more sensitive to this interacting threat, and therefore require additional investigation.

In the area of axial loads, soil-pipe interaction also plays a role, and the experimental part of this investigation could be performed in a soil box, thus accounting for soil restraint effects when applying the four-point bending conditions.

In addition, other diameters and defect shapes are also of interest to enhance the representativeness of Dent and Gouge defects with respect to operational conditions.

Finally, Dent and Gouge defects removed from service would need to undergo a similar procedure for comparison purposes. While finding systematically similar defects as those created on purpose cannot be guaranteed, it is an area of research that is important to in order to compare real world and laboratory results.

2.3 Stress Corrosion Cracking Colonies and SDO Modeling Coordination

Performing SCC full scale crack propagation tests is a very long endeavor, as time has to be allowed for the electrochemical phenomena to develop. The first results are encouraging, as they confirm some of the existing results. However, more varied conditions are required in order to cover a wider range of parameters, especially in terms of pipe materials and diameter.

3 Team Project Activities

This project was divided into nine tasks described below, along with the corresponding project deliverables.

3.1 *Task 1: Project Kick-Off Meeting*

The stakeholders used the Kick-Off meeting to review the project scope, schedule, relevant past work, technical details and finalize the test plan and matrices for full-scale testing. The deliverables for this task included meeting minutes presented in the DOT Quarterly Status report.

3.2 *Task 2a-b: Material Selection, Acquisition and Characterization*

The objective of this task was to select, procure and characterize the materials that were used in this experimental testing program. Data and testing results on material properties for the selected linepipe are presented in the Quarterly and Final Reports.

3.3 *Task 3a-b: Baseline existing features*

The team identified and characterized the pre-existing features (dents, corrosion features, Dent and Gouges, SCC) in the pipes removed from service. The deliverables for this task included a catalogue of the pre-existing flaws used in the experimental test program and are also reported in the Quarterly and Final Reports.

3.4 *Task 4: Full Scale Testing of Complex Dents*

This task focused on creating a variety of experimental dent shapes in the various linepipe materials and then measure their fatigue performance. A description of the testing procedures and the results of the experimental program were provided in the Quarterly and Final Reports.

3.5 *Task 5a,b,c: Full Scale Testing of Dent and Gouge Defects*

In this task, the team created and tested additional Dent and Gouge defects which extends the previous database established by PHMSA and PRCI Projects^{1,2} in order to fill the following knowledge gaps concerning effects of different parameters on defect behavior. A description of the testing procedures and the results of the experimental program are provided in the Quarterly and Final Reports. This task was split into three sub-tasks related to the knowledge gaps:

- *Task 5a: Dent and Gouge Severity*
- *Task 5b: Interaction between Defects*
- *Task 5c: Dent and Gouge Defects Removed from Service*

3.6 *Task 6a,b: Stress Corrosion Cracking Colonies and SDO Modeling Coordination*

The team experimentally investigate pipes containing three SCC patches when the coalescence of adjacent SCC cracks occurs during crack growth. The goal was to determine when cracks coalesce and the conditions that differentiate failure by leak or rupture. The team also performed full-scale tests to consider variable loading conditions that best represent pipeline operating conditions and test the model predictions. Testing included monitoring crack growth with Jentek MWM sensors at regular intervals.

The tests also considered representative environmental conditions, allowing a thorough evaluation of predictions from both the latest University of Alberta models and previous related PHMSA sponsored are provided in the Quarterly and Final Reports. This task evolved as the project developed as described in Section 0 below.

3.7 *Task 7: Finite Element Analysis of Longitudinal Strain*

The objective of this task was to use finite element analysis (FEA) to understand the effect of longitudinal strain on pipes affected by dents and dents on corrosion features or welds. The findings developed in this task were used to develop a test plan for future tests intended to evaluate the effect of longitudinal strain on the various mechanical damage features.

3.8 *Task 8: Dissemination of Results*

The purpose of this task was to disseminate the findings to further the current state of knowledge pertaining to mechanical damage and SCC testing and assessment to industry stakeholders and Standards Development Organization (SDO) groups. The team accomplished this through three activities:

- Formation of a Technical Advisory Board (TAB)
- Final Technical Review Meeting and Workshop
- SDO outreach and coordination

3.9 *Task 9: Reporting and Project Management*

This task involved the coordination of the project team and reporting. The team held phone or web-based meetings on a regular basis and when needed. The reporting delivered in this task included the monthly status updates and Quarterly and Final reports.

3.10 *Deliverables*

1. **Meeting:** Conduct kick-off team meeting.
COMPLETED: 01/21/2014
2. **Reporting:** Monthly status updates due to DOT in accordance the basic agreement.
COMPLETED every month of the project
3. **Reporting:** Quarterly Status and Progress reports due to DOT in accordance with the basic agreement.
COMPLETED every quarter of the project
4. **Documentation:** Develop an electronic database of full-scale mechanical damage test data and stress corrosion cracking colonies supported by a complete description of the testing process and results as well as complete linepipe material characterization data. Test data includes:
 - Complex dents including complex shapes, corrosion and weld interaction
 - Dent and gouges including environmentally assisted cracking, high loads, interaction between defects, and in-service defects
 - Effect of stress corrosion crack colonies**COMPLETED: 09/30/2017**
5. **Meeting:** Conduct final technical review meeting with the DOT to present program findings.
COMPLETED: 10/24/2017
6. **Reporting:** Submit final written report documenting program activities and findings, including:
 - Materials selection and characterization
 - Mechanical damage test data
 - Stress corrosion cracking test data
 - Finite element analysis of longitudinal strain
 - Technical advisory panel feedback
 - Standards development organization coordination**COMPLETED: 09/30/2017**
7. **Reporting:** Submit a Public Paper documenting program activities and findings.
COMPLETED: 10/24/2017

- 8. Final Technical Review Meeting:** Hold a one day workshop describing the state of knowledge in mechanical damage behavior testing and assessment. The results of this project and previous work will be demonstrated and discussed with pipeline industry stakeholders.
COMPLETED: 10/24/2017
- 9. Pipeline Safety Research Peer Review:** PowerPoint template and attendance at two (2) online peer review meeting as specified by the DOT.
COMPLETED: 05/22/2014
COMPLETED: 05/27/2015
COMPLETED: 05/26/2016

4 Full Scale Testing of Complex Dents (Task 4)

4.1 Background

The objectives of the test program were to create a detailed experimental database of physical trial results describing dent response under pressure loading considering:

- Plain dent fatigue life with symmetric and asymmetric dent shapes,
- Fatigue life reduction due to dent interaction with realistic corrosion features, and
- Fatigue life reduction due to dent interaction with welds.

The experimental data generated will be used to calibrate and validate models that can be used for dent integrity management and assist in developing/ improving dent remediation and repair criteria.

The task focused on creating a variety of experimental dent shapes in two linepipe geometries and material grades with and without secondary features to evaluate their fatigue performance. The experimental trials included

- Dent shapes (created using elliptical/dome, and long bar shaped indenters),
- Dents on long seam welds and
- Dents created on real corrosion features in pipe removed from service.

The dents were tested in the restrained condition, where the indenter was kept in place during cyclic pressure loading and the unrestrained condition where the indenter was removed after dent creation allowing the dent to rebound during cyclic pressure loading. The samples were instrumented to provide data describing dent formation strains, cyclic strains, dent geometry and fatigue lives.

Long bar indenters were used to create complex asymmetric dents in the axial orientation, dents in the transverse orientation and dents at 45 degree angle to the pipe longitudinal axis. Dents were also created using semi-elliptical/dome shape indenters.

4.1.1 Test Matrix

Two linepipe materials were used in the test program, noted as D and F. Table 1 provides details of the pipe geometries, material grades and year of manufacture. The indenters used in the current test program were bar type indenters and semi-elliptical indenters. Four indenters were used to create dents of different shape and size in the current test program and are listed in Table 2. Table 3 and Table 4 provide details about the test matrix including pipe ID, indenter type, dent interaction, dent depth, restraint condition and cyclic pressure loading condition.

Table 1: Linepipe Details Used in the Current Test Program

Pipe Id.	Nominal OD mm (in)	Nominal Wall Thickness mm (in)	Grade	Year
D	609.6 (24)	9.525 (0.375)	X70	1998
F	508 (20)	7.137 (0.281)	X52	1970's

Table 2: Listing of Indenters Used in the Current Test Program

Item #	Indenter Type	Indenter Diameter mm (in)	Indenter Length mm (in)
1	Semi Elliptical	305 (12)	N/A
2	Semi Elliptical	610 (24)	N/A
3	Long bar	102 (4)	508 (20)
4	Short bar	102 (4)	254 (10)

Table 3: Dent Shape and Dent Interaction Test Matrix

Spec. #	Pipe Characteristics				Indenter Type	Secondary Feature Characteristic*
	Pipe Id.	OD (in)	WT (in)	Grade	Bar Elliptical (OD)	
1	D	24	0.375	X70	Long Bar - Transverse	Plain dent
2	D	24	0.375	X70	Long Bar - Transverse	Plain dent
3	D	24	0.375	X70	Short Bar - Axial	Plain dent
4	D	24	0.375	X70	Short Bar - Axial	Plain dent
5	D	24	0.375	X70	Long Bar - Transverse	GW at C/L
6	D	24	0.375	X70	Long Bar - Transverse	GW at C/L
7	D	24	0.375	X70	Short Bar - Axial	GW 5.3 in offset
8	D	24	0.375	X70	Short Bar - Axial	GW 5.5 in offset
9	D	24	0.375	X70	Long Bar - Transverse	LSW 6.0 in offset
10	D	24	0.375	X70	Long Bar - Transverse	LSW 7.0 in offset
11	D	24	0.375	X70	Long Bar - Transverse	Plain dent
12	D	24	0.375	X70	Short Bar - Axial	LSW at C/L
13	D	24	0.375	X70	Long Bar - Transverse	Plain dent
14	F	20	0.281	X52	Elliptical (12 in)	Plain dent
15	F	20	0.281	X52	Elliptical (24 in)	Plain dent
16	F	20	0.281	X52	Elliptical (24 in)	42% Corrosion at C/L
17	F	20	0.281	X52	Elliptical (24 in)	17% Corrosion at C/L
18	F	20	0.281	X52	Elliptical (12 in)	30% Corrosion at C/L
19	F	20	0.281	X52	Elliptical (12 in)	16% Corrosion at C/L
20	F	20	0.281	X52	Elliptical (24 in)	8% Corrosion at C/L
21	F	20	0.281	X52	Elliptical (24 in)	26% Corrosion at C/L
22	F	20	0.281	X52	Elliptical (12 in)	9% Corrosion at C/L
23	F	20	0.281	X52	Elliptical (12 in)	39% Corrosion at C/L
24	F	20	0.281	X52	Long Bar @ 45 deg	Plain dent
25	F	20	0.281	X52	Elliptical (24 in)	Plain dent
26	F	20	0.281	X52	Elliptical (24 in)	20% Corrosion 3.5 in Offset
27	F	20	0.281	X52	Elliptical (24 in)	35% Corrosion 3.5 in Offset
28	F	20	0.281	X52	Long Bar @ 45 deg	28% Corrosion 4.5 in Offset
29	F	20	0.281	X52	Long Bar @ 45 deg	23% Corrosion 4.5 in Offset
30	F	20	0.281	X52	Long Bar @ 45 deg	LSW 3.2 in offset

* GW = Girth Weld, C/L = Centre Line, LSW = Long Seam Weld

Table 4: Dent Fatigue Test Matrix

Spec. #	Pipe Id.	Restraint Condition	Indenter Travel	Dent Depth	Indentation Pressure	First Cyclic Pressure	Cyclic Pressure
		(R/U)*	(% OD)	(% OD)	(% PSMYS)	(%PSMYS)	(%PSMYS)
1	D	U	10	2	15	80	10 to 70
2	D	U	14	2	15	80	10 to 70
3	D	R	4	4	0	90	10 to 70
4	D	R	6	6	0	90	10 to 70
5	D	U	10	2	15	80	10 to 70
6	D	U	12	2	15	80	10 to 70
7	D	R	3	3	0	90	10 to 70
8	D	R	6	6	0	90	10 to 70
9	D	U	10	2	15	80	10 to 70
10	D	U	13	2	15	80	10 to 70
11	D	U	5	1	15	80	10 to 70
12	D	R	3	3	0	90	10 to 70
13	D	U	5	1	15	80	10 to 70
14	F	U	10	2	30	70	10 to 60
15	F	U	10	2	0	60	5 to 55
16	F	U	10	1	0	60	5 to 55
17	F	U	10	2	0	60	5 to 55
18	F	U	10	2	30	70	10 to 60
19	F	U	10	2	30	70	10 to 60
20	F	U	10	1	0	60	5 to 55
21	F	U	10	1	0	60	5 to 55
22	F	U	10	2	30	70	10 to 60
23	F	U	10	1	30	70	10 to 60
24	F	R	6	6	0	80	10 to 70
25	F	R	6	6	0	80	10 to 70
26	F	R	6	6	0	80	10 to 70
27	F	R	6	6	0	80	10 to 70
28	F	R	6	6	0	80	10 to 70
29	F	R	6	6	0	80	10 to 70
30	F	R	6	6	0	80	10 to 70

* R: restrained dent condition, U: unrestrained dent condition

4.1.2 Test Set-Up

Figure 1a shows the dent test rig used to create dents. Cyclic pressure is generated using the pump, shown in Figure 1b, capable of total water flow of 40 gallons per minute (GPM) at continuous operating pressure of 3500 psi. Figure 2 shows the control system used to control the cyclic pressure test. The test system is capable of running two tests, simultaneously.



Figure 1: (a) Dent Rig with 24 inch Pipe (b) Pump & Motor Assembly and Water Reservoir

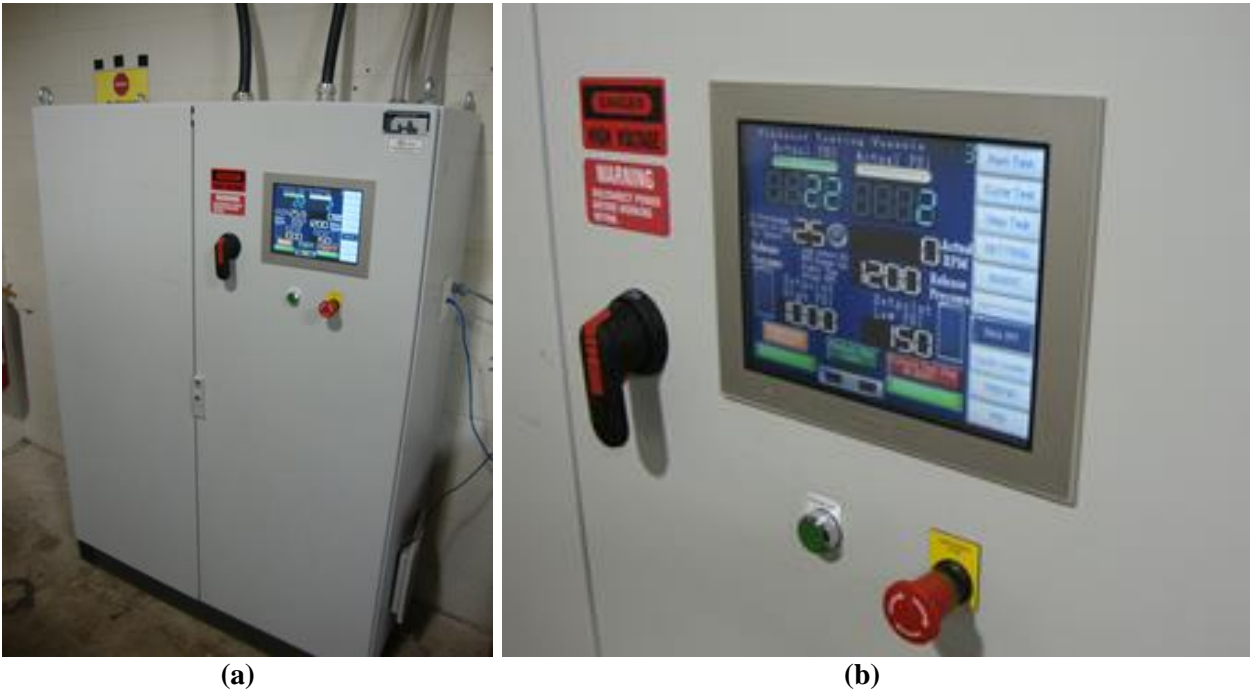
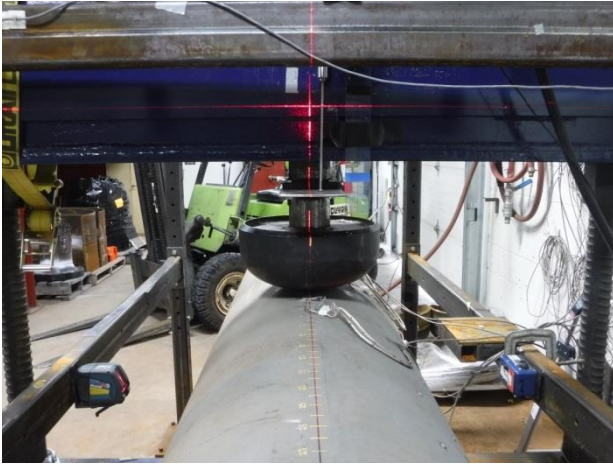


Figure 2: (a) Control System for Cyclic Pressure Fatigue Test (b) Control Panel enlarged view

Figure 3 through Figure 5 show the different indenters that were used in the current test program to create dents. Figure 6 shows interacting features, dents interacting with a weld and dent interacting with a corrosion feature, respectively.



(a)



(b)

Figure 3: Elliptical Indenters (a) 12in Indenter (b) 24 in Indenter

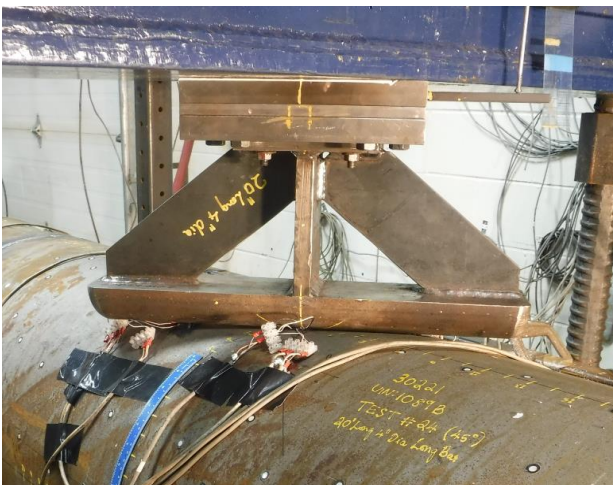


(a)



(b)

Figure 4: Cylindrical Bar Indenters (a) 10in short Axial Bar Indenter (b) 20in Long Transverse Bar Indenter



(a)



(b)

Figure 5: 20in Long Bar Indenter at 45 degree to Pipe longitudinal Axis (a) View 1 (b) View 2



(a) (b)
Figure 6: Dent Interacting with (a) Girth Weld (b) Corrosion

4.2 Baseline Existing Features (Task 3)

Based on the ILI data made available on Pipe F, several pipe joints that had a range of corrosion features were identified and selected. Laser scanning of the selected pipe joints was carried out to characterize and confirm the corrosion features. Corrosion features were first identified based on their depths. Further selection of corrosion features for full scale tests was based on their lengths and widths. Longer and wider corrosion features were favored as compared to smaller size features of the same depth. Figure 8 shows a snapshot of the laser scan of one pipe joint with all the corrosion features and subsequent selection of the corrosion feature for full scale testing.

Figure 7 and Figure 8 show example of a corrosion feature selection process. Table 5 lists the dimensions of the corrosion features that were used for the various dent corrosion interaction full scale fatigue tests. The corrosion depths identified in Table 5 are the depths of the deepest pits identified from the laser scan data and confirmed with ultrasound thickness gauge.

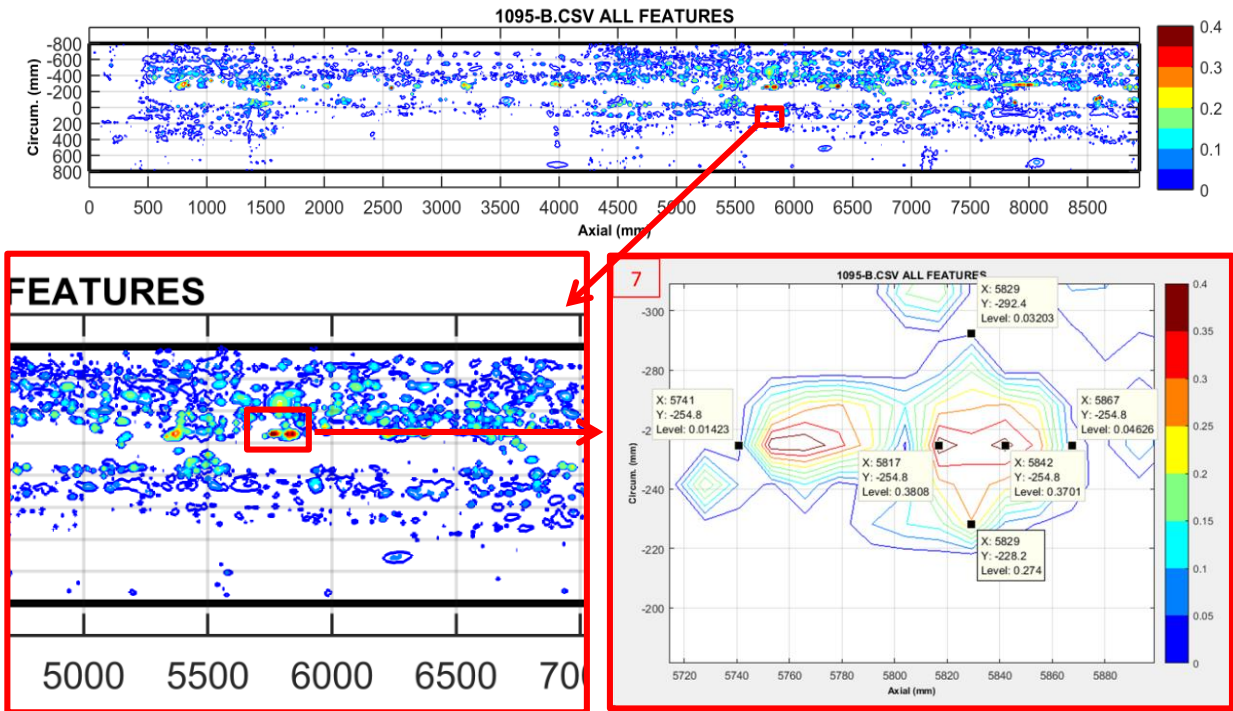
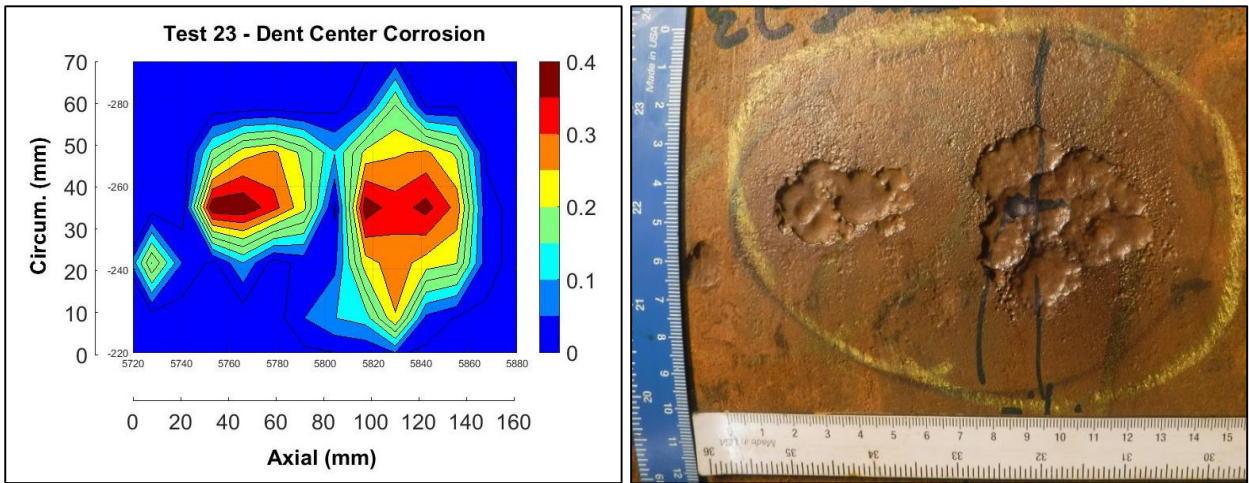


Figure 7: 39% Corrosion Selection Procedure



(a) (b)
Figure 8: 39% Corrosion Feature (a) Scan plot (b) Feature

Table 5: Corrosion Feature Dimensions Used in the Current Test Program

Corrosion #	Spec. #	Corrosion Depth	Corrosion Length	Corrosion Width
		(% WT)	mm (in)	mm (in)
1	16	42%	226 (8.9)	60 (2.4)
2	17	17%	28 (1.1)	39 (1.5)
3	18	30%	141 (5.6)	58 (2.3)
4	19	16%	93 (3.7)	86 (3.4)
5	20	8%	88 (3.5)	61 (2.4)
6	21	26%	130 (5.1)	66 (2.6)
7	22	9%	181 (7.1)	146 (5.7)
8	23	39%	111 (4.4)	49 (1.9)
9	26	20%	340 (13.4)	190 (7.5)
10	27	35%	235 (9.3)	58 (2.3)
11	28	28%	200 (7.9)	89 (3.5)
12	29	23%	108 (4.3)	74 (2.9)

4.2.1 Material Characterization

Detailed material characterization was carried out on Pipe D and Pipe F. Material characterization included chemical analysis, tensile property determination, and Charpy tests. Tensile properties were measured in both the longitudinal and the transverse orientation. Base material Charpy tests were performed on specimens in transverse orientation. In addition, strain life fatigue tests and crack tip opening displacement (CTOD) fracture toughness tests were carried out on Pipe D. CTOD tests were carried out on base material, weld metal (girth weld) and 50% heat affected zone (HAZ). The test temperature was -5°C. Strain life fatigue tests were carried out on the base material. The specimen orientation was along the pipe longitudinal axis.

Table 6 provides the results of the chemical analysis for both pipe materials. Table 7 shows the tensile test results. Table 8 shows the Charpy impact test results for the specimen sizes tested. For Pipe D, 2/3 Charpy specimen size was tested and for Pipe F, the Charpy specimen size was 1/2 size. Vickers hardness measurements carried out using a 10 kg load are listed in Table 9.

Table 10 provides the results of the CTOD fracture toughness tests. Figure 9a and Figure 9b show the strain life fatigue data and the cyclic stress strain curve, respectively.

Table 6: Chemical Composition for Pipe D and Pipe F

Pipe	Al (%)	B (%)	C (%)	Co (%)	Cr (%)	Cu (%)	Mn (%)	Mo (%)	Nb (%)	Ni (%)	P (%)	S (%)	Si (%)	Ti (%)	V (%)
D	0.036	<0.0005	0.06		0.03	0.02	1.27	<0.01	0.056	0.01	0.011	0.007	0.26	0.014	0.034
F	<0.005	<0.0005	0.21	<0.005	0.03	0.02	1.13	0.01	<0.005	0.02	0.09	0.014	0.02	<0.005	0.06

Table 9: Vickers Hardness (10 kg) values for Pipe D and F

Orientation	Location	Pipe D	Pipe F
		(HV ₁₀)	(HV ₁₀)
Trans	OD	217	180.5
	Center		167.6
	ID	232	183.4
Axial	OD	219	182.1
	Center		167.7
	ID	227	184.1

Table 10: CTOD Fracture Toughness Results for Pipe D

Location	δ_{el} (mm)	δ_{pl} (mm)	δ_{tot} (mm)	Failure Type
Base Metal	0.024	0.16	0.184	δ_u
	0.025	0.175	0.2	δ_u
	0.025	0.162	0.186	δ_u
Girth Weld (weld center line)	0.018	0.201	0.219	δ_m
	0.019	0.209	0.229	δ_m
	0.019	0.203	0.222	δ_m
50% HAZ	0.019	0.39	0.409	δ_m
	0.017	0.241	0.259	δ_m
	0.02	0.526	0.545	δ_m

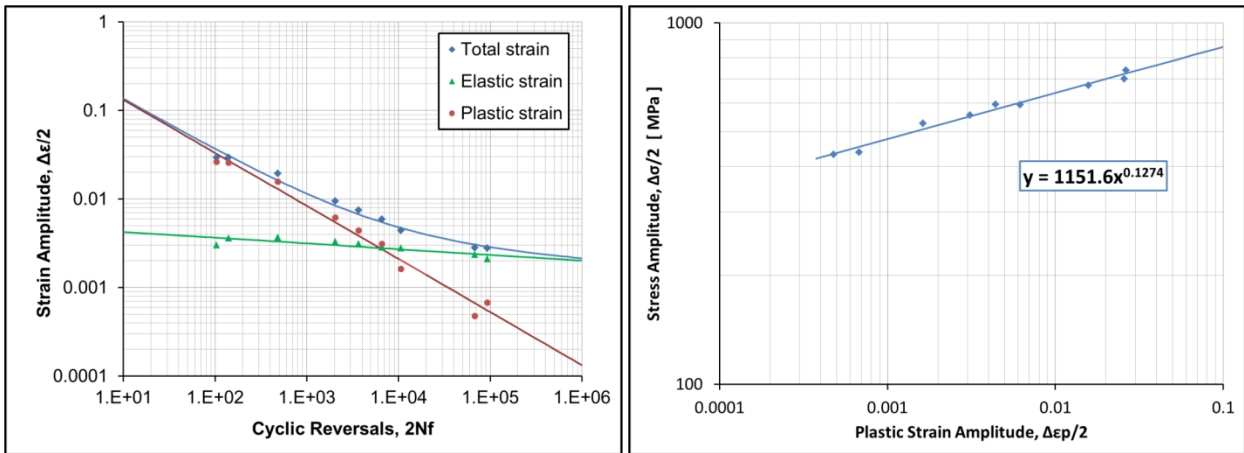


Figure 9: Pipe D Characteristic curves (a) Strain life fatigue curve (b) Cyclic stress-strain curve

4.2.2 Experimental Approach

Pipe test specimens, 10 feet long, were fabricated by welding on end caps. Baseline measurements of axial and transverse profiles were carried out using Vernier caliper at the proposed dent region after the test completion. The instrumentation and sensors were used during the test to measure the force, indenter travel, and strain during dent creation. During cyclic pressure loading, pressure and strain gauge data was recorded. Dent axial and circumferential profiles were also measured and recorded. For restrained dent tests the indenter was held in place during the entire test duration and removed after test completion, when there was a leak in the dent region. For unrestrained dent tests the indenter was removed after dent creation, before the test specimen was subjected to pressure loading.

Strain gauge locations varied from test to test depending upon the individual test parameters. Figure 10 shows an example of a strain gauge schematic, prepared for each test specimen. Figure 11a and Figure 11b show a photograph of a typical end-capped pipe specimen and a close up of the strain gauges installed on a pipe test specimen. Figure 12 shows photographs of dents created with round bars in transverse and axial orientation. Figure 13 shows photographs of dents created with 12 inch and 24 inch semi-elliptical indenters.

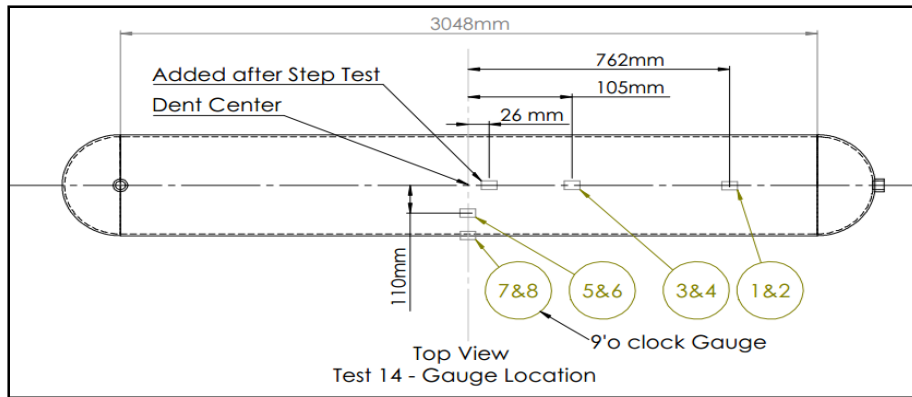
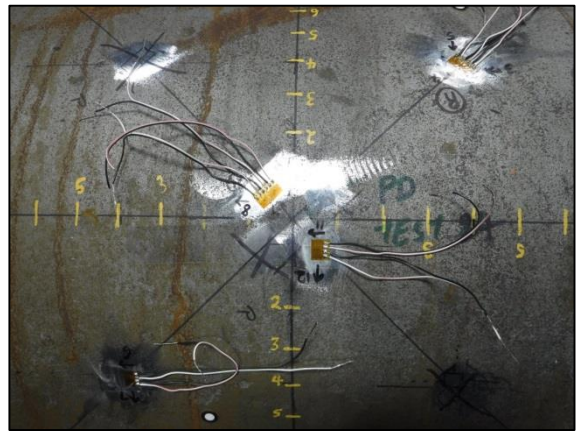


Figure 10: Test 14 – Gauge Schematic

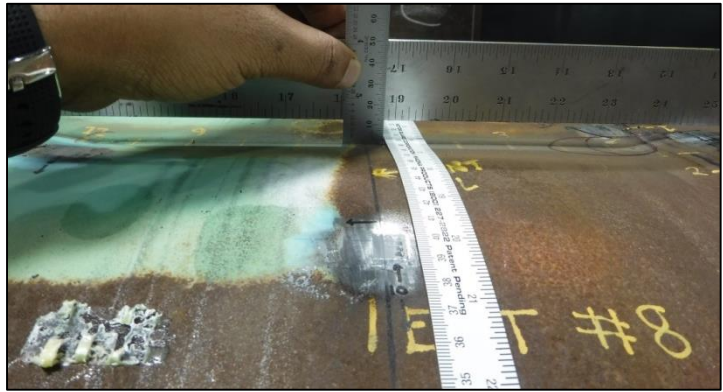


(a)

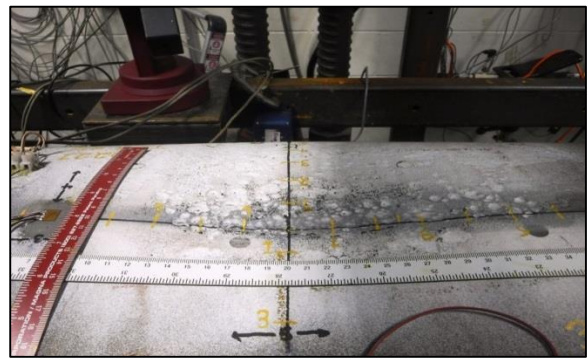


(b)

Figure 11: (a) Pipe Test Specimen with End Caps (b) Close up of the Strain Gauges Installed on a Test Specimen



(a) (b)
Figure 12: Dent Shape with (a) Transverse Bar (b) Axial Bar



(a) (b)
Figure 13: Dent Shape with (a) 12 in Indenter (b) 24 in Indenter

The location of strain gauges on individual test specimens was chosen based on the FE modeling results. For each test parameter identified in Table 3 and Table 4, FE modeling was carried out before commencing the full scale test. Figure 14 through Figure 16 show the comparison of FE modeling results with experimental data. Figure 14 shows comparison between dent axial profile and dent indentation force and indenter displacement during dent creation. Figure 15 shows comparison of strains resulting from dent creation at different strain gauge locations. Figure 16 shows comparison of cyclic strains during pressure loading cycles. The comparison between the experimental and FE model results indicates that the experimental results correlate very well with the FE models.

The FE modeling results were used to identify the critical location within the dent region and this information was used to position the weld and corrosion feature at the critical location. This was done to ensure that the interacting features are located at the critical location within the dent region which would result in the maximum reduction in fatigue life due to dent weld and dent corrosion interaction. The dent interaction results were compared with the similar plain dent tests to quantify the reduction in life due to weld and corrosion feature interaction.

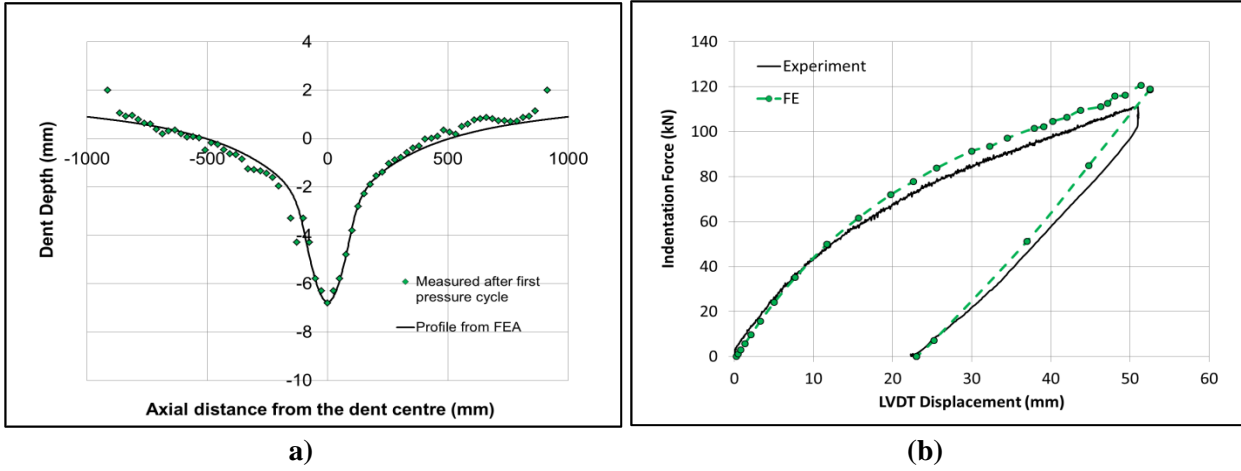


Figure 14: Experiment vs FEA (a) Axial Dent Profile (b) Force vs LVDT Displacement

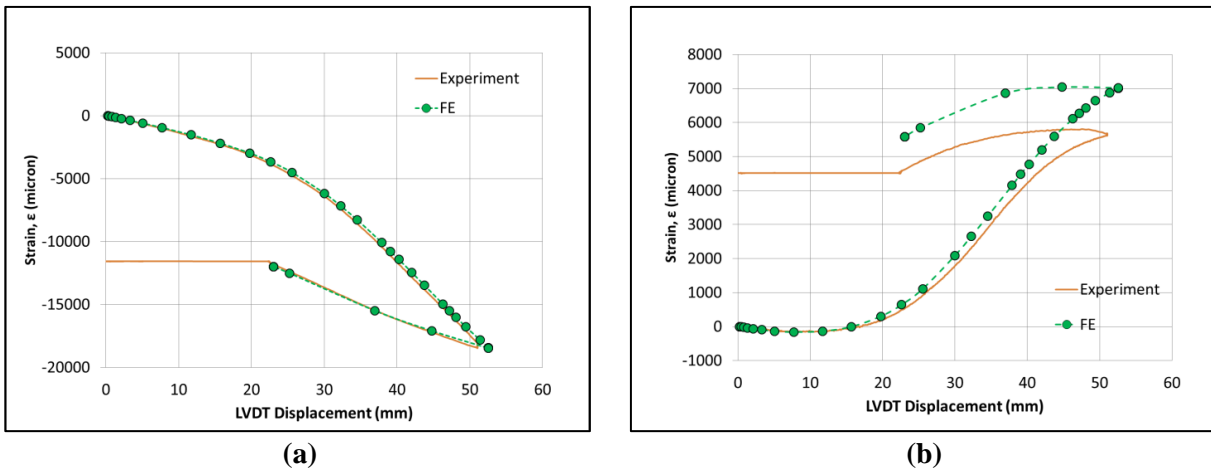


Figure 15: Test 15 Indentation Strains – 120mm Longitudinal Gauge (a) Hoop (b) Axial

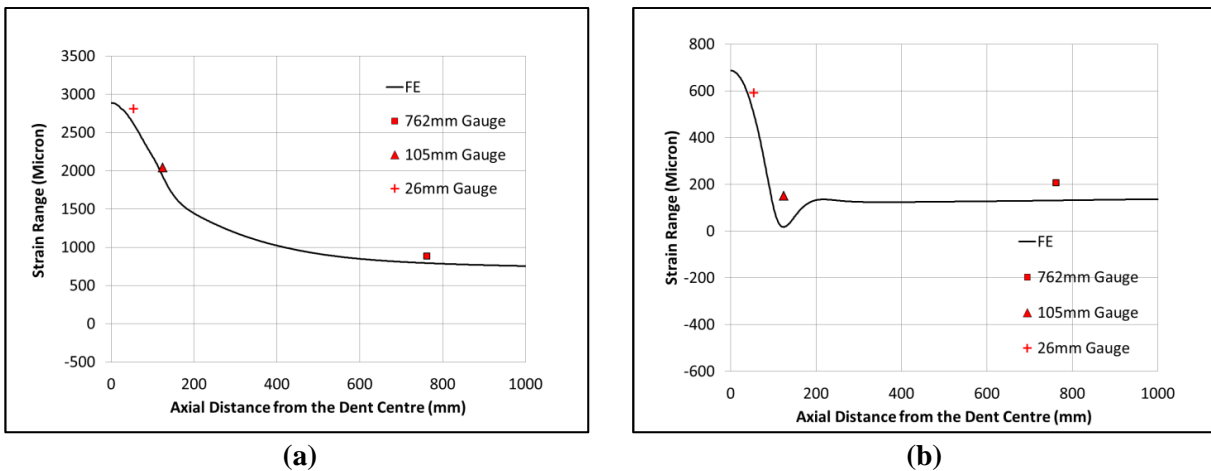


Figure 16: Test 15 Cyclic Strains (a) Hoop (b) Axial OD Strain Ranges on Axial Path from 5% to 55% PSMYS Cycles

4.3 *Experimental Results*

Thirty full scale fatigue tests were carried out under the current test program. Table 11 shows the number of cycles to failure for each individual test.

Table 11: Full Scale Dent Fatigue Test Results

Spec. #	Dent Depth	Restraint Condition	Interaction	Cyclic Pressure	Crack Orientation	Crack Surface	Cycles to Failure
	% OD	R/U		% PSMYS			
1	2	U	Plain Dent	10 to 70	Axial	ID	12716
2	2	U	Plain Dent	10 to 70	Axial	ID	9851
3	3	R	Plain Dent	10 to 70	Axial	ID	10945
4	6	R	Plain Dent	10 to 70	Circumferential	ID	7701
5	2	U	GW	10 to 70	Circumferential	OD	8300
6	2	U	GW	10 to 70	Circumferential	OD	6568
7	3	R	GW	10 to 70	Axial	ID	10963
8	6	R	GW	10 to 70	Circumferential	ID	10130
9	2	U	LSW	10 to 70	Axial	ID	12689
10	2	U	LSW	10 to 70	Axial	ID	7569
11	1	U	Plain Dent	10 to 70	Axial	ID	37776
12	3	R	LSW	10 to 70	Axial	ID	6415
13	1	U	Plain Dent	10 to 70	Axial	ID	23119
14	2	U	Plain Dent	10 to 60	Axial	OD	18346
15	2	U	Plain Dent	5 to 55	Axial	OD	21812
16	1	U	Corrosion	5 to 55	Axial	OD	1943
17	2	U	Corrosion	5 to 55	Axial	OD	13215
18	2	U	Corrosion	10 to 60	Axial	OD	4714
19	2	U	Corrosion	10 to 60	Axial	OD	9738
20	1	U	Corrosion	5 to 55	Axial	OD	12261
21	1	U	Corrosion	5 to 55	Axial	OD	5476
22	2	U	Corrosion	10 to 60	Axial	OD	14099
23	1	U	Corrosion	10 to 60	Axial	OD	5032
24	6	R	Plain Dent	10 to 70	32 deg with the axial baseline	ID	17495
25	6	R	Plain Dent	10 to 70	Circumferential	ID	34301
26	6	R	Corrosion	10 to 70	Circumferential	ID	33771
27	6	R	Corrosion	10 to 70	Axial	OD	20192
28	6	R	Corrosion	10 to 70	32 deg with the axial baseline	ID	23604
29	6	R	Corrosion	10 to 70	42 deg with the axial baseline	ID	22786
30	6	R	LSW	10 to 70	42 deg with the axial baseline	ID	15971

Failure was identified when a through thickness crack developed in the dent region resulting in a leak. Table 11 also shows the crack orientation and crack initiation location (OD surface or ID surface) for each individual test.

Figure 17a shows a photograph of the magnetic particle inspection (MPI) carried out on an unrestrained plain dent. Figure 17b shows the MPI carried out on the ID surface for the same test specimen. In unrestrained dents fatigue cracks initiate on the OD surface and are in the axial orientation. In smooth shallow unrestrained dents, created with large indenters, the fatigue cracks initiated close to the dent peak. Deeper and sharper unrestrained dents promoted fatigue crack initiation away from dent peak. Multiple crack indications can be seen on the OD surface and resemble SCC colonies as seen in pipelines. This observation is consistent with previous full scale dent fatigue test results^{3, 4, 5, 6}. However, the multiple cracks are similar to what is typically seen in low cycle fatigue tests. It is conceivable that there can be scenarios present in existing pipelines where unrestrained dents may see similar stress ranges as generated in the present test program and therefore promote multiple low cycle fatigue cracks and may potentially be mis-characterized as SCC colonies.

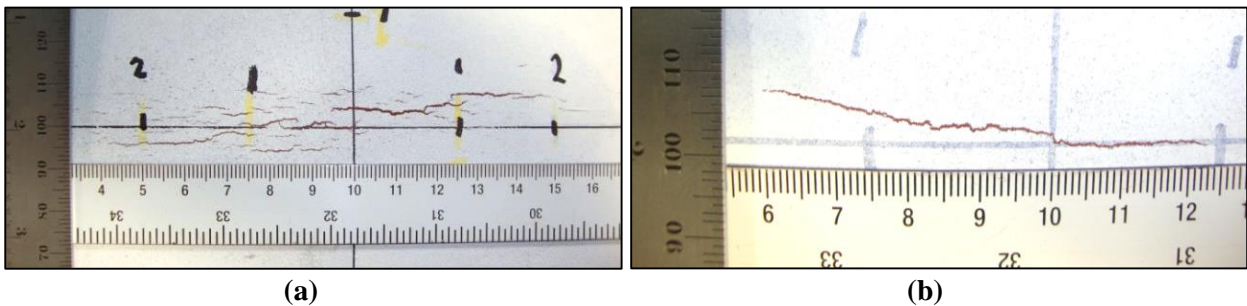


Figure 17: Plain Pipe Unrestrained Dent MPI (a) OD MPI - Axial OD Cracks (b) ID MPI - Axial OD Crack

Figure 18a and Figure 18b show photographs of the MPI carried out on a restrained plain dent. Fatigue cracks initiated on the ID surface in the case of restrained dents. The crack orientation depended upon the dent depth. Shallow restrained dents promoted cracks along the axial orientation and, as dent depth increased, the fatigue crack orientation changed to be at an angle to the longitudinal axis. In deeper restrained dents, fatigue cracks initiated in circumferential orientation away from the dent peak.

³ Brock Bolton, Vlado Semiga, Aaron Dinovitzer, Sanjay Tiku, “Towards a Validated pipeline Dent Integrity Assessment Model”, IPC2008-64621, Proceedings of the 7th International Pipeline Conference IPC 2008.

⁴ Brock Bolton, Vlado Semiga, Sanjay Tiku, Aaron Dinovitzer, Joe Zhou, “Full Scale Cyclic Fatigue Testing of Dented Pipelines and Development of a Validated Dented Pipe Finite Element Model” IPC2010-31579, Proceedings of the 8th International Pipeline Conference IPC 2010.

⁵ Sanjay Tiku, Vlado Semiga, Aaron Dinovitzer, Geoff Vignal, “Full Scale Cyclic Fatigue testing of Dented Pipelines and Development of a Validated Dented pipe Finite Element Model”, IPC2012-90427, Proceedings of the 9th International Pipeline Conference IPC 2012.

⁶ Sanjay Tiku, Amin Eshraghi, Vlad Semiga, Luis Torres, Mark Piazza, “Improved Pipeline Dent Integrity Management” IPC2016-64530, Proceedings of the 10th International Pipeline Conference IPC 2016.

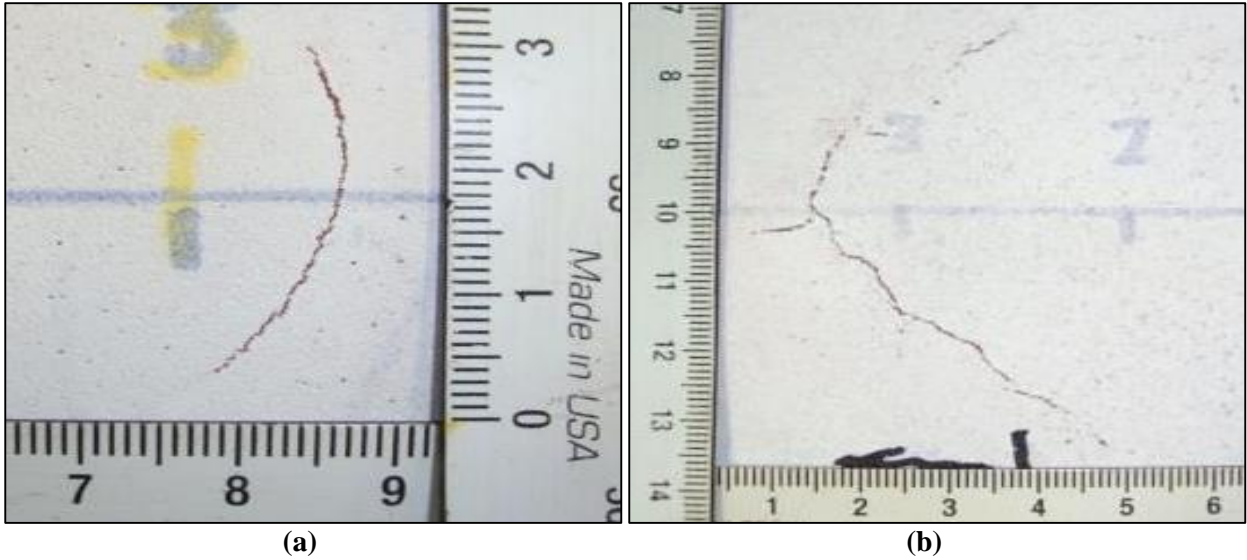


Figure 18: Plain pipe Restrained Dent MPI (a) OD MPI - Circumferential ID Crack (b) ID MPI - Circumferential ID Crack

Figure 19a and Figure 19b show MPI photographs of the OD surface and ID surface for an unrestrained dent interacting with a corrosion feature, respectively. For dents interacting with corrosion features, the fatigue cracks initiated in the corrosion feature and were mostly confined within the corrosion feature. In dents interacting with corrosion features, the tendency to have multiple parallel fatigue cracks/crack colonies was lower as compared to the similar plain unrestrained dents.

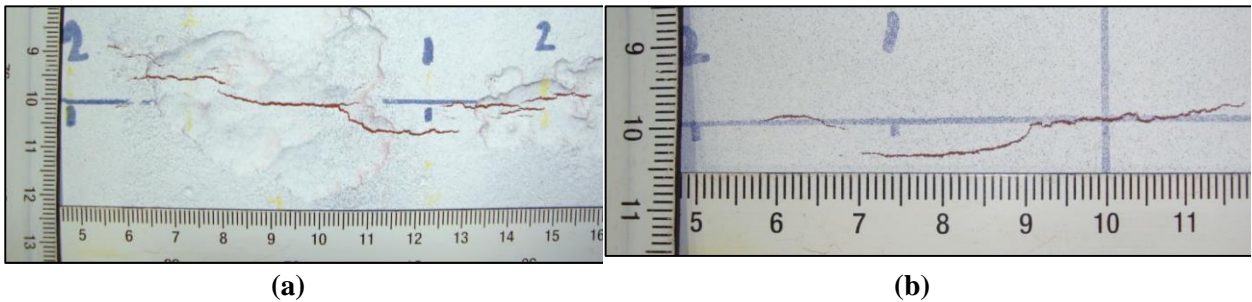


Figure 19: Corroded Pipe (a) OD MPI - Axial OD Cracks (b) ID MPI - Axial OD Cracks

Figure 20 shows a cross-section metallograph of a dent fatigue crack test specimen. There is some crack branching observed when the crack grows through thickness. The through thickness crack branching is possibly a result of a combination of complex stress state in the dent region and due to the microstructure (laminations/inclusions) rather than effect of environment.

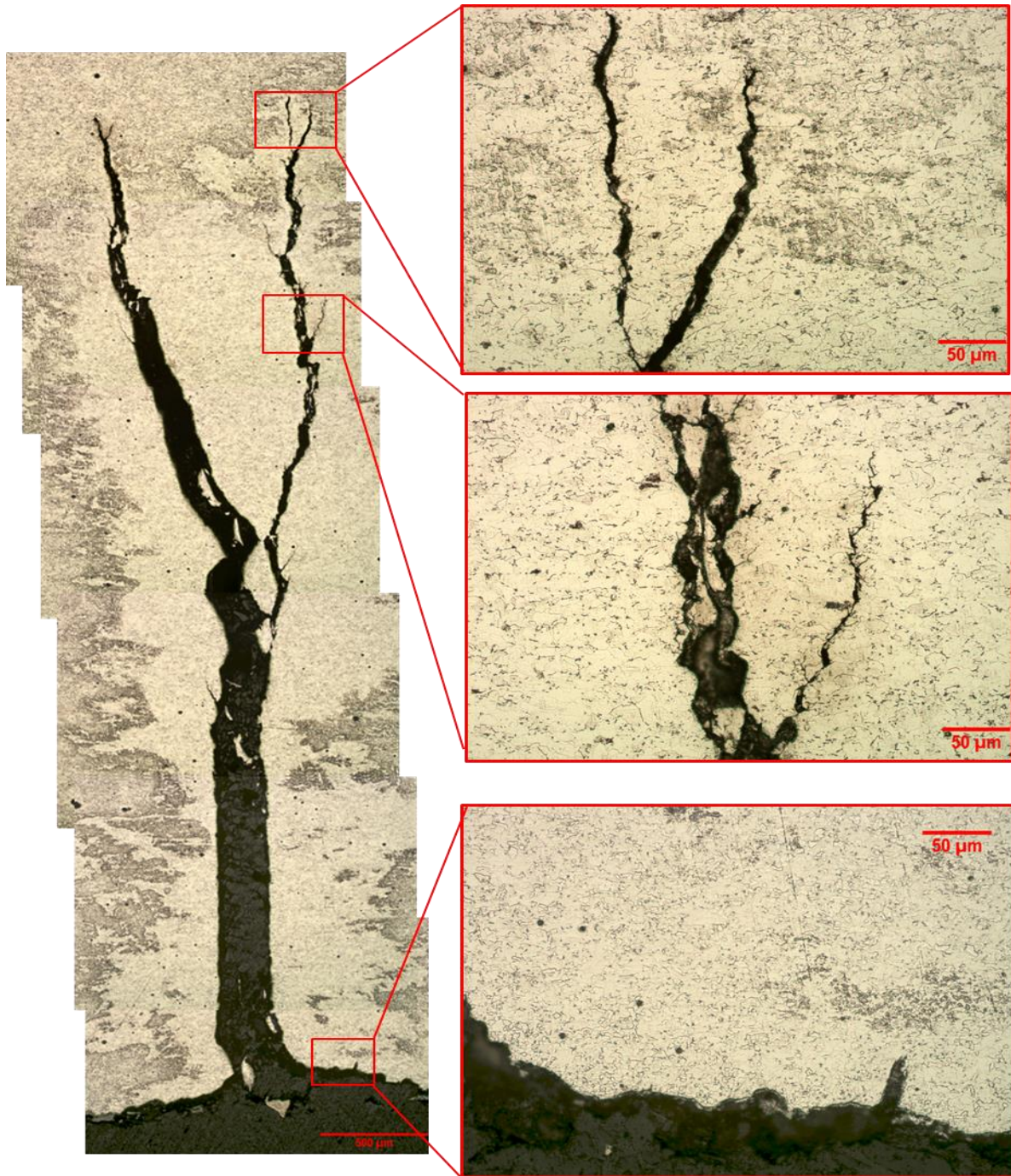


Figure 20: Cross-Section Metallograph of Fatigue Crack in Test Specimen 13

Figure 21 shows a photograph of the fracture surface for an unrestrained dent. The fracture surface looks like a typical fatigue fracture with ratcheting marks, shown as red arrows, on the OD surface where fatigue crack initiated. In some unrestrained dents, there is also indication of fatigue crack initiation on the ID surface as shown by black arrows. The fatigue cracks on the ID surface are less than 1 mm deep and may have initiated at a later stage after the initiation and growth of OD surface cracks.

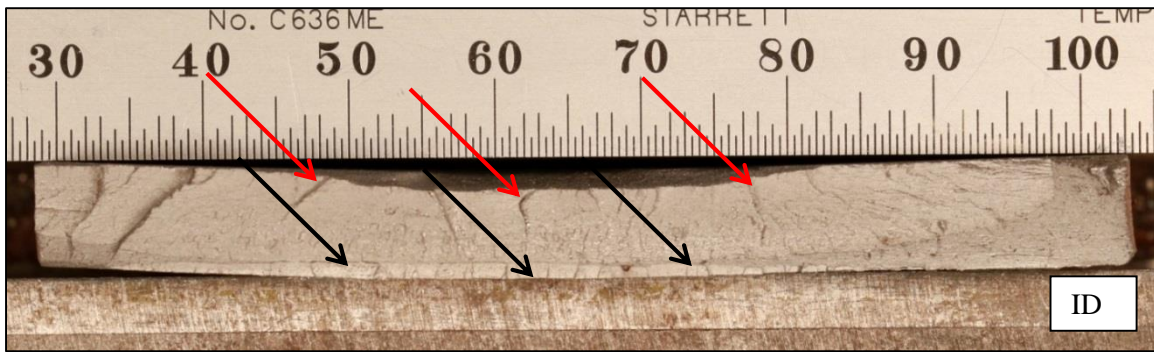


Figure 21: Test # 17 Fracture Photograph

Figure 22 shows a plot of stress range versus number of cycles (SN curve) for plain dent tests carried out in the current test program. As discussed earlier, FE modeling of the full-scale tests was carried out and the maximum surface stress range for each test specimen model was extracted and plotted against the experimental number of cycles to failure. The FE modelling tool used was developed using the measured material properties and was demonstrated to agree with the measured pipe response. Figure 22 also shows BS 7608 Class D mean curve and BS 7608 Class D mean-1SD curve⁷. BS 7608 Class D mean-1SD curve provides a conservative prediction for all the plain dents tested in the current program. BS 7608 Class D mean curve provides conservative prediction for all the plain dents except two, encircled in red, tested in the current program. The two dents circled in red were created with the transverse long bar and resemble more of a buckle than a dent.

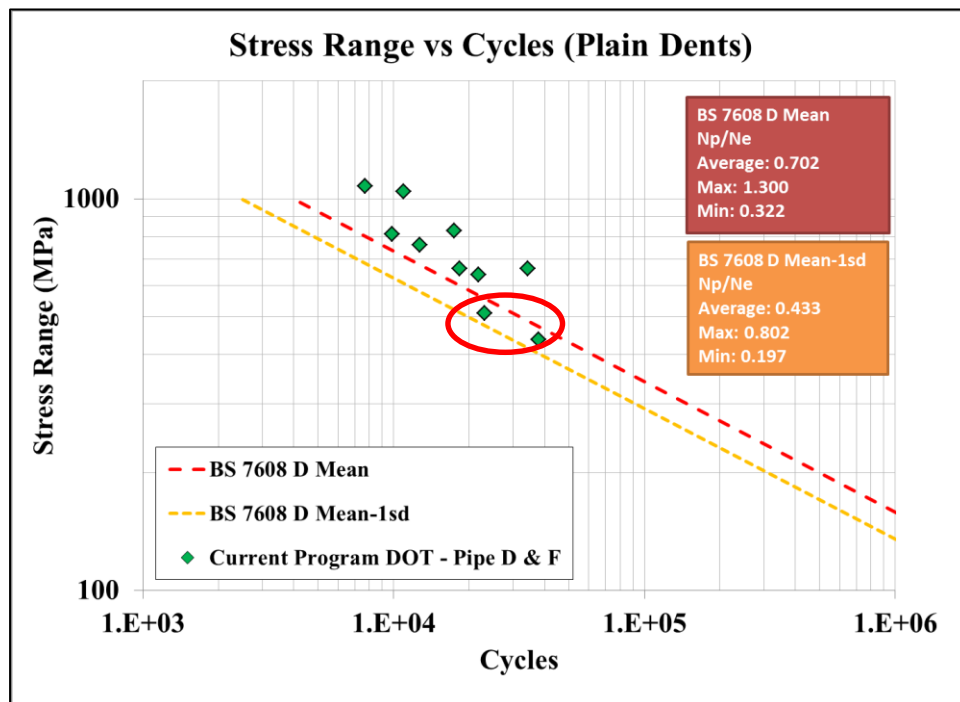


Figure 22: Pipe D & F Plain Dents - Stress Range vs Experimental Life

Figure 23 shows the same SN plot as shown in Figure 22 and includes plain dent full scale test data generated under previous full scale test projects^{3,4,5,6}. Figure 22 includes dent fatigue test data carried out

⁷ Fatigue design and Assessment of Steel Structures, BS 7608: 1993.

on linepipes of vintage 1950's, 1970's, 1990's and 2005. It includes restrained and unrestrained dents created by 2, 4, 8, 12, and 24 inch semi-elliptical indenters and 10 and 20 inch long Bar indenters. The pipe diameters used were 18, 20, and 24 inch and includes X-52 and X-70 grades. Based on the prediction for the full-scale dent fatigue tests, presented in Figure 23 results in an average predicted fatigue life of 0.40 (~2.5X lower) of the experimentally measured life based on the BS 7608 Class D mean-1sd curve. The predicted fatigue life ranges from a minimum of 0.1 (10X lower) to a maximum of 0.8 (20% lower) of the experimentally measured fatigue life.

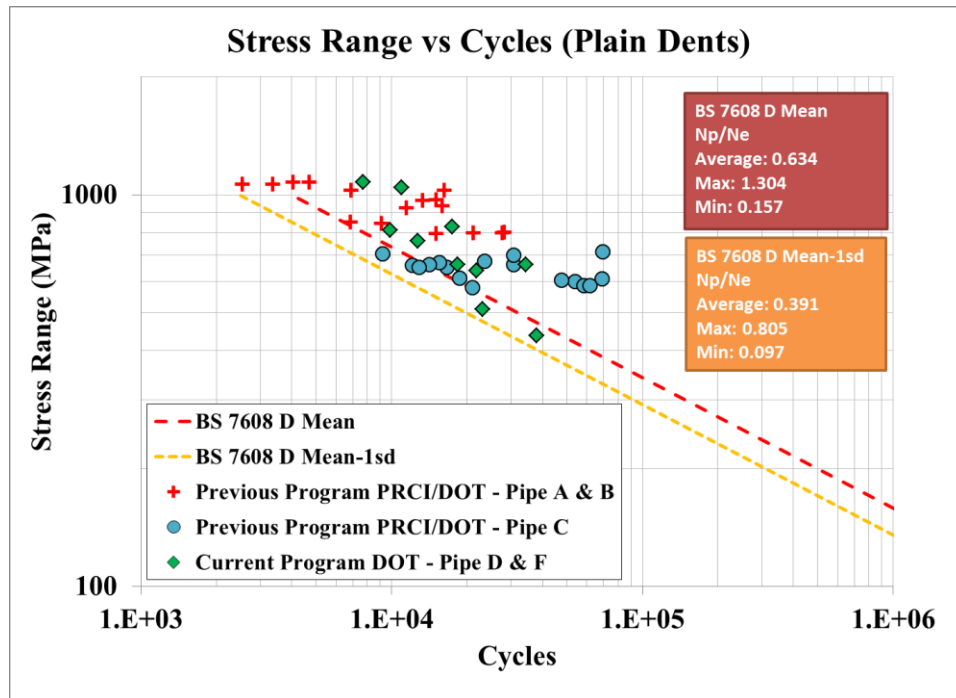


Figure 23: All Plain Dents - Stress range vs Experimental Life

Based on the BS 7608 Class D mean curve, the prediction for the full-scale dent fatigue tests results in an average predicted fatigue life of 0.63 (~1.6X lower) of the experimentally measured life. The predicted fatigue life ranges from a minimum of 0.16 (6.25X lower) to a maximum of 1.3 (30% higher) of the experimentally measured fatigue life. The 30% higher un-conservative prediction is related to the two transverse bar dents as discussed earlier.

BS 7608 Class D mean-1sd curve provides a lower bound (conservative) prediction to all of the plain dent full-scale fatigue tests and BS 7608 Class D mean curve provides conservative prediction for most of the plain dent tests (excluding six) carried out under current and previous full scale test^{3,4,5,6}. Figure 24 and Figure 25 show SN plot of unrestrained and restrained dents separately. BS7608 Class D curves provide a much more conservative prediction of fatigue life for restrained dents as compared to unrestrained dents.

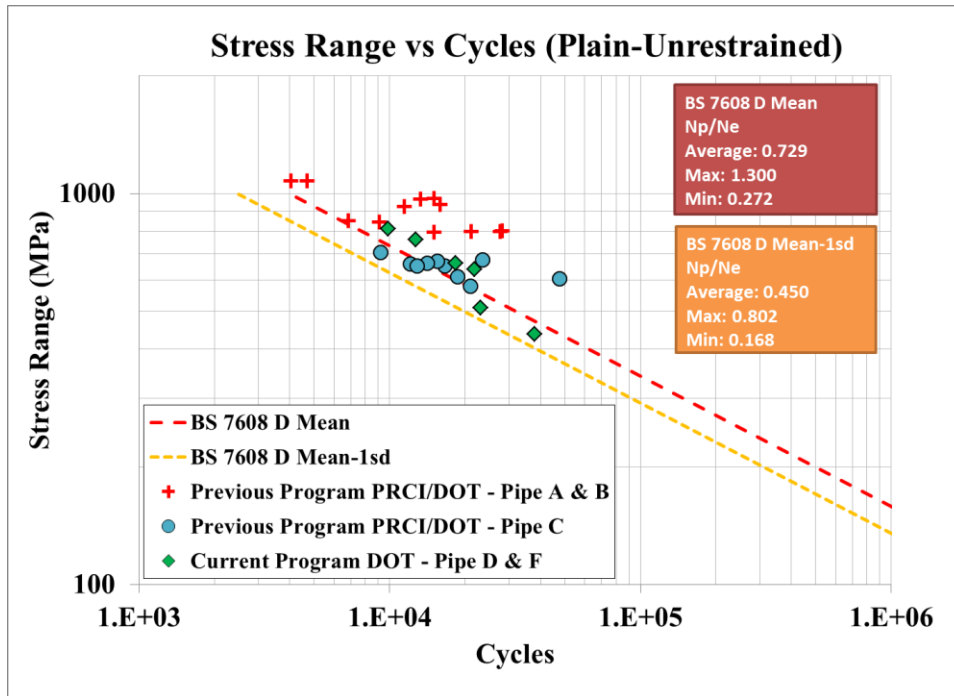


Figure 24: Unrestrained Dents - Stress range vs Experimental Life

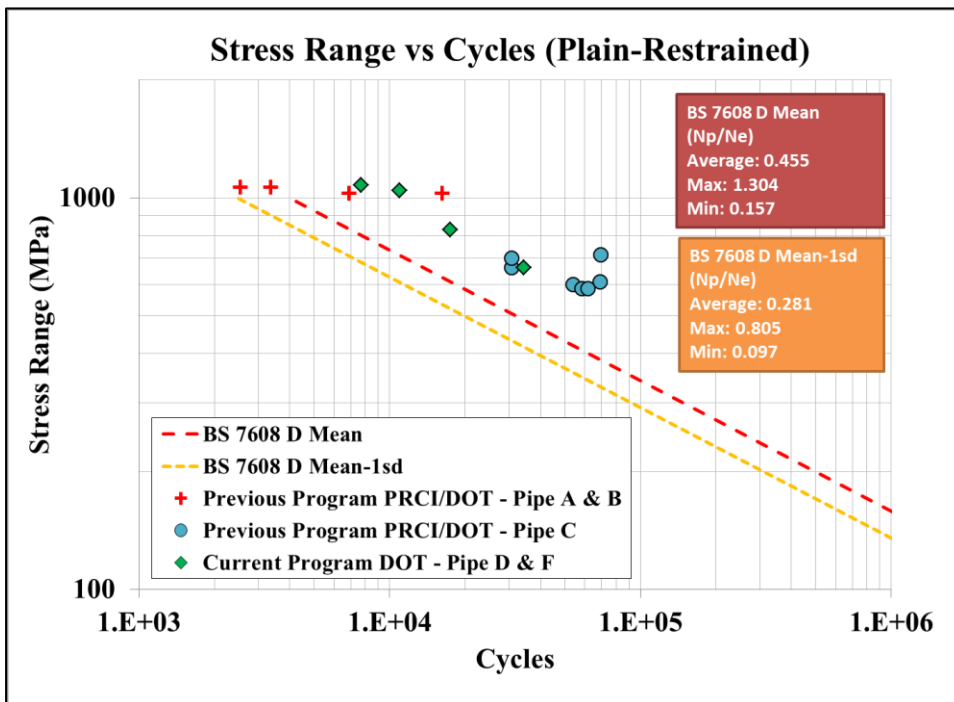


Figure 25: Restrained Dents - Stress range vs Experimental Life

Dent weld interaction tests carried out on dents created with round bars, under the current test program resulted in a maximum reduction of 2 times in fatigue life as compared to the plain dent life, as shown in Figure 26a. The maximum reduction in fatigue life, due to dent weld interaction, of 6 times was observed in the previous test program^{3,4,5,6} as shown in Figure 26b.

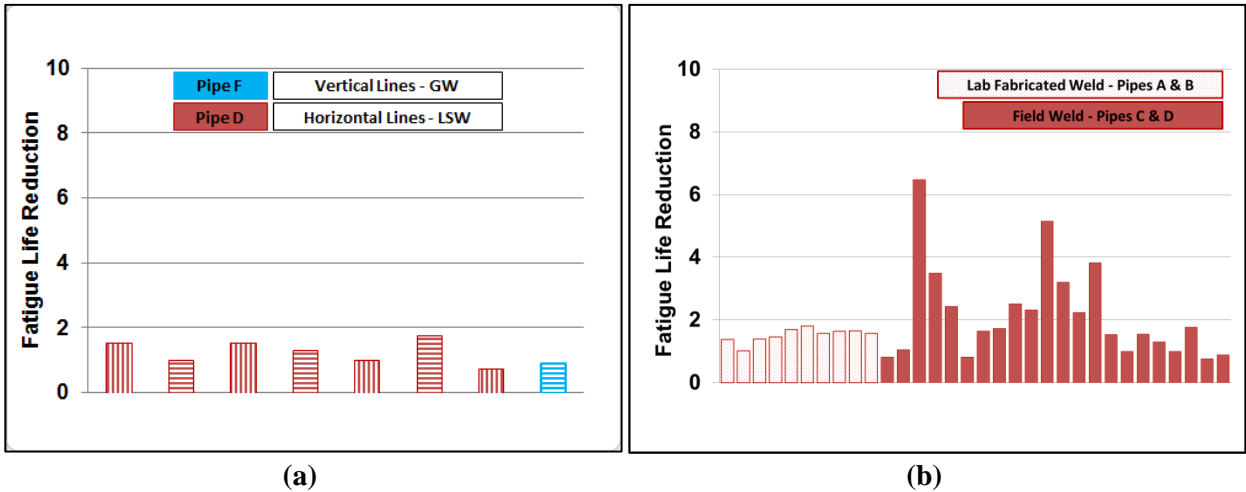


Figure 26: Fatigue Life Reduction due to Long Seam and Girth Welds (a) Current Test Program (b) Previous and Current Test Program

Figure 27a, and Figure 27b show the results for fatigue life reduction due to dent corrosion interaction for unrestrained dents. The fatigue life was reduced by a maximum of 4 times for dent corrosion interaction when the corrosion depth was less than 40%. In one test, where the corrosion depth was 42%, fatigue life reduction of 11 times was observed. The reduction in fatigue life observed in test data will be due to a combination of the effect of reduced wall thickness and surface finish.

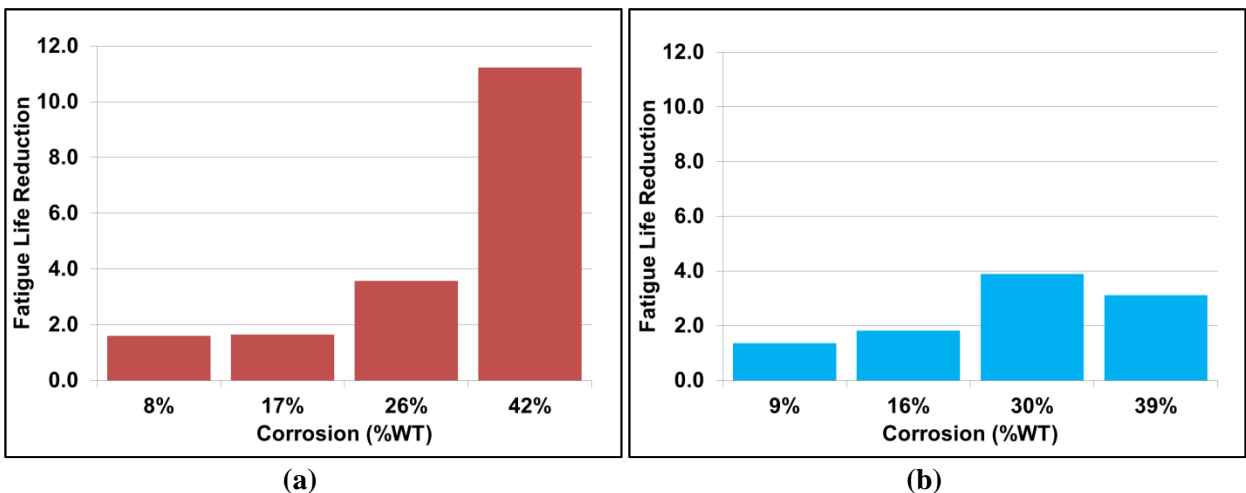


Figure 27: Fatigue Life Reduction due to Corrosion interaction (a) Unrestrained Dent with 24 in Indenter and 10% Travel (b) Unrestrained Dent with 12 in Indenter and 10% Travel

Figure 28a, and Figure 28b show the results for fatigue life reduction due to dent corrosion interaction for restrained dents. Maximum reduction in fatigue life of 1.4 times was observed for dent corrosion interaction when the corrosion depth was less than 35%. The reduction in fatigue life due to dent corrosion interaction is lower in the case of restrained dents as compared to the unrestrained dents shown earlier. Fatigue cracks initiated on the ID surface in the restrained dents and on the OD surface in unrestrained dents is consistent

with the previous full scale test program⁵. Therefore, in the case of restrained dents the effect of surface finish due to the presence of corrosion feature present on the OD surface, is not going to have an impact on the fatigue life.

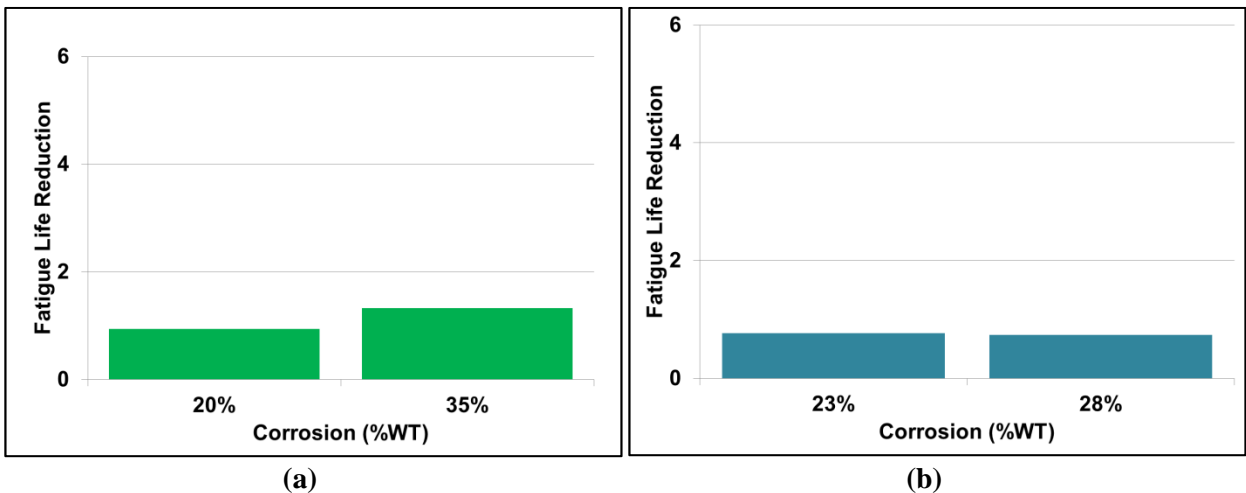


Figure 28: Fatigue Life Reduction Due to Corrosion Interaction with Restrained Dent (a) Restrained Dent with 24 in Indenter with 6% Travel (b) Restrained Dent with 20in Long Bar Indenter with 6% Travel

Detailed test data or results for individual tests are shown in Annexes (see Section 10).

4.4 Concluding Remarks and Next Steps

Thirty full scale dent fatigue tests were carried out on plain dents, dents interacting with welds and dents interacting with corrosion features. The tests involved generating data for both restrained dents and unrestrained dents. The following observations can be made based on the full scale test program:

- The plain dents test data generated on asymmetric shapes was within the scatter band of the previous full scale symmetric plain dent fatigue test data. BS 7608 Class D mean curve provides a reasonable mean life estimate and BS 7608 Class D mean-1sd curve provide a lower bound estimate of dent fatigue lives.
- For dents interacting with welds tests, the maximum reduction in fatigue life, as compared to the plain dent fatigue life, observed in the current program was 2 times which is below the maximum reduction in fatigue life, 6 times, observed in the previous fatigue test program.
- The maximum reduction in fatigue life of 4 times was observed for dents interacting with corrosion features of 40% of the pipe wall thickness or below as compared to the plain dent fatigue life. For one test with a corrosion feature depth of 42% of the pipe wall thickness, maximum reduction in life of 11 times was observed. The reduction in fatigue life due to dent interacting with corrosion features was lower (1.4 times) in the case of restrained dents.
- The location, orientation and initiation surface of fatigue cracks depended upon the dent restraint condition and the indenter size. The observation was consistent with earlier full scale test results. Deeper restrained dents approximately $\geq 4\%$ depth, in general, lead to circumferential fatigue cracks initiating on the ID surface. Shallower restrained dents, in general, result in axial cracks initiating on the ID surface. In the case of unrestrained dents the fatigue cracks initiated on the OD surface located either in the dent peak or away from the dent peak in the dent shoulder region depending upon the indenter size.
- The multiple axially oriented fatigue cracks were observed in unrestrained plain dent cases were similar to the ones observed in previous test program [3] and resemble SCC colonies as seen in pipelines. However, in the current tests the multiple cracks are similar to what is typically seen in

low cycle fatigue tests. It is conceivable that there can be scenarios present in existing pipelines where unrestrained dents may see similar stress ranges as generated in the present test program and therefore promote multiple low cycle fatigue cracks and may be mis-characterized as SCC colonies.

- In the case of dents interacting with corrosion features, there was a lower number of multiple fatigue cracks observed as compared to plain dent cases and the fatigue cracks usually followed the corrosion feature.
- To date, all the dents for the dent fatigue test program have been created in the laboratory using artificial indenters. It is recommended to carry out full scale fatigue tests on dents removed from the field and obtain fatigue life data on realistic dent shapes. The fatigue lives of field dents can then be compared against laboratory created dents and the applicability of the current standardized curve (BS7608 Class D) can be further validated.
- Dents created with round bar in the transverse orientation to the pipe longitudinal axis in the present program looked similar to buckles and had lower fatigue lives compared with other dent shapes. It is recommended to carry out additional full scale fatigue tests on dents created with transverse bars of different sizes to generate additional transverse dent shapes and corresponding fatigue life data to develop a separate fatigue life curve that will be more applicable to transverse dent that look similar in shape to buckles.
- To date, all the full scale dent fatigue tests have been carried out on dents that are either fully restrained or in unrestrained condition. There are possible scenarios where a dent in a pipeline can be partially restraint and/or the restraint condition of the dent may change depending upon the mean pressure of the pipeline. It is recommended to carry out additional full scale fatigue tests where dent is partially restraint or its restraint condition changes during the cyclic pressure loading. The work would also involve carrying out detailed FE modeling to assist in experimental design. The fatigue life data generated for the partially restrained dent will be compared against the restrained and unrestrained dent fatigue tests carried out previously and applicability of the current standardized curve (BS7608 Class D) can be further validated.

The full scale dent fatigue tests involving dent interaction with secondary features (welds and corrosion features) focused on positioning secondary features at the critical locations in order to obtain the maximum reduction in fatigue life due to interacting features. It is recommended to carry out additional full scale tests to identify the minimum distance a feature has to be from the dent peak where it would not affect the dent fatigue life. This will enable to better define when a dent is considered to be interacting with a secondary feature and therefore requires repair/remediation. This study was completed numerically for welds. It is recommended to complete this numerical evaluation for metal loss and complete full scale trials for welds and metal loss to validate these results.

5 Full Scale Testing of Dent and Gouge Defects (Task 5)

5.1 Background and plan of investigation

In this task, additional Dent and Gouge defects were created and tested in order to extend the previous database established by previous PHMSA and PRCI projects^{1,2} so as to fill some knowledge gaps concerning effects of different parameters on defect behavior. The graph in Figure 29 shows the existing database and the possible investigation field at project beginning.

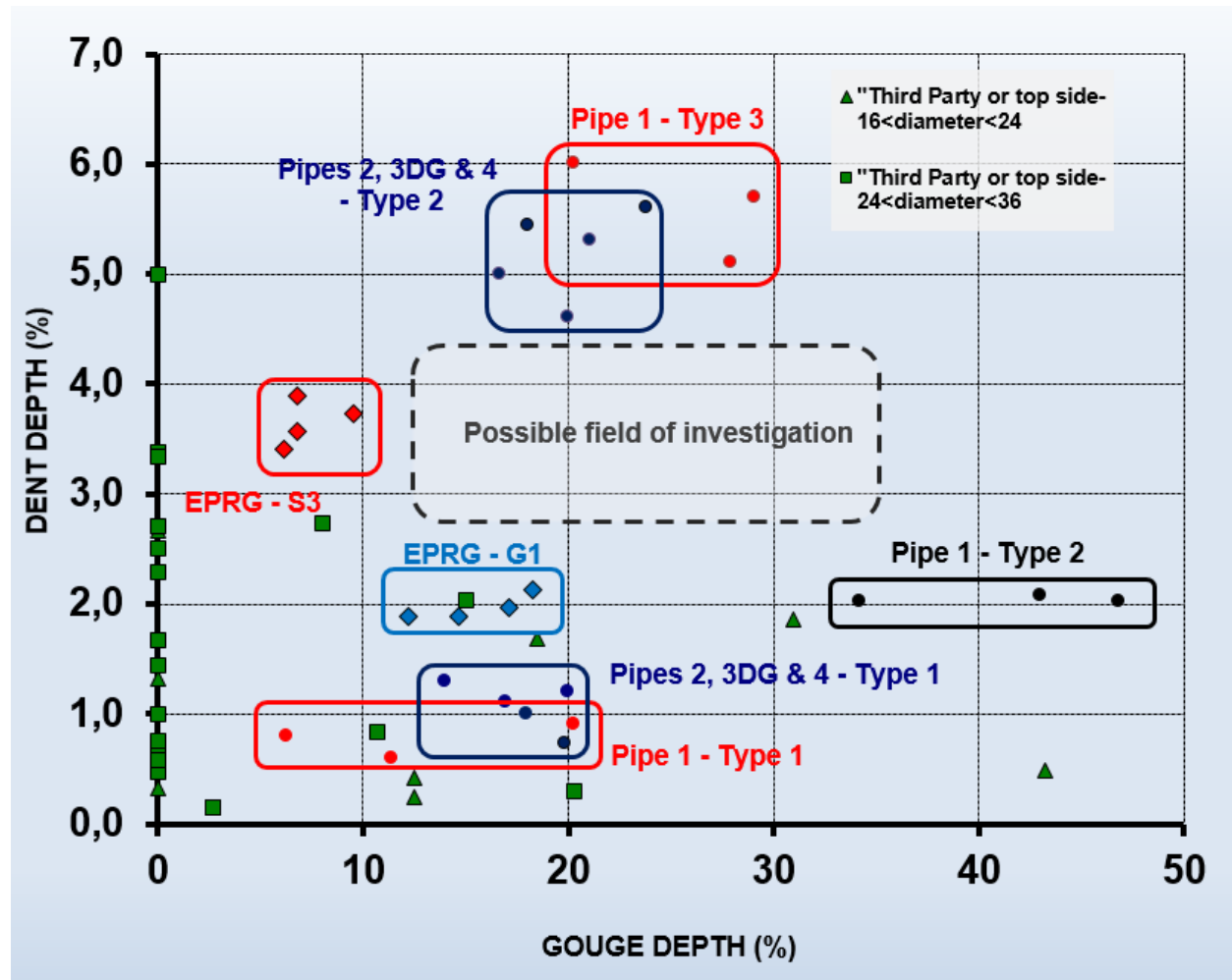


Figure 29: State of the art of Dent and Gouge defect database and possible field of investigation at the beginning of the project t; some results are provided by the European Pipeline Research Group (EPRG)

Throughout the scope of this task, 19 Dent and Gouge defects were created and 16 were tested (three defects were considered not to be fit according to graph of Figure 29). In addition, two defects were retrieved from the field and tested (on one defect, it was not possible to measure the gouge depth due to the field configuration). Thus, a total of 18 defects were tested for this task.

Graph of Figure 30 shows the Dent and Gouge defect database that were completed. Pipe 5 and 6 were bought and two pipes (Pipe 7 and 8) were retrieved from the field to accomplish this task. Three different tools (type 4, 5 and 6) were used for defect creation on Pipe 5 and 6 in order to have different defect dimensions to fill in the gaps of Figure 29.

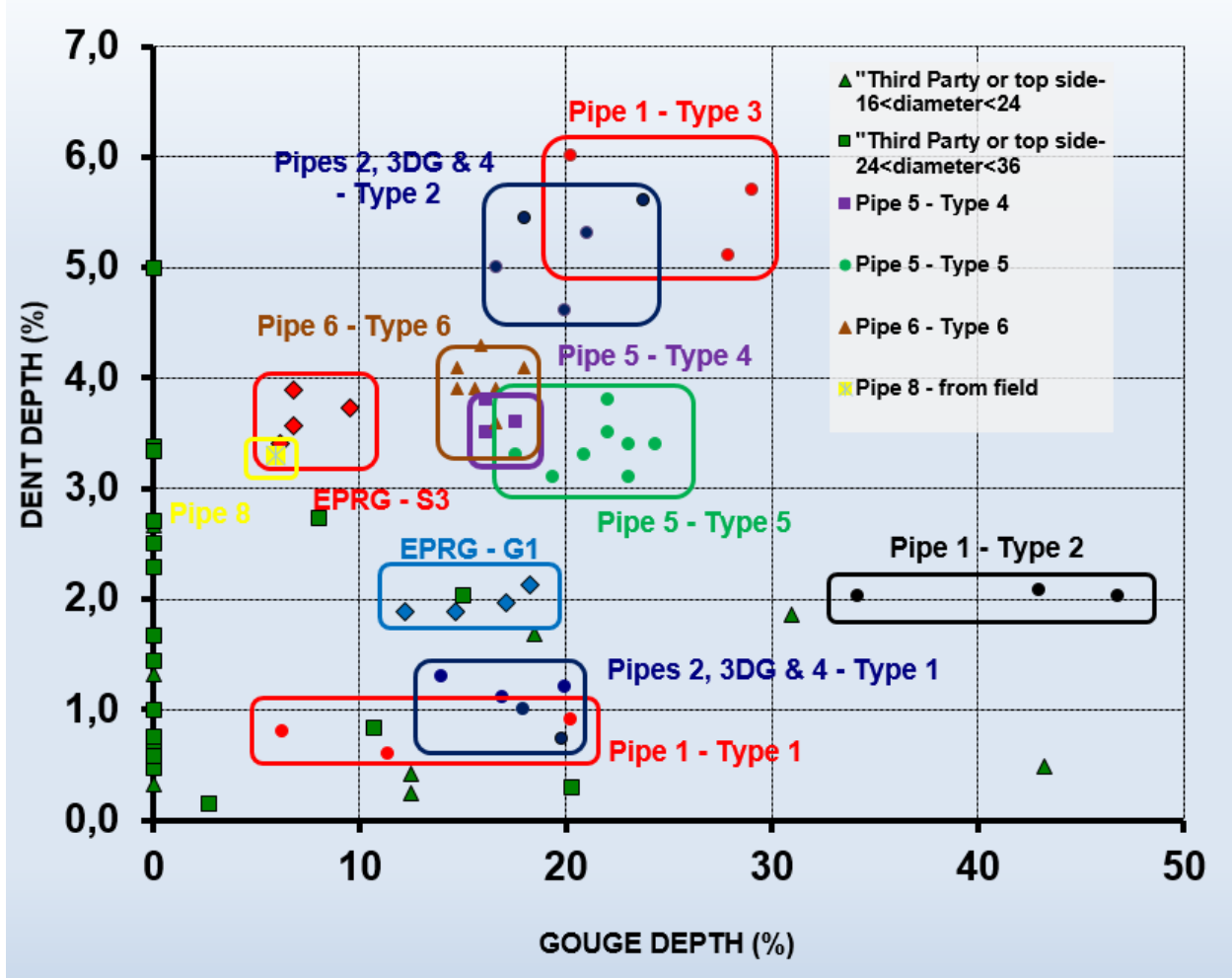


Figure 30: State of the art of Dent and Gouge defect database and defects created during the project. Pipe 7 is not represented because gouge depth measurement had too high uncertainties due to defect configuration

5.1.1 Test Matrix

To better highlight the test matrix, it was decided to split this task into three sub-tasks:

- Task 5a, Dent and Gouge Severity (Pipe 5 and 6),
- Task 5b, Interaction Between Defects (Pipe 5),
- Task 5c, Dent and Gouge Defects Removed from Service (Pipe 7 and 8).

The three sub-tasks are summarized in Table 12. Task 5a was performed on two different pipes (Pipe 5 and Pipe 6). Task 5c was performed on two different pipes retrieved from service (Pipe 7 and Pipe 8). Task 5b was performed on a single pipe, which was also used in Task 5a (Pipe 5).

Table 12: Dent and gouge defect test matrix, covering one task, three sub-tasks, four pipes, eighteen Dent and Gouge defects

	PIPE 5 (24") Task 5a & Task 5b		PIPE 6 (12") Task 5a	PIPE 7 (8.6") PIPE 8 (16") Defects removed from service Task 5c
Material characterization	Pipe 5 characterized		Pipe 6 characterized	Pipe 7 characterized Pipe 8 characterized
Destructive characterization	5.4.1	5.5.1	6.6.1	na
Burst test	5.4.2	5.5.2	6.6.2	7.ext1.2
Pressure Swings Fatigue test	5.4.3	5.5.3	6.6.3	na
Fatigue test & CP overprotection = environmentally assisted cracking with H2 diffusion	na	5.5.3.cp	na	8.ext2.3cp(*)
Fatigue test interacting defects, 2 spacings: i1 & i2 (Task 5b)	na	5.5.3i1 & 5.5.3i1' spacing 600 mm	na	na
		5.5.3i2 & 5.5.3.i2' spacing 0 mm		
Burst test combined with <u>axial</u> <u>load</u>	na	na	6.6.2a	na
Pressure swings fatigue test with combined <u>axial</u> <u>load</u>	na	na	6.6.3a	na
Legend		Destructive characterization / Burst test / Fatigue test performed		
		Completed test / Destructive characterization ongoing		
Note	(*) Defect 8.ext2.3cp has not failed and thus has not been destructively characterized			

The goal of Task 5 was to provide a very detailed experimental database to expand the knowledge about realistically created Dent Gouge defects (i.e. both are created simultaneously during the impact). This realistic creation process using a Pipe Aggression Rig ensures similar geometric, mechanical and metallurgical features upon defect creation as Dent and Gouge defect found in service. Results of detailed, including destructive characterization are reported for some of the defects. The database also includes experimental results for several different Dent and Gouge defect types in terms of burst pressure, fatigue life, and related detailed post-failure investigations. All of these experimental investigation results can be used to improve models developed to ascertain how a feature was created, and assessments of burst pressure and fatigue life of Dent and Gouge defects.

This task complemented and expanded results produced during prior PHMSA and PRCI projects^{1,2}, involving full-scale testing of Dent and Gouge mechanical damage defects that are related to external interference (i.e., machinery). PRCI's project test matrix included the creation of 15 realistic Dent and Gouge defects also using ENGIE's Pipe Aggression Rig and PHMSA's project included 21 realistic Dent and Gouge defects. The fabricated features were then subjected to full-scale testing to determine burst failure under monotonic loading conditions and fatigue failure due to cycling loads (pressure fluctuations), as well as, a detailed non-destructive and destructive defect characterization.

The work completed for this project includes testing on modern steel with three different types of Dent and Gouge defects created using a slower aggression mode. Each defect type created is then subjected to a series of detailed geometry, mechanical state and local material characterization tests and burst and fatigue testing, with the burst and fatigue test being highly instrumented to provide detailed and comprehensive measurement data for the development of the improved severity assessment models.

5.1.2 Defect creation process

The defects are identified by three characters **X.Y.Z.** which are numbers:

X.Y.Z.—**X** identifies the **Pipe X** material which is noted by 5, 6, 7 or 8 in this program;

X.Y.Z.—**Y** defines the **type of Dent and Gouge defect** characterized by its geometry notably in terms of dent depth and length, and gouge depth and length. The value of Y can range from 1 to 3 for defects created in the laboratory facilities, *ext1 for Pipe 7* and *ext2 for Pipe 8* retrieved from service.

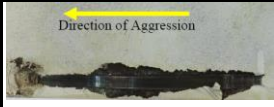
X.Y.Z.—**Z** is the **defect number in the defined defect type.**

- $Z = 1$ is for a detailed geometrical, mechanical and metallurgical in-depth defect characterization after its creation.
- $Z = 2$ is a similar defect for the burst test to evaluate the defect behavior of under monotonous pressure load.
- $Z = 3$ is a similar defect for the fatigue test to evaluate the defect behavior under cyclic variation of internal pressure.
- $Z = 3cp$ is a similar defect for a fatigue test with cathodic overprotection environment.
- $Z = 2a$ is a similar defect for the burst test to evaluate the defect behavior of under monotonic pressure load combined with an axial load.
- $Z = 3a$ is a similar defect for the fatigue test to evaluate the defect behavior under cyclic variation of the internal pressure combined with an axial load.

The objectives of this task compared to previous Dent and Gouge defect life assessment was to examine the following new features:

- Interaction between closely spaced Dent and Gouge defects, and spacing effect on fatigue life;
- Effect of cathodic overprotection on fatigue life of Dent and Gouge;
- Additional axial load effect on fatigue life; and
- Burst or fatigue test on pipe with Dent and Gouge defect retrieved from service.

Table 13: Dent and Gouge defect test matrix

Pipe 5		Pipe 6	Pipe 7	Pipe 8
Type 4	Type 5	Type 6	Ext1	Ext2
5.4.1	5.5.1	6.6.1	7.ext1.2	8.ext2.3cp
				
5.4.2	5.5.2	6.6.2		
				
5.4.3	5.5.3	6.6.3		
				
	5.5.3cp	6.6.2a		
				
	5.5.3i1	6.6.3a		
				
	5.5.3i1'			
				
	5.5.3i2			
				
	5.5.3i2'			
				

During defects' creation, forces, aggression tooth displacement and time are recorded to determine the energy to create defects which was below 10,000 Joules. Figure 31 provides energy versus time during defect creation of Dent and Gouge defect 6.6.1.

DEFECT 6.6.1

X energy, Z energy and total absorbed energy versus time

Actual load factor :
Internal pressure (bar) : 30
Total absorbed Energy (J) : 5267
Tooth type : DIV00824



Diameter (mm) : 323,9
Thickness (mm) : 5,9
Grade : L360MB
Pipe number : 6

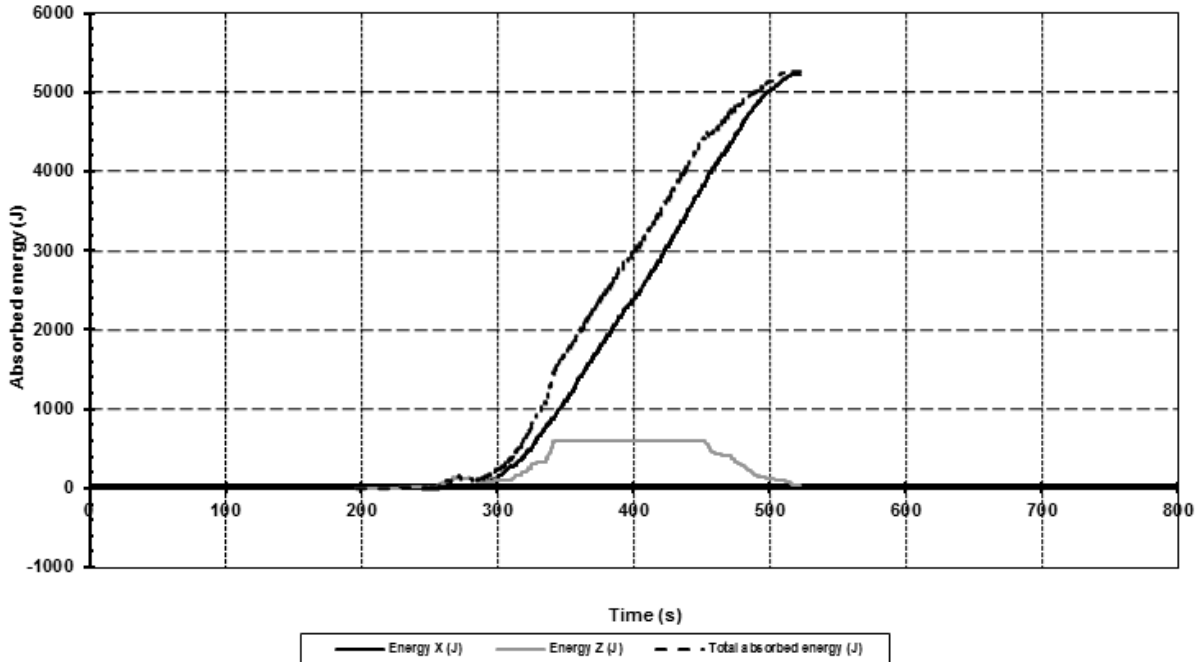


Figure 31: Energy spent to create defect 6.6.1 by slow dynamic aggression (5,267 Joules)

Each defect was characterized by 3D Seikowave measure to determine the dimensions (see Figure 32). Each defect was checked by magnetic particle inspection (MPI) to detect micro-cracks at the gouge bottom (see Figure 32). There is no evidence of micro-cracks for the defects created. It is consistent with the observation performed during the previous PHMSA project¹ with defects created by slow aggression.

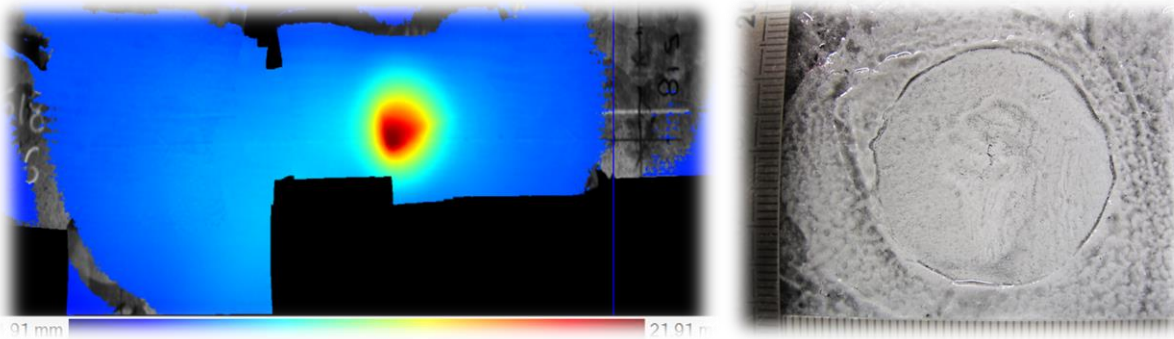


Figure 32: Seikowave measure for defect 7.ext2.2 dimensions (left); MPI on defect 8.ext2.3cp (right);

5.1.3 Experimental Approach for Burst tests

Detailed instrumentation included a longitudinal dent profiler positioned along the defect length to measure the vertical displacement during pressure increase to failure. Figure 33 represents defect re-rounding as it responds to increasing pressure. The curves with the largest outward motion (evolution) correspond to the deepest locations in the dent, and those with a more limited outward motion correspond to the edges of the dent. The team has identified and distinguished two phases in the outward motion of the deepest part of the Dent and Gouge defect:

- Pop-up: this corresponds to the rapid (i.e., for a limited pressure increase) re-rounding that occurs above the denting pressure, and brings the Dent and Gouge bottom close to the initial position. Reverse dent bending is the dominant mode in this phase.
- Bulging: re-rounding and even peaking occurs over a wider pressure interval – membrane stretching seems to be the dominant mechanism, with a smaller amount of associated reverse bending.

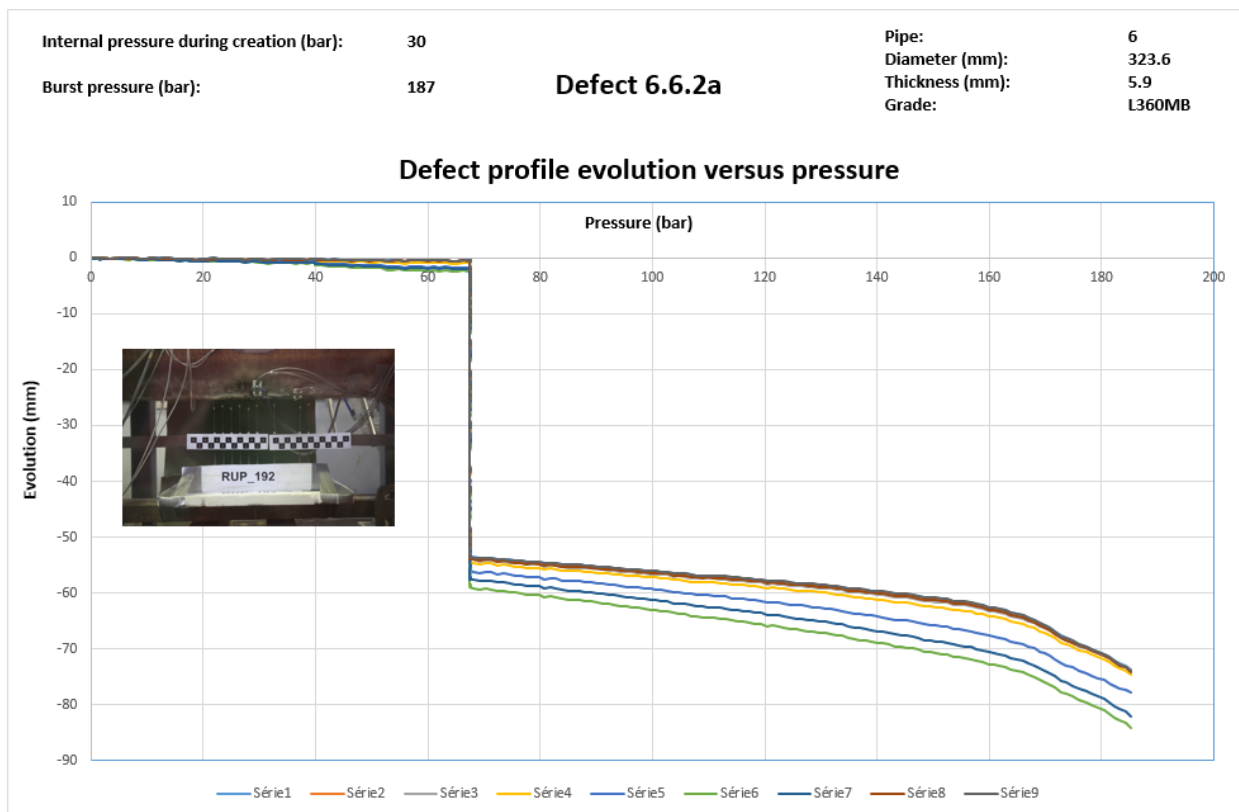


Figure 33: Dent pop-up of Dent and Gouge 6.6.2 followed by significant dent bulging for pressure increase at 67 bar when the four-point bending load was imposed.

Dent and Gouge defects are also instrumented with an opening displacement clip gauge in order to measure the opening of the defect during pressure increase or cycling (see Figure 34).

Internal Pressure during defect creation (bar): 30
 Burst Pressure (bar): 175,2

Defect 6.6.2

Pipe 6
 Diameter (mm) 323
 Thickness (mm) 5,9
 Grade L360MB

Evolution of opening displacement (clip gauge) versus pressure

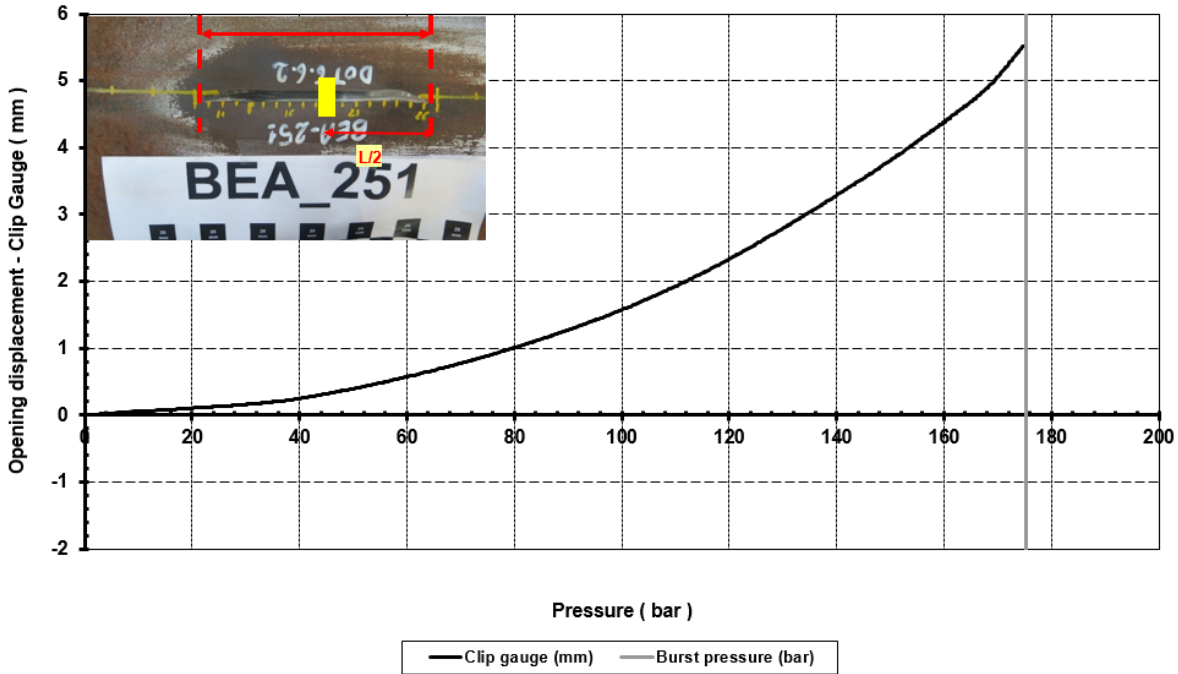


Figure 34: Opening displacement clip gauge for burst test of Dent and Gouge defect 6.6.2

5.2 Material Selection, Acquisition and Characterization (Task 2)

Four different pipe materials were utilized and characterized for the experimental test program relative to Task 5 (split into sub-tasks 5a, 5b and 5a), see Table 14.

Table 14: Overview of the four materials used in Task 5

Pipe#	Sub-Task#	External Pipe Diameter mm (in)	Pipe Thickness mm (in)	Grade (specified)	Year
Pipe 5	Task 5a, 5b	609.6 (24)	7 (0.276)	unknown	unknown
Pipe 6	Task 5a	323.9 (12.8)	5.9 (0.232)	X52	1959
Pipe 7	Task 5c	219.1 (8.6)	5.9 (0.232)	A37 HLE	1971
Pipe 8	Task 5c	406.4 (16)	7.0 (0.276)	A42 SHLE	1959

Material property characterization was carried out for each of the four pipes materials. The characterization effort included:

- Chemical analysis
- Tensile tests in both the longitudinal and transverse directions
- Charpy impact testing

Table 15: Pipe materials transverse tensile properties

Pipe# transverse direction	Measured Values					
	0.2% Yield Strength		Ultimate Tensile Strength		Elongation	Area Reduction
	(MPa)	(ksi)	(MPa)	(ksi)	(%)	(%)
Pipe 5	406	58.9	578	83.8	25.2	50.7
Pipe 6	441	64.0	534	77.5	30.5	52.9
Pipe 7	284	41.2	441	63.9	37.4	47.3
Pipe 8	331	48.0	503	73.0	32.0	48.0

Table 16: Pipe materials longitudinal tensile properties

Pipe# longitudinal direction	Measured Values					
	0.2% Yield Strength		Ultimate Tensile Strength		Elongation	Area Reduction
	(MPa)	(ksi)	(MPa)	(ksi)	(%)	(%)
Pipe 5	412	59.7	562	81.5	28.5	67.1
Pipe 6	437	63.3	528	76.6	31.1	62.0
Pipe 7	333	48.2	450	65.3	35.4	49.5
Pipe 8	315	45.6	493	71.6	32.2	53.7

Table 17: Pipe materials transverse Charpy impact properties

Pipe# TL direction	Test Temperature		Impact Energy	
	(°C)	(°F)	(J) (ft-lb)	(J.cm ⁻²)
Pipe 5	22	72	16.5 (12.2)	41.0
Pipe 6	20	68	23.7 (17.5)	125.0
Pipe 7	23	73	13.0 (9.6)	66.0
Pipe 8	20	68	8.3 (6.2)	41.2

Table 18: Pipe materials longitudinal Charpy impact properties

Pipe# LT direction	Test Temperature		Impact Energy	
	(°C)	(°F)	(J) (ft-lb)	(J.cm ⁻²)
Pipe 5	22	72	52.8 (38.9)	130.7
Pipe 6	20	68	26.3 (19.4)	131.7
Pipe 7	23	73	64.0 (47.2)	158.0
Pipe 8	20	68	16.0 (11.8)	80.0

Table 19: Pipe materials chemical composition

Pipe#	C %	Mn %	Si %	P %	S %	Al %	Cr %	Cu %	Ni %	Mo %	Nb %	N2 %	Ti %	V %
Pipe 5	0.230	1.270	0.030	0.009	0.015	0.010	0.040	0.030	0.030	0.010	0.030	0.004	0.010	0.010
Pipe 6	0.085	0.920	0.180	0.015	0.007	0.050	0.030	0.060	0.050	0.010	0.020	0.006	< 0.010	< 0.010
Pipe 7	0.140	0.520	0.200	0.028	0.025	0.010	0.020	0.020	0.050	0.010	0.010	0.004	0.010	0.010
Pipe 8	0.160	0.790	0.190	0.012	0.032	0.050	0.070	0.210	0.250	0.040	< 0.010	< 0.005	< 0.010	< 0.010

The detailed results of the material characterizations are available in the Annex.

It appears that pipes tested have a medium to high toughness.

5.3 *Test set-ups for Task 5*

5.3.1 Dent and Gouge Severity (Task 5a)



Figure 35: Test set-up for Dent and Gouge defect 5.4.1 (Task 5a)



Figure 36: Test set-up for Dent and Gouge defect 5.5.3cp (Task 5a)

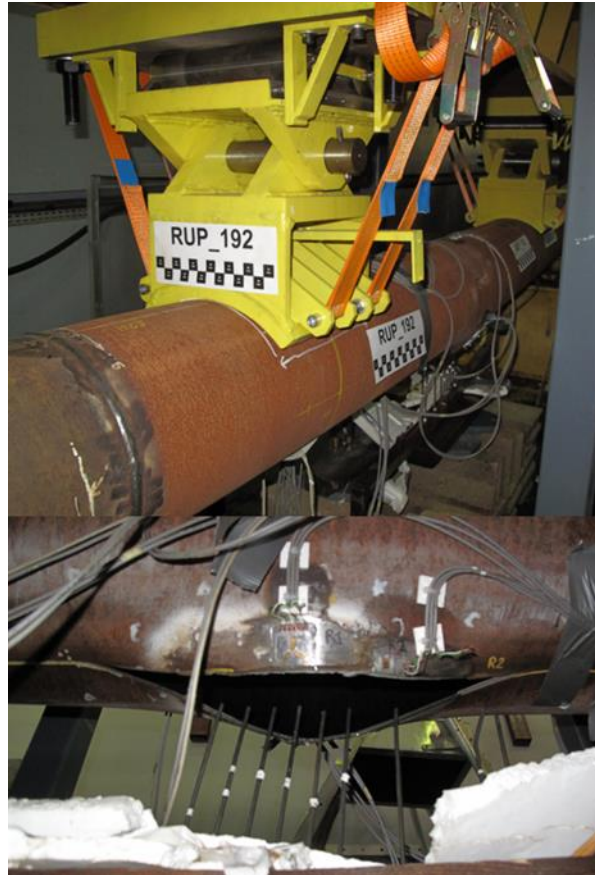


Figure 37: Test set-up for Dent and Gouge defect 6.6.2a burst test with axial load by means of a 4-points-bending loading (Task 5a)

5.3.2 Interaction between Dents with Severe Dent and Gouge defect profiles (Task 5b)



Figure 38: Test set-up for Interacting Dent and Gouge defects 5.5.3i2 and 5.5.3i2' (Task 5b)

5.3.3 Dent and Gouge Defects Removed from Service (Task 5c)



Figure 39: Test set-ups for Dent and Gouge defects 7.ext1.2 (burst test, *top*) and 8.ext2.3cp (fatigue test under over cathodic protection, *bottom*) retrieved from service (Task 5c).

5.4 *Results and Conclusions (Task 5)*

5.4.1 Burst tests

Results for the burst tests are summarized in Table 20, in which the load factors are expressed as the ratio of the hoop stress in the flawless pipe (in the considered conditions) to the actual yield strength. The load factor is one way to assess Dent and Gouge defect severity, as their burst pressure can be related to the commonly used load factors for the maximum allowable operating pressure (MAOP) determination, and more particularly indicate defect severity in given class locations.

The most noticeable aspect is that defects created on Pipe 5 are very severe, resulting in low burst pressures, particularly for Dent and Gouge defect 5.4.2, below a typical location class 1 MAOP of the pipe. As the pipe grade for Pipe 5 is unknown (retrieved from service), the use of the actual yield strength is conservative. All load factor at burst based on actual yield strength values are lower than when using the specified yield strength. Aside from Dent and Gouge defect 5.4.2, all other would have failed well above MAOP, and this is highly probable but not known with certainty for defect 5.4.2.

The severity of these Dent and Gouge defects is mainly due to a sharp edge on one side of the aggression tool. This edge was rounded out between Dent and Gouge defects 5.4.2, then 5.5.2, and subsequently more significantly for Dent and Gouge defects introduced in Pipe 6. This aspect highlights a reason why Dent and Gouge defects are so difficult to assess, they are significantly more complex than dents, especially in terms of local attributes, like minimum curvature range in the gouge, micro-cracks in the gouge, etc.

The burst strength results are significantly higher for defects in Pipe 6 as compared to Pipe 5, which illustrates the sensitivity of results to defect severity, in this case based on just one parameter, the curvature radius of the excavator tooth in the plane perpendicular to the aggression trajectory plane.

This relatively wide range of load factors at burst indicate a broad coverage of defect severity in this study, even though based on one parameter. In the previous PHMSA study¹, two types of Dent and Gouge defects were studied, one with a sharp new tooth under highly dynamic aggression, that almost systematically produced micro-cracks. The other had a worn tooth in a slower aggression mode that did not produce micro-cracks. In the current study, a combination of the two previous modes was tried, i.e. a sharp tooth with a slower aggression mode. While no clear micro-crack indications appeared, the changes in curvature radius created very different defects in terms of burst and fatigue resistance (see also below). Completing the test matrix with other values of these parameters appears as a gap to be filled.

It is also noteworthy that the main subject of this project, i.e. interacting threats, provides a very reassuring result. For the axially oriented Dent and Gouge defect studied, the presence of the defect in the worst case conditions (on the pipe extrados during four-points bending) with simultaneous bending and pressurization, led to a slightly higher burst pressure. In other terms, the influence of the axial loading seems to be second order in this case, as compared to small variations in defect shape. This evidence suggests that circumferentially oriented Dent and Gouge defects that are more likely to be sensitive to axial loads, would be ideal candidates for further testing of Dent and Gouge resistance when simultaneously submitted to axial and internal pressure loads.

The actual Dent and Gouge defect removed from service survived to a rather high failure pressure, as the load factor is based on actual rather than specified yield strength figures. This suggests that additional full scale testing of Dent and Gouge defects removed from service, with even more detailed geometry characterization would be beneficial.

Table 20: Results of burst tests for Task 5 pipes

Pipe number	Defect number	Subtask #	Type of mechanical aggression for defect creation	Dent depth without pressure (%)	Pressure during creation (bar)	Pressure during creation (psi)	Load factor during creation (w/r to actual YS) (%)	Burst pressure (bar)	Burst pressure (psi)	Load factor @ burst w/r to actual YS (%)
Pipe 5 unknown grade	5.4.2	<i>Task 5a</i>	Slow dynamic aggression	3.8	10	145.04	11%	66.0	957.2	71%
	5.5.2	<i>Task 5b</i>	Slow dynamic aggression	3.3	10	145.04	11%	81.1	1176.3	87%
Pipe 6 X52 grade	6.6.2	<i>Task 5a</i>	Slow dynamic aggression	3.6	30	435.11	19%	175.2	2541.1	109%
	6.6.2a	<i>Task 5a</i>	Slow dynamic aggression	3.9	30	435.11	19%	187.5	2719.5	116%
Pipe 7 A37 HLE grade	7.ext1.2	<i>Task 5c</i>	<i>unknown</i>	10.0	<i>unknown</i>	<i>unknown</i>	<i>unknown</i>	166.8	2419.2	93%

Fatigue test results summarized in Table 21 also cover a wide variety of conditions, in terms of:

- Providing a baseline for Dent and Gouge defects without interacting threats
- Pressure cycling range, with a factor of 2 between 20 and 40 bar
- Fatigue cycling of closely interacting Dent and Gouge defects, or more remotely located Dent and Gouge defects
- Fatigue cycling sometimes coinciding with cathodic overprotection as an aggravating factor
- Fatigue cycling under simultaneous axial loading, as four point bending
- Fatigue cycling of a Dent and Gouge defect removed from service.

Table 21: Results of fatigue tests for Task 5 pipes

Pipe number	Defect number	Subtask #	Type of mechanical aggression for defect creation	Dent depth without pressure (%)	Pressure during creation (bar)	Pressure during creation (psi)	Fatigue pressure range Pmax-Pmin (bar)	Fatigue pressure range Pmax-Pmin (psi)	Fatigue load factor range (%)	Number of cycles to failure	Failure mode
Pipe 5 unknown grade	5.4.3	Task 5a	Slow dynamic aggression	3.5	10	145.04	20.0	290.1	[31% ; 53%]	13,347	leak
	5.5.3	Task 5a & Task 5b	Slow dynamic aggression	3.3	10	145.04	40.0	580.2	[21% ; 64%]	1,794	rupture
	5.5.3cp	Task 5a	Slow dynamic aggression	3.1	10	145.04	40.0	580.2	[20% ; 63%]	4	rupture
	5.5.3i1' (**)	Task 5b	Slow dynamic aggression	3.4	10	145.04	40.0	580.2	[21% ; 64%]	1,794	rupture
	5.5.3i2 (***)	Task 5b	Slow dynamic aggression	3.8	10	145.04	40.0	580.2	[21% ; 64%]	2	rupture
Pipe 6 X52 grade	6.6.3	Task 5a	Slow dynamic aggression	3.9	30	435.11	30.0	435.1	[24% ; 42%]	30,000	no failure
							40.0	580.2	[47% ; 72%]	14,137	leak
	6.6.3a	Task 5a	Slow dynamic aggression	4.1	30	435.11	40.0	580.2	[44% ; 69%]	29,266 (****)	leak
Pipe 8 A42 SHLE grade	8.ext2.3cp	Task 5c	unknown	2.3	unknown	unknown	20.0	290.1	[33% ; 51%]	11,968	no failure (*)
							40.0	580.2	[33% ; 51%]	1,366	no failure (*)
							27.0 (*****)	391.6	[45% ; 68%]	1,015	no failure (*)

(*) Dent and Gouge defect 8.ext2.3cp did not fail

(**) Defect 5.5.3i1 of Dent and Gouge defect 5.5.3i1' failed and was not further tested

(***) Defect 5.5.3i2' of Dent and Gouge defect 5.5.3i2 failed and was not further tested

(****) Dent and Gouge defect 6.6.3a was depressurized to 0 bar during fatigue cycling due to an unexpected power supply failure

(*****) An issue with the computer induced an unplanned value of Pmin = 51 bar instead of 38 bar, that is the reason why Delta P = 27 bar instead of 40 bar for the last 1,015 cycles

Defects 5.4.3 and 5.5.3 served as baseline fatigue behavior for Dent and Gouge defects, as they were not interacting with any other threat. As seen in Table 20, defect 5.4.2, the sibling of 5.4.3, failed at the lowest pressure, so fatigue loading was limited to 20 bar, less severe than in previous cases, like previous studies^{1,2}, when it was 40 bar. There was almost one order of magnitude reduction in fatigue life survived by defect 5.4.3 compared to the geometrically more severe defect 5.5.3. Indeed defect 5.5.2 was similar to 5.5.3, but burst at a higher pressure than defect 5.4.2 which was similar to defect 5.4.3.

Cathodic overprotection proved to have a particularly strong effect as an accelerator of Dent and Gouge 5.5.3cp defect to premature failure after only 4 40-bar amplitude cycles. Significant hydrogen penetration into the damaged and highly stressed material at the sharp edge on one side of the gouge bottom, and

subsequent embrittlement may explain such a rapid failure at a significantly lower pressure (53 bar) than the similar Dent and Gouge Defect 5.5.2 without cathodic overprotection during its burst test (81.1 bar).

Indeed, at the other end of the Dent and Gouge behavior range when submitted to cathodic overprotection, defect 8.ext2.3cp removed from service, with a not very severe gouge, did not fail under multiple cycles at higher amplitude and increasingly severe cathodic overprotection conditions. This identifies cathodic overprotection as an area for further investigation, in an attempt to better identify the most important parameters that control such a wide ranging response. Indeed, it is important for an operator to understand which conditions are subject of concern vs. those that do not represent a significant threat, and this project contributed to highlighting the fact that there are conditions under which this coincident threat does not create a critical situation, and others where it may be so, when the aggression tool is very sharp.

Another particularly and unexpectedly rapid failure was experienced with closely interacting Dent and Gouge defects that were adjacent in terms of dents, not of gouges. In this case Dent and Gouge defect 5.5.3i2 failed after only 2 40-bar cycles, at less than 60 bar, while it was similar to defect 5.5.2, with a burst strength of 81.1 bar. This close interaction condition requires also more extended exploration, in order to better define boundaries for severe vs. innocuous interaction conditions.

The last case of coincident threats tested was that of axial loads acting simultaneously to fatigue cycling: with Dent and Gouge defect 6.6.3 survived 30,000 30-bar cycles followed by 14,137 40-bar cycles before a leak appeared. This was compared to defect 6.6.3a, also submitted to four-point bending during fatigue cycling, and failed after 29,266 40-bar cycles. Although not perfectly comparable, the fatigue behavior is not significantly affected by the axial load, similar to the burst strength behavior of these axially oriented Dent and Gouge defects. As mentioned above, circumferentially oriented Dent and Gouge defects, or such defects oriented at an angle to the pipe axis, may exhibit different burst and fatigue strengths, and need investigation.

5.4.2 Uncertainties related to some tests

Two issues arose during performance of Task 5:

1. Difficulty to assess when the gouge shape is too sharp for realistically created Dent and Gouge defects
2. Uncertainty concerning the gouge dimensions of Dent and Gouge defects in vintage pipes retrieved from service

In Task 5a and Task 5b, defects 5.5.X were created with a new tooth featuring a very sharp profile. Indeed, a specific excavator tooth was machined in order to comply with the investigation plan presented in Table 20 then aggression conditions were iterated during defects creation until Dent and Gouge dimensions complied with expectations, but the process led to one side of the tooth being very sharp. It can be seen in Table 20 that burst pressure was significantly reduced compared to the other defects of this test program but also compared to the burst pressures reported in the previous project ¹. This had the unexpected effect to drastically reduce the fatigue lives of defects 5.5.3cp and 5.5.3i2, as reported in Table 21. Indeed, defects 5.5.3cp and 5.5.i2 were under very severe conditions during the test. Dent and Gouge defect 5.5.3cp was loaded with hydrogen produced on purpose by the cathodic overprotection setup, and Dent and Gouge defect 5.5.2i2 was closely interacting with Dent and Gouge defect 5.5.3i2' (they were adjacent).

As planned, the team actively searched for Dent and Gouge defects retrieved from service. The first Dent and Gouge defect retrieved from service, 7.ext1.2 was submitted to a burst test, but the defect configuration induced a high uncertainty on gouge depth. The second Dent and Gouge defect 8.ext2.3cp retrieved from service had a smooth profile without any micro-cracks. More severe testing loading conditions were implemented without leading to failure: Cathodic overprotection of about -14 mA.cm⁻², pressure range comprised between 20 bar and 40 bar, P_{max} was chosen for a load factor of 72 % of yield stress. Dent and

Gouge defect 8.ext2.3cp resistance is an interesting result by itself, which has to be confirmed by further investigation: a not very severe Dent and Gouge defect, with no micro-crack, under very severe fatigue cycling and cathodic overprotection conditions resisted far beyond predictions of a current Dent and Gouge fatigue life prediction model.

5.4.3 Observations

The following observations were made during this study:

- Close interaction between severe Dent and Gouge defects may affect fatigue life: Very close severe (sharp gouge profile) Dent and Gouge defects interact and reduce significantly fatigue life. In this particular study, the severity of the gouge transverse profile proved to be the factor with the highest influence, leading to premature failure in several fatigue tests.
- Effect of cathodic overprotection on fatigue life of Dent and Gouge defects: This test matrix provides first elements in terms of interacting threats, i.e. Dent and Gouge defects submitted to fatigue cycling under cathodic overprotection, which the team recommends for further investigation.
- Additional axial load effect on fatigue life: A computational 3D FE model was developed by the team (not included in the initial scope of work) in order to choose the best conditions to perform the burst test and fatigue test on Dent and Gouge defects 6.6.2a and 6.6.3a under an axial load imposed with a full scale four-points-bending test rig on fully instrumented 7 m long pipe spools. The computational model showed that the worst position for the defect was at six o'clock, i.e. with the Dent and Gouge defect on the extrados of the bent pipe. Table 20 shows that the burst pressure for Dent and Gouge defect 6.6.2a under axial load is not affected by the additional load. Table 21 shows that fatigue life for Dent and Gouge defect 6.6.3a under axial load is hardly reduced by this additional axial loading.
- Burst and fatigue tests on pipes with Dent and Gouge defect retrieved from service: Behavior of two pipes with Dent and Gouge defects retrieved from service showed good agreement with the behavior of the pipes where Dent and Gouge defects were realistically created.

5.4.4 Conclusions and Gap analysis

The analysis of test results showed the added value of the current work on Dent and Gouge defects, both realistically created, and retrieved from service. The experimental approach covered a wide range of threat interaction cases, each time trying to compare the baseline burst and fatigue resistance with corresponding burst and fatigue resistance of the combined threats.

The findings of this work show that based on defect geometry, the additional interacting threats can play a significant role in bringing already severe defects closer to failure, like cathodic overprotection or close geometric interaction. For less severe defects the additional interacting threats did not significantly influence their burst or fatigue resistance. Additional investigation on better defining the Dent and Gouge severity limits for those defects that become sensitive to other interacting threats is recommended.

Based on current experimental findings, defect severity is a key factor when it comes to adding cathodic overprotection or close defect interaction. These aspects require clearly more work to define the key parameters in terms of defect severity that would make such defects more sensitive to these threat interactions. To perform this work, a combined experimental and FE modeling approach seems to be the most appropriate.

Concerning superimposed axial loads, while axially oriented defects haven't seen their burst and fatigue strength significantly affected by axial loads generated with four-point bending, circumferentially oriented

Dent and Gouge defects or such defects oriented at an angle with the pipe axis may be more sensitive to this interacting threat, and therefore require additional investigation.

In the area of axial loads, soil-pipe interaction also plays a role, and the experimental part of this investigation could be performed in a soil box, thus accounting for soil restraint effects when applying the four-point bending conditions.

In addition, other diameters and defect shapes are also of interest to enhance the representativeness of Dent and Gouge defects with respect to operational conditions.

Finally, Dent and Gouge defects removed from service would need to undergo a similar procedure for comparison purposes. While finding systematically similar defects to be able to compare burst and fatigue strength for similar defects, as those created on purpose cannot be guaranteed, they should be looked for.

6 Stress Corrosion Cracking (SCC) Colonies and Standard Development Organization (SDO) Modeling Coordination (Task 6)

6.1 Background

Numerous studies have been performed on SCC with fruitful results, but important knowledge gaps remain, including information on crack colonies coalescence and improved modeling. In this task, the team experimentally investigates on pipes containing SCC colonies when the coalescence of adjacent SCC cracks occurs during crack growth. The goal is to determine when cracks coalesce and the conditions that differentiate failure by leak or rupture. A specific test bench has been developed to apply a mechanical loading and an electrochemical environment on SCC colonies. Specific electrochemical cells have been designed and manufactured in order to:

- Prevent any leak from the liquid and/or oxygen pollution in the liquid all along the SCC test duration;
- Be able to be easily removed from the pipes sections to allow the sizing of the features periodically or at specific times during the SCC tests.

A picture of the designed cell is given in Figure 40.

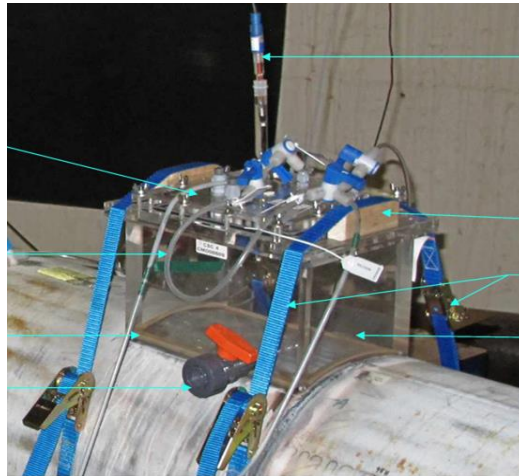


Figure 40: Air-tight electrochemical cell for full scale near neutral SCC crack propagation tests

6.2 Material Selection, Acquisition and Characterization (Task 2)

Two different pipe materials were utilized and characterized for the experimental test program relative to Task 6, see Table 22.

Table 22 : Overview of the two materials used in Task 6

Pipe#	External Pipe Diameter mm (in)	Pipe Thickness mm (in)	Grade (specified)	Year
HP20	457.2 (18)	6 (0.236)	X63	1974
R156	457.2 (18)	6 (0.236)	X63	unknown

Material property characterization was carried out for each of the two pipe materials. The characterization effort included:

- Tensile tests in both the longitudinal and transverse directions (Table 23, Table 24)
- Charpy impact testing (Table 25,
- Table 26)
- Chemical analysis (Table 27)

Table 23: Task 6 pipe materials transverse tensile properties

Pipe# transverse direction	Measured Values					
	0.2% Yield Strength		Ultimate Tensile Strength		Elongation	Area Reduction
	(MPa)	(ksi)	(MPa)	(ksi)	(%)	(%)
HP20	476	69.1	593	86	23.5	44.1
R156	433.7	62.9	581.7	84.4	26.5	41.7

Table 24: Task 6 pipe materials longitudinal tensile properties

Pipe# longitudinal direction	Measured Values					
	0.2% Yield Strength		Ultimate Tensile Strength		Elongation	Area Reduction
	(MPa)	(ksi)	(MPa)	(ksi)	(%)	(%)
HP20	436	63.3	571	82.9	26.2	61.2
R156	435.7	63.2	587.7	85.2	27.2	59.7

Table 25: Task 6 pipe materials transverse Charpy impact properties

Pipe# TL direction	Test Temperature		Impact Energy	
	(°C)	(°F)	(J) (ft-lb)	(J.cm ⁻²)
HP20	22	68	14.06	35
R156	27	80.6	10	50

Table 26: Task 6 pipe materials longitudinal Charpy impact properties

Pipe# LT direction	Test Temperature		Impact Energy	
	(°C)	(°F)	(J) (ft-lb)	(J.cm ⁻²)
HP20	22	68	38.88	97
R156	27	80.6	20	100

Table 27: Task 6 pipe materials chemical composition

Pipe#	C %	Mn %	Si %	P %	S %	NI %	Cr %	Cu %	Mo %	V %	Al %	Nb %	Ti %	C %
HP20	0.18	1.37	0.27	0.02	0.017	0.04	0.02	0.05	0.01	<0.01	0.03	0.04	<0.01	0.18
R156	0.15	1.3	0.27	0.021	0.015	0.04	0.02	0.07	<0.01	<0.01	0.05	0.02	<0.01	0.15

6.3 Baseline Existing Features (Task 3)

A specific SCC crack sizing equipment was delivered to ENGIE. It is a Grid Station D8000 β equipment by Jentek with two sensors: a FA28 MWM sensor for crack mapping and a FA214 Meandering Winding Magnetometer (MWM) sensor for crack depth estimation. MPI was performed on the SCC colonies on the SCC-1 vessel and will be successively compared to MWM crack mapping. SCC-1 vessel is composed by HP20 pipe. Five SCC colonies were studied.

Results are presented for the C8 colony defect and are illustrated by the comparison of the MPI results in Figure 41 and the C-scan with MWM in terms of magnetic relative permeability (Figure 42) and in terms

of estimated crack depth (Figure 43). We observe a good match in terms of mapping between MPI and magnetic relative permeability C-scan data.

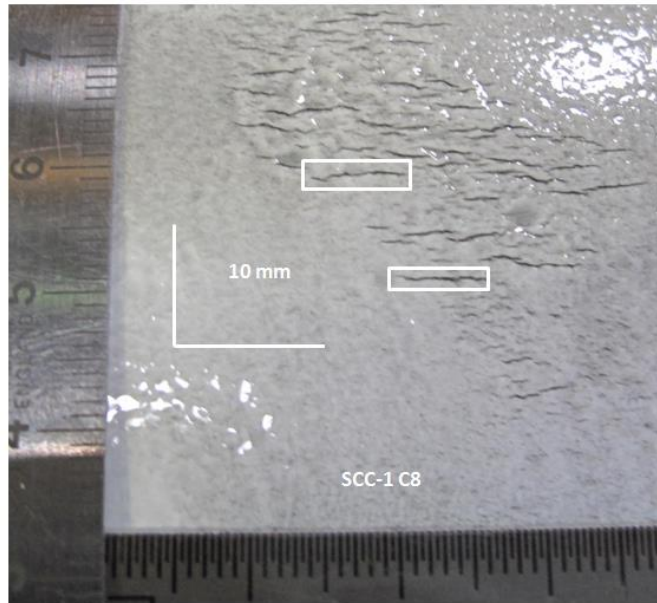


Figure 41: View of the defect C8 after Magnetic Particle Inspection in which the location of the deepest cracks according to sizing with MWM FA214 Jentek Sensor is highlighted.

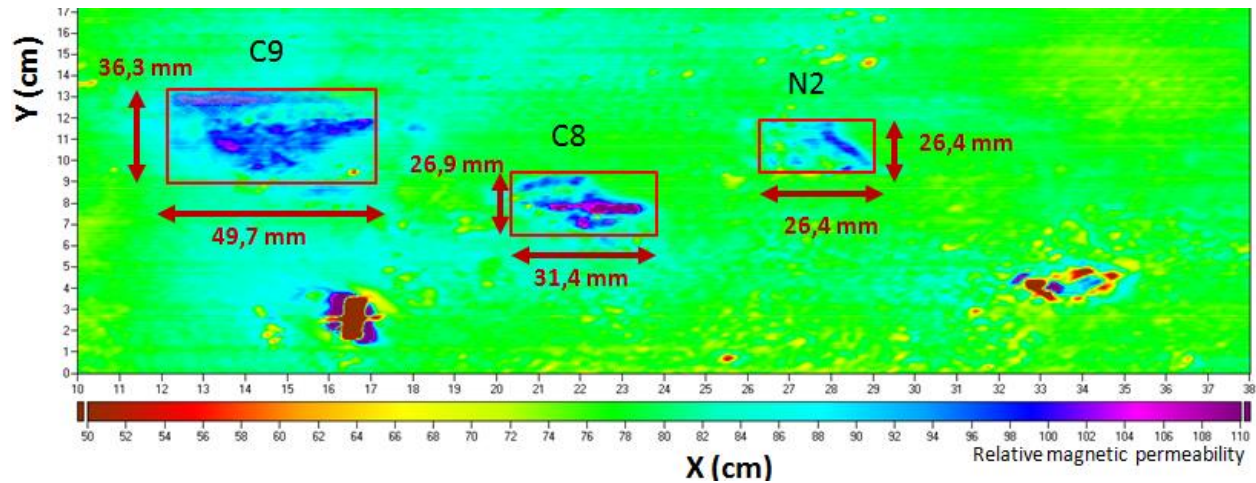


Figure 42: C-SCAN of magnetic relative permeability for colonies C9-C8-N2 colonies, as measured by MWM FA214 Jentek Sensor.

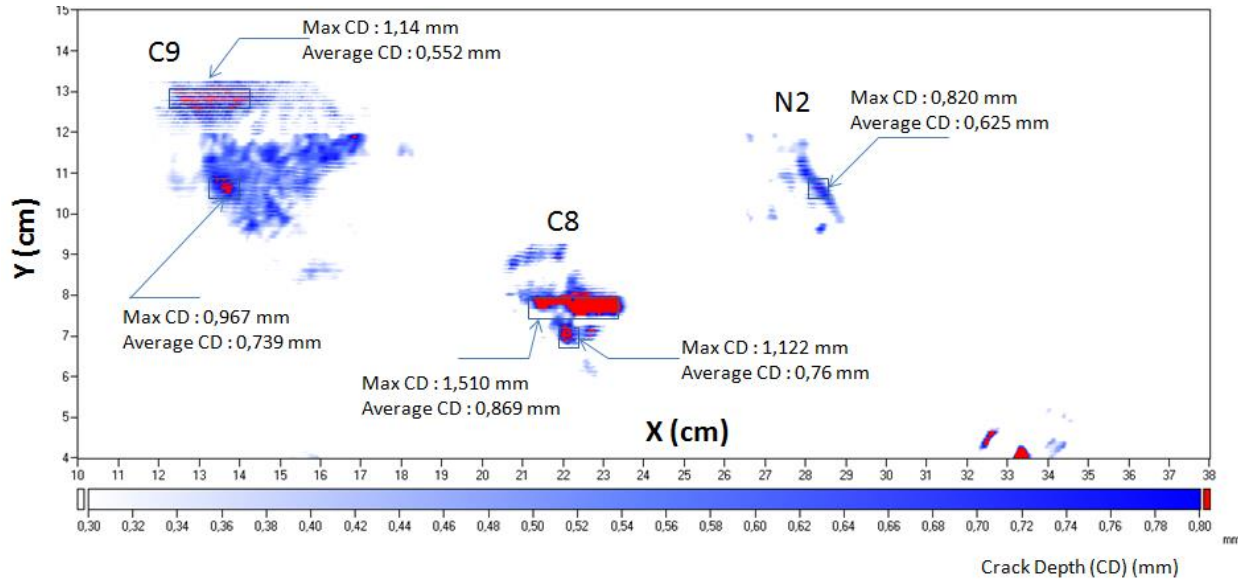


Figure 43: C-SCAN of crack depths in C9-C8-N2 colonies as measured with MWM FA214 Jentek Sensor.

SCC colonies on SCC-1 pipe were characterized in both length and in depth. MPI was also performed on the different SCC colonies of the SCC-1 vessel. Deepest cracks are located in the different MPI views for the five colonies to measure their lengths. Main characteristics are provided in Table 28 in terms of colony length, maximum crack depth and crack length of the deepest single crack according to sizing.

Table 28: Main characteristics of SCC colonies on pipe SCC-1 according to sizing by MWM FA214 Jentek Sensor.

Colony ID	Colony Max Length (mm)	Max. crack depth (mm)	Max length of the deepest single crack in colony (mm)
B30	217.2	1.1	40
B31	60.6	1.2	7
C9	49.7	1.	31
C8	31.4	1.5	6
N2	26.4	0.8	10

Results show that estimated maximal depths are low. The difficulty is to find a deep enough crack in a SCC colony which is susceptible to coalesce with the neighboring cracks. If the crack depth is low, it would be difficult to propagate it and to achieve coalescence between several cracks.

Another colony has been studied on pipe R156. The maximal measured depth is 1.7 mm and the length of the associated crack is 6 mm. The crack colony is shown in Figure 44.

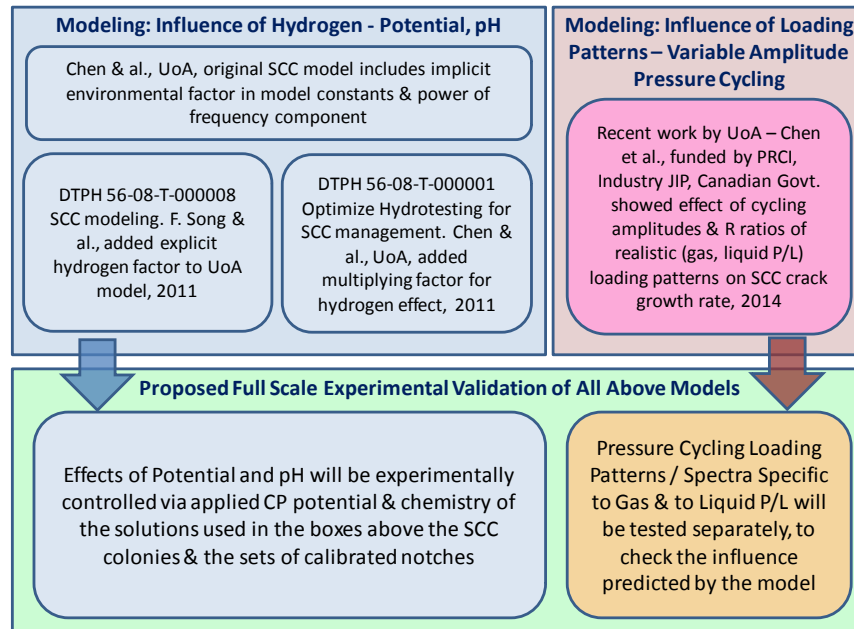


Figure 44: Crack colony R156-im1

6.4 Results

6.4.1 Experimental approach

The DOT PHMSA has been supporting work on optimizing hydrotesting to manage SCC by University of Alberta (UoA)⁸, as well as, SCC modeling⁹.



An implicit environmental effect is already embedded in the UoA model through the model constants and the power of the frequency component (number of cycles / year) of the model equation. A hydrogen effect has also been reported by UoA and added to its model as a multiplying factor. The work and model reported by Frank Song, et al., applies an explicit hydrogen factor to the UoA model to further account for the effects of potential and pH.

Significant additional model development has been performed by UoA since 2011, and is ongoing, supported by PRCI, other joint industry programs, and Canadian government research. Recent developments have included the effect of load/pressure interactions (obtained from operating SCADA data) on the crack growth rate, where some loading spectra may result in lower or greater crack growth rates.

⁸ DTPH-56-08-T-000008 – June 2011

⁹ DTPH-56-08-T-000001 – June 2011

This development also enables differentiation of different gas and oil lines or segments through characterization of their specific SCADA operating data, potentially providing a very useful screening procedure. These recent developments and enhancements make the UoA model the most advanced model of today, considering both environmental conditions and loading conditions from both a mechanistic and empirical perspective. Recent advances concerning the role of different cycling loading spectra for oil and gas pipelines were presented at the 2014 International Pipeline Conference (IPC)¹⁰.

The team has proposed to expand the original work scope beyond the investigation of crack coalescence into the parallel full scale investigation of the combined effect of load interactions and pH / potential conditions, both for two specific conditions:

- One typical of oil transmission pipeline load spectra,
- The other typical of gas transmission load spectra

For each vessel, specific oil and gas transmission pipelines loading patterns have been determined by applying the UoA interpretation of cyclic loading with different amplitude cycles to SCADA data from one oil pipeline and from one gas pipeline. The large amplitude cycles has been singled out, and for each case, a sequence of large amplitude cycles followed by the typical amplitude pattern, already determined, has been applied to the corresponding vessel. The frequency has also been adjusted to be both realistic and close to the range where the crack growth rate depends only weakly on loading frequency, while being compatible with realistic time-scales for performing the full scale tests. The following R ratio ($R=P_{\min}/P_{\max}$) have been chosen for the typical amplitude pattern:

- $R=0.5$ for oil conditions, and
- $R=0.85$ for gas conditions.

6.4.2 Oil Condition Test

Three vessels have been used for the oil condition test and Electrical Discharge Machining (EDM) notches have been machined:

- SCC1a is a part of pipe R156 which contain the crack colony named R156-im1. The zone near R156-im1 crack colony has been examined by MPI in order to control that there is no other crack at locations where EDM notches have been machined.
- SCC1b is a part of pipe HP20. The zone where EDM notches have been machined was examined by magnetic particle inspection in order to control that there is no crack.
- SCC1c is a part of pipe HP20. The zone where EDM notches have been machined was examined by magnetic particle inspection in order to control that there is no crack.

UoA proposed to model near neutral pH crack growth rate by a relationship using a combined factor ($\Delta K^2 K_{\max} / f^{0.1}$) between the stress intensity factor variation (ΔK) between P_{\max} and P_{\min} , the maximal stress intensity factor (K_{\max}) and loading frequency (f). Combined factor values were calculated for each EDM notch and were ordered from the lowest combined factor value to the highest combined factor value. They have been divided in three groups. Notches with low combined factor values will be machined near the real crack colony on vessel SCC-1a. Notches with intermediate combined factor values will be machined on vessel SCC-1b, and notches with high combined factor values will be machines on vessel SCC-1c. If crack dimensions become excessively high for longer notches, fatigue tests can be continued on the two other vessels.

Moreover, 8 EDM notches have been machined outside of the electrochemical cell zone in order to compare their behavior with or without electrochemical environment.

¹⁰ Mengshan Y., "Depressurization-Induced Crack Growth Enhancement for Pipeline Steels Exposed to Near-Neutral pH Environments", International Pipeline Conference, 2014

Expected crack growth during fatigue in air have been estimated by API579 level 2¹¹ calculation using a Paris law in order to ensure crack initiation before Near Neutral pH SCC (NNPHSCC) testing.

EDM notches map for the oil transmission pipeline test are presented in Figure 45, Figure 46 and Figure 47:

- On pipe SCC-1a, expected combined factor values range from 2000 to 4700 after fatigue in air.
- On pipe SCC-1b, expected combined factor values range from 4800 to 6700 after fatigue in air.
- On Pipe SCC-1c, expected combined factor values range from 6800 to 10700 after fatigue in air.

The nomenclature of each defect is the following:

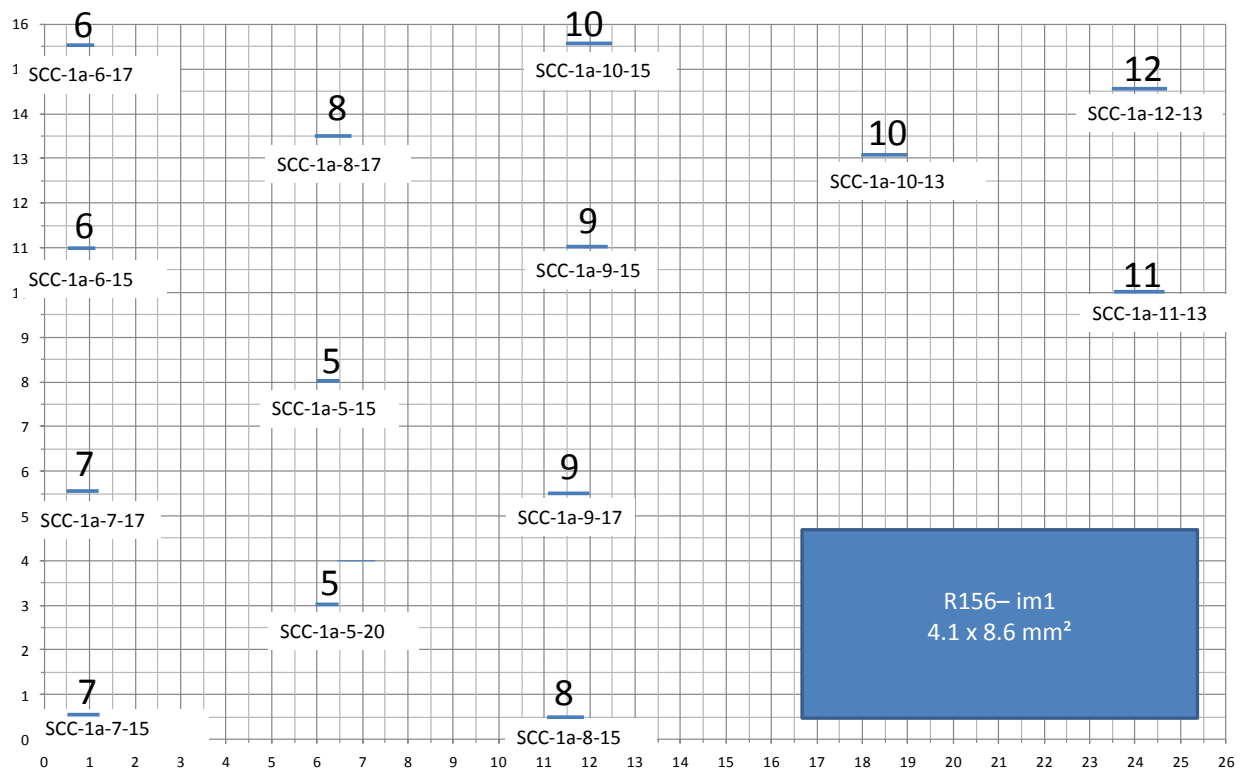
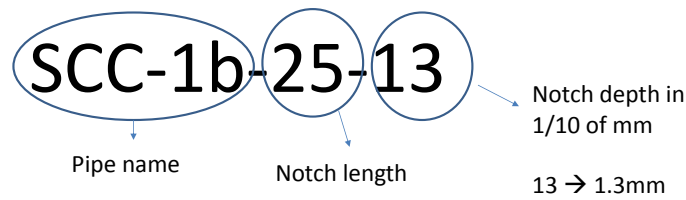


Figure 45: EDM notches + real SCC colony map for pipe SCC1a

¹¹ Fitness-for-Service, API recommended practice 579, first edition, 2007

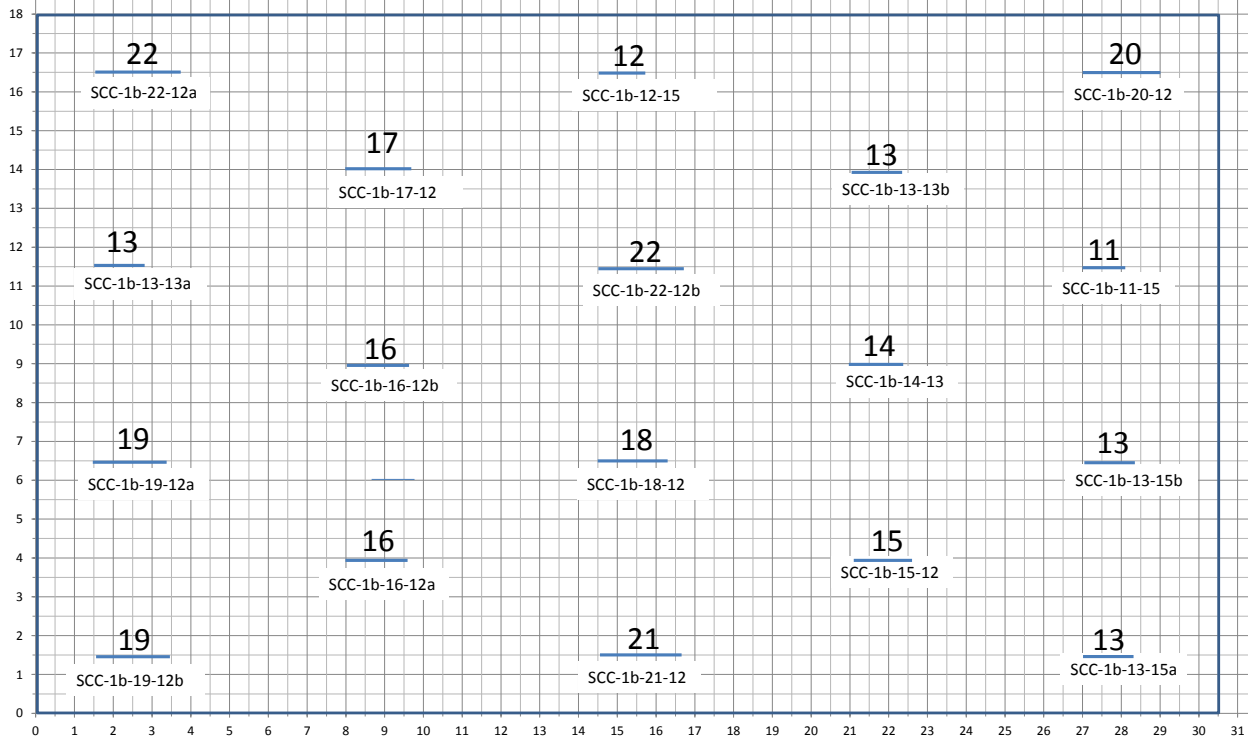


Figure 46: EDM notches map for pipe SCC1b

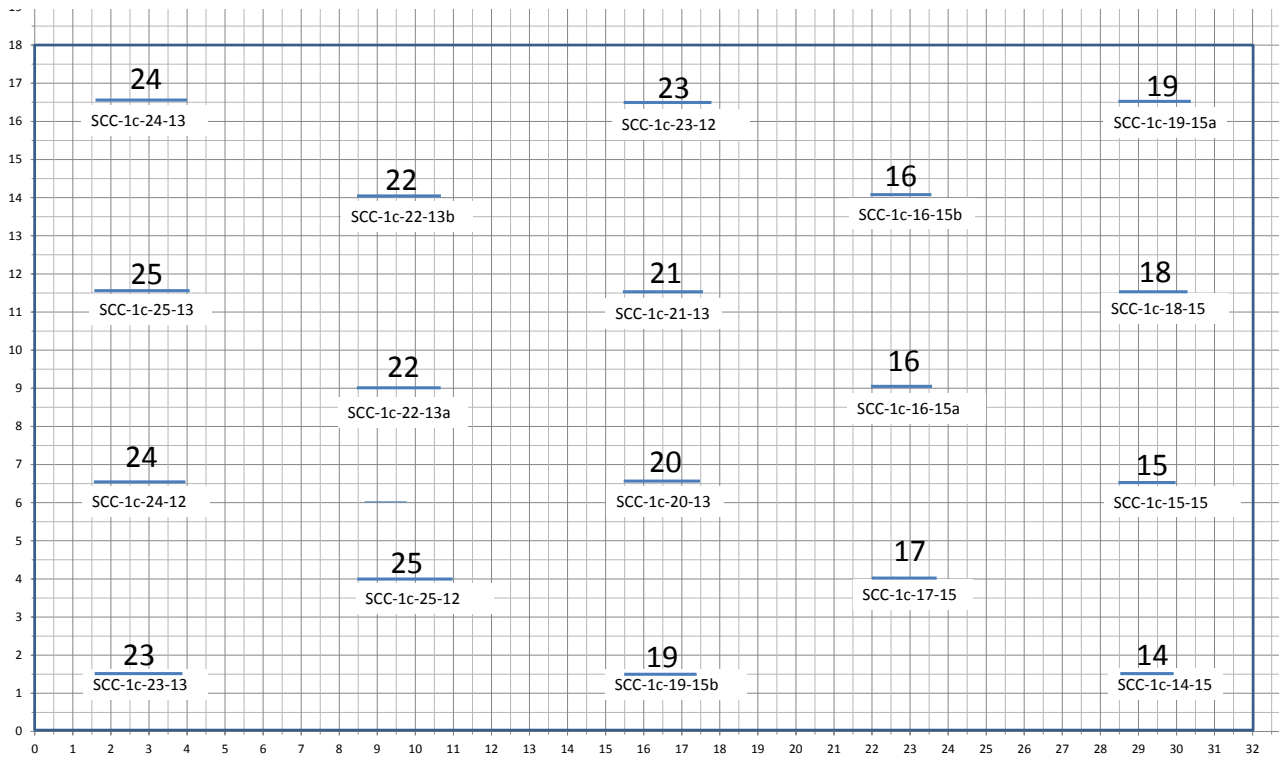


Figure 47: EDM notches map for pipe SCC1c

As described previously, boxes with environmental solution, controlled pH and potential have been mounted above the SCC colony as well as above controlled EDM notches introduced on the pipe. The

testing will be performed in a near-neutral pH-cracking environment referred to as C2 electrolyte, which is based on cracking electrolytes used by the University of Alberta SCC tests. The composition of the C2 electrolyte is given in Table 29.

Table 29: Composition of simulation NNPHSCC soil solutions (C2). Concentrations are in g/liter.

Electrolyte	KCl	NaHCO ₃	CaCl ₂ .2H ₂ O	MgSO ₄ .7H ₂ O	CaCO ₃	pH
C2	0.0035	0.0195	0.0255	0.0274	0.0606	6.29

The C2 electrolyte has been sparged with 7% CO₂ balance N₂ before starting the test and continuously sparged during the tests. The targeted oxygen average content in the liquid tight cell is 500 ppb (w).

A protocol has been proposed for the oil conditions tests. The aim is to optimize test duration in order to perform the maximum number of cycles. The critical aspect of these loading sequences is to demonstrate the effect of underloading (accelerating effect) and overloading (decelerating effect) on NNPHSCC crack growth rates (CGR). The combinations of these different cycling profiles are quantified as a combined mechanical factor which is used subsequently. Each vessel have been fatigue tested in air in order to initiate cracks on the EDM notches before the actual testing sequences described below.

Table 30: Oil Condition Test Step 0: Fatigue in air

Loading shape	Sinus
Maximal pressure (bars)	67.7
Minimal pressure (bars)	6.7
R –Ratio (P_{min}/ P_{max})	0.1
Cycle duration (s)	
Minimal number of cycles	5000 depending on measured CGR
Environment over the features	Air

Table 31: Oil Condition Test Step 1: Effect of underloading on the SCC growth rate

Loading shape	Asymmetric triangular
Maximal pressure (bars)	67.7
Minimal pressure (bars)	33.9 or 6.7 every 615 cycles block
R –Ratio (P_{min}/ P_{max})	0.5 or 0.1 every 615 cycles block
Cycle frequency (Hz)	1.25x10 ⁻³
Loading rate (bars /sec)	Around 0.056
Unloading rate (bars /sec)	Around 0.169
Minimal number of cycles	6150 depending on measured CGR
Environment over the features	C2 solution with sparging N ₂ + 5% CO ₂

Pressure vessel will be decreased down to 6.7 bars after each 615 cycles block. Each will be sized in length and in depth by MWM FA214 Jentek sensor. The real SCC colonies will be sized in depth and a picture will be taken after a magnetic particle examination. Those pictures will be used to identify and study coalescence indications due to crack interactions.

Table 32: Oil Condition Test Step 2: SCC growth rates along constant loading conditions

Loading shape	Asymmetric triangular
Maximal pressure (bars)	67.7
Minimal pressure (bars)	33.9
R –Ratio (P_{min} / P_{max})	0.5
Cycle frequency (Hz)	1.25×10^{-3} Hz
Loading rate (bars /sec)	Around 0.056
Unloading rate (bars /sec)	Around 0.169
Minimal number of cycles	2120 (depending on measured CGR)
Environment over the features	C2 solution with sparging 95% N ₂ + 5% CO ₂

The real SCC colonies will be sized in depth and a picture will be taken after a magnetic particle examination. Those pictures are intended to identify and study coalescence indications due to crack interactions.

Table 33: Oil Condition Test Step 3: Effect of overloading on the SCC growth rate

Loading shape	Asymmetric triangular
Maximal pressure (bars)	67.7 for the first 2400 cycles then 77.7 bars every 250 cycles blocks
Minimal pressure (bars)	33.85 or 6.77 every 500 cycles blocks during the first 2400 cycles
R –Ratio (P_{min} / P_{max})	0.5
Cycle frequency (Hz)	$1,25 \times 10^{-3}$ Hz
Loading rate (bars /sec)	Around 0.056
Unloading rate (bars /sec)	Around 0.169
Minimal number of cycles	4400 depending on measured CGR
Environment over the features	C2 solution with sparging N ₂ + 5% CO ₂

The vessels will be depressurized down to 6.7 bars after each 600 cycles block during the first 2400 cycles. Each feature will be sized in length and in depth after each 600 cycles block and at the end of step 3. The real SCC colonies will be sized in depth and a picture will be taken after a MPI. Those pictures will be used to identify and study coalescence indications due to crack interactions.

The oil pipe loading profile is presented in Figure 48.

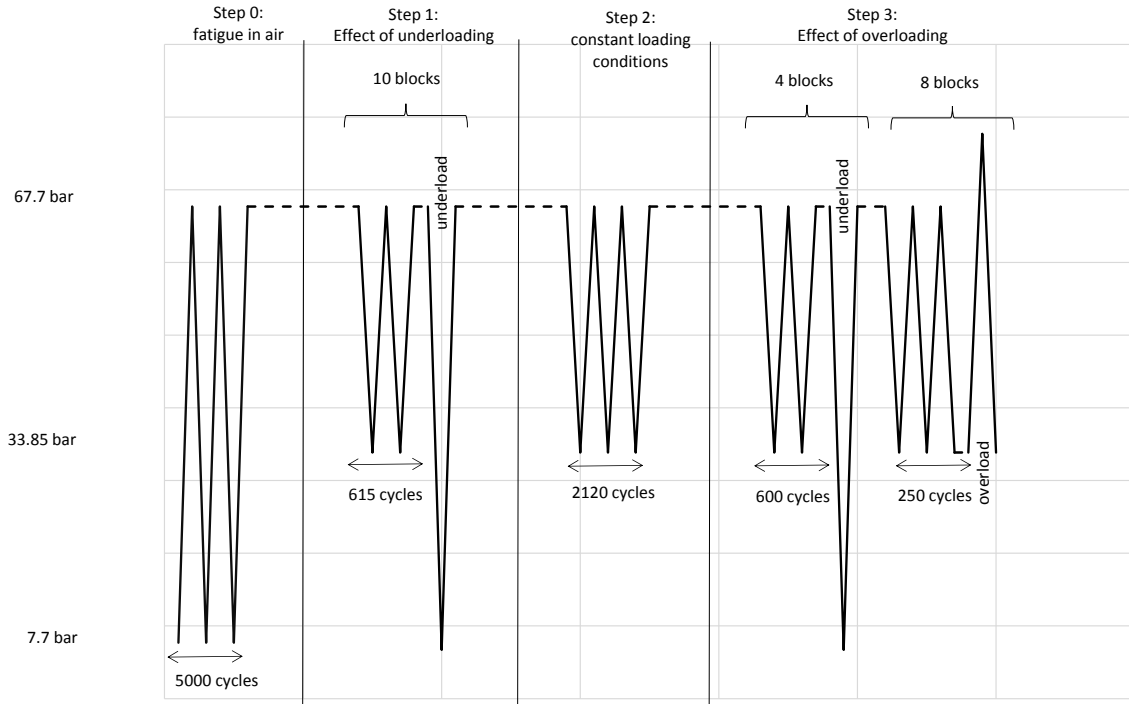


Figure 48: Oil pipe loading profile

After fatigue test in air (phase 0 of oil condition protocol), pipes SCC1a, SCC1b and SCC1c have been scanned by JENTEK sensor. Results shows that defect depth seemed to have increased during fatigue test (depth propagation from 0.1mm to 0.7mm, Figure 49).

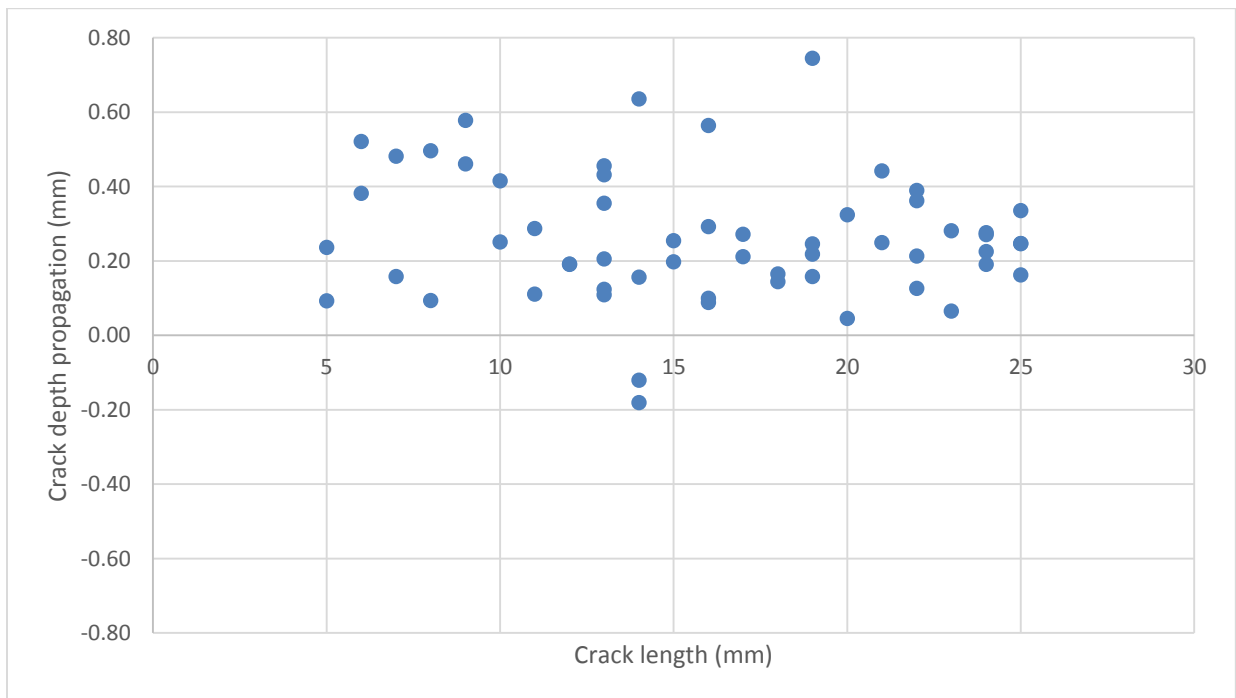


Figure 49: Crack depth propagation during phase 0 (fatigue in air)

Figure 50 shows the 3 vessels with their electrochemical cells.



Figure 50: SCC1a, SCC1b and SCC1c pipes with electrochemical cells

After 9 blocks of 615 cycles, EDM notch sizing by JENTEK sensor showed that there is no crack propagation. Moreover, no crack coalescence on the real SCC colony on pipe SCC1a have been detected. So, the team, after discussion with PHMSA and the technical advisory board agreed to increase the number of underloads in order to activate crack propagation. So, the test has changed from one underload every 615 to one underload every 200 cycles (Figure 51).

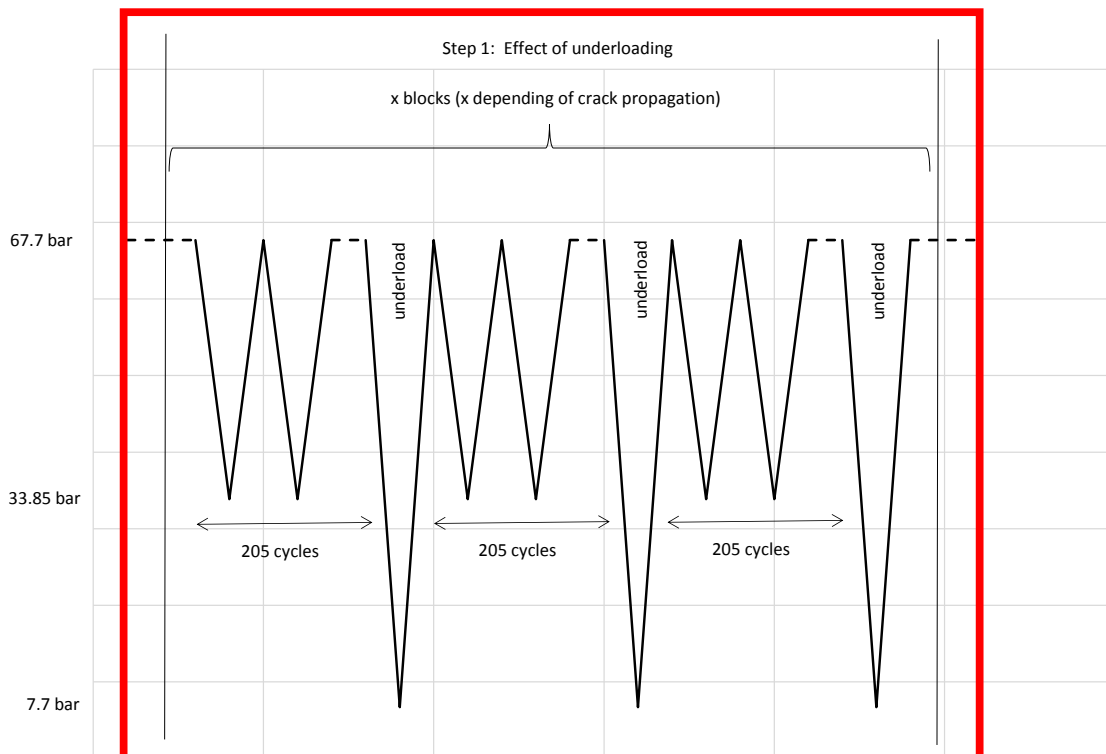


Figure 51: Modified oil test conditions for step 1 - 1 underload each 205 cycles

With these conditions 22 blocks of 205 fatigue cycles were performed. Overall 9761 cycles with $R=0.5$ and 31 underloads were applied to the three vessels. Results of MPI show that there is no crack coalescence on the real SCC colony on pipe SCC1a as shown in Figure 52 (at the beginning of the test) and in Figure 53 (after 9792 cycles).



Figure 52 : Magnetic particle inspection of real SCC colony before step 1 of oil condition test



Figure 53 : Magnetic particle control of real SCC colony after 9792 cycles of step 1 of oil condition test

Crack depth measurements showed no significant enhancement of crack propagation. Moreover, it seems that there are some unexpected results concerning crack depth measurements which seem less deep than in previous measurements. Crack depth measurements since the beginning of the test are presented in Figure 54. One block corresponds to a given crack. Measurements are sorted chronologically. The first measurement is the value before test, the second measurement corresponds to the value after 5000 cycles of fatigue in air, the other measurements correspond to subsequent values during phase 1 of oil condition test ($P_{min}/P_{max} - R=0.5$ - with underload). A way to explain these variations could be the dislocations that appear during the course of fatigue cycling, which have an effect on eddy currents, and can therefore impact JENTEK sensor measurements. As will be explained below, crack propagation was limited to the order of magnitude of JENTEK sensors uncertainties in this test sequence, so it is not surprising that a significant advance could not be measured.



Figure 54: Crack depth measurements during oil conditions test

In order to confirm crack propagation at the tip of EDM notches, 7 notches were chosen on pipe SCC1b to perform a destructive observation of the crack propagation (Figure 55).



Figure 55: 7 EDM notches chosen for destructive observation.

An example of microscopic observation is presented in Figure 56. It shows a crack which propagates at the tip of the EDM notch (SCC1b-12-15). Results for the seven analyzed notches are presented in Table 34. The initial measured depth corresponds to the EDM notch depth before test. The crack propagation corresponds to the depth of the crack at the tip of the EDM notch. The crack growth rate is calculated by UoA considering the total number of fatigue cycles with electrochemical cell (9792 cycles).

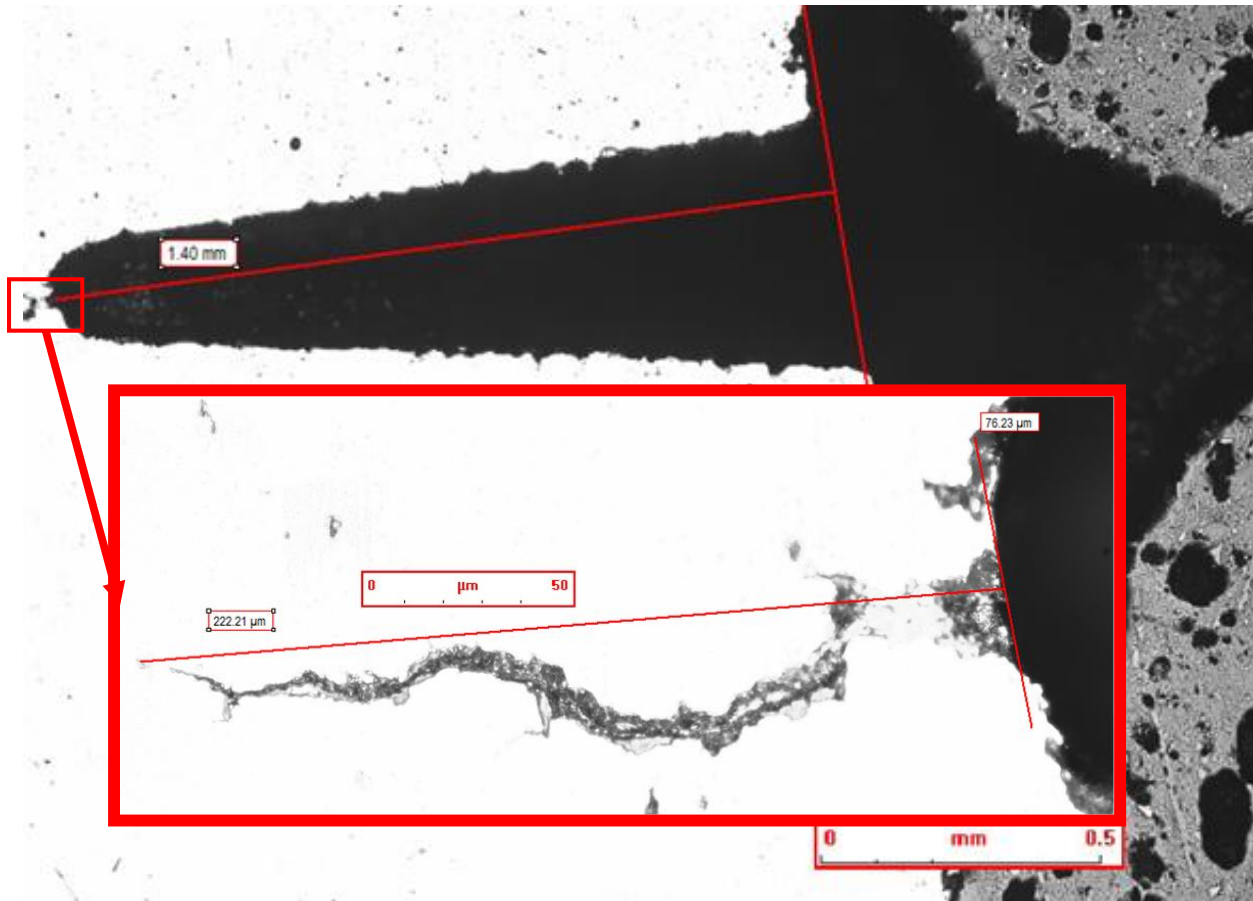


Figure 56: Microscopic observation of SCC1b-12-15 defect after oil conditions test

Table 34: Crack depths and crack growth rates

Notch	Initial measured depth (mm)	Crack propagation (mm)	Crack growth rate (mm/cycle)
SCC1b-12-15	1.4	0.222	2.26716E-05
SCC1b-22-12b	1.18	0.19	1.94036E-05
SCC1b-18-12	1.12	0.064	6.53595E-06
SCC1b-14-13	1.27	0.116	1.18464E-05
SCC1b-15-12	1.16	0.113	1.154E-05
SCC1b-13-13b	1.24	0.191	1.95057E-05
SCC1b-21-12	1.15	0.082	8.37418E-06

Results have been compared to results summarized by UoA and presented at the 2008 International Pipeline Conference¹² (Paper # IPC2008-64475) as shown in Figure 57. Final crack depths have been taken into account to calculate the combined factor. Results show good agreement with crack growth rates reported by UoA.

¹² Chen W., "Crack Growth Model of Pipeline Steels in Near-Neutral pH Soil Environments", International Pipeline Conference, 2008

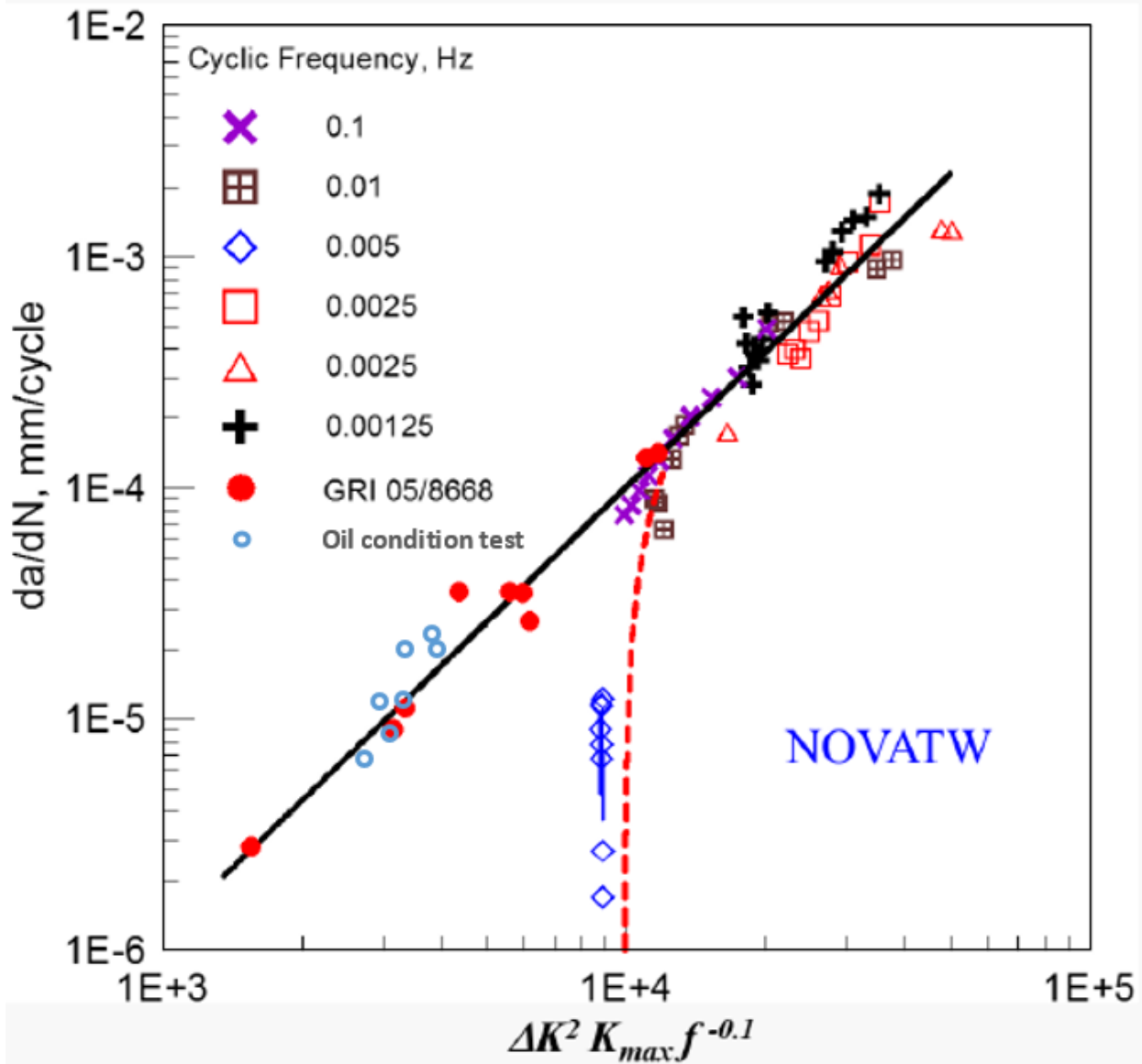


Figure 57: Comparison of oil condition test results and University of Alberta summary of results (paper # IPC2008-64475)

6.4.3 Gas Transmission Pipeline Condition Test

Pipes tested during oil pipeline condition test were also used for the gas pipeline condition test. The only difference consists in pipe SCC1b where 7 defects were destructively observed after the oil pipeline condition test. The seven defects were located on a same ring to minimize impact. The two parts with the other defects were welded in order to create a new vessel. The new defect mapping for pipe SCC1b is presented on Figure 58. The 3 defects named SCC1b-14-13bis, SCC1b-13-15bis and SCC1b-13-13bis, which were outside the electrochemical cell during the oil pipeline condition test, will be located now in the electrochemical cell during the gas pipeline condition test.

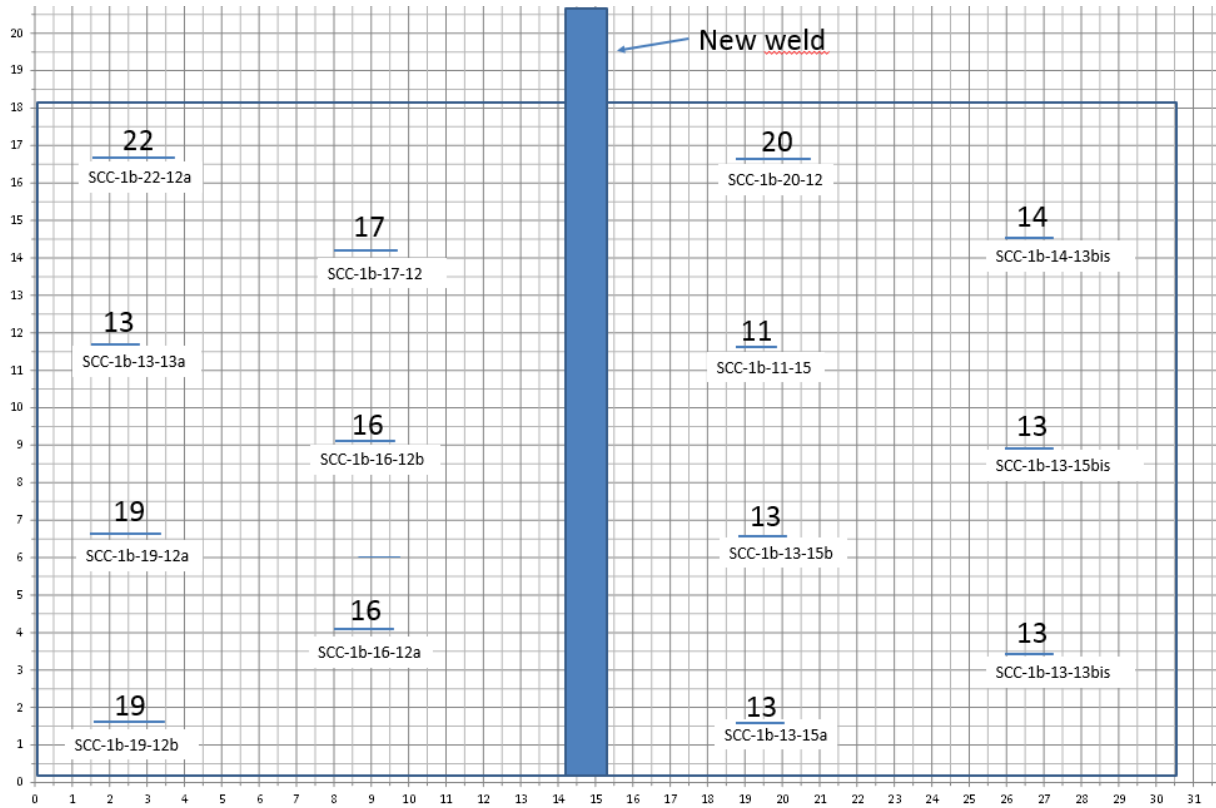


Figure 58: EDM notches map for pipe SCC1b during gas pipeline test condition

In the same way as during the oil pipeline condition test, boxes with environmental solution, controlled pH and potential control were mounted above the SCC colony as well as above controlled EDM notches introduced on the pipe. Testing was performed in a near-neutral pH- environment favoring cracking referred to as C2 electrolyte, which is based on electrolytes favoring cracking used by the University of Alberta SCC tests. The composition of the C2 electrolyte is given in Table 35.

Table 35: Composition of simulation NNPHSCC soil solutions (C2) used for gas condition test.
Concentrations are in g/liter.

Electrolyte	KCl	NaHCO ₃	CaCl ₂	MgSO ₄ .7H ₂ O	CaCO ₃	Expected pH
C2	0.0035	0.0195	0.0255	0.0274	0.0606	6.29

The C2 electrolyte was sparged with 7% CO₂ and balance of N₂ before starting the test and continuously sparged during the tests. pH has been checked in the three cells during the test. A value of 6.2 was measured. The targeted oxygen average content in the liquid tight cell is below 300 ppb (w). The O₂ concentration measured during the test is presented in Figure 59.

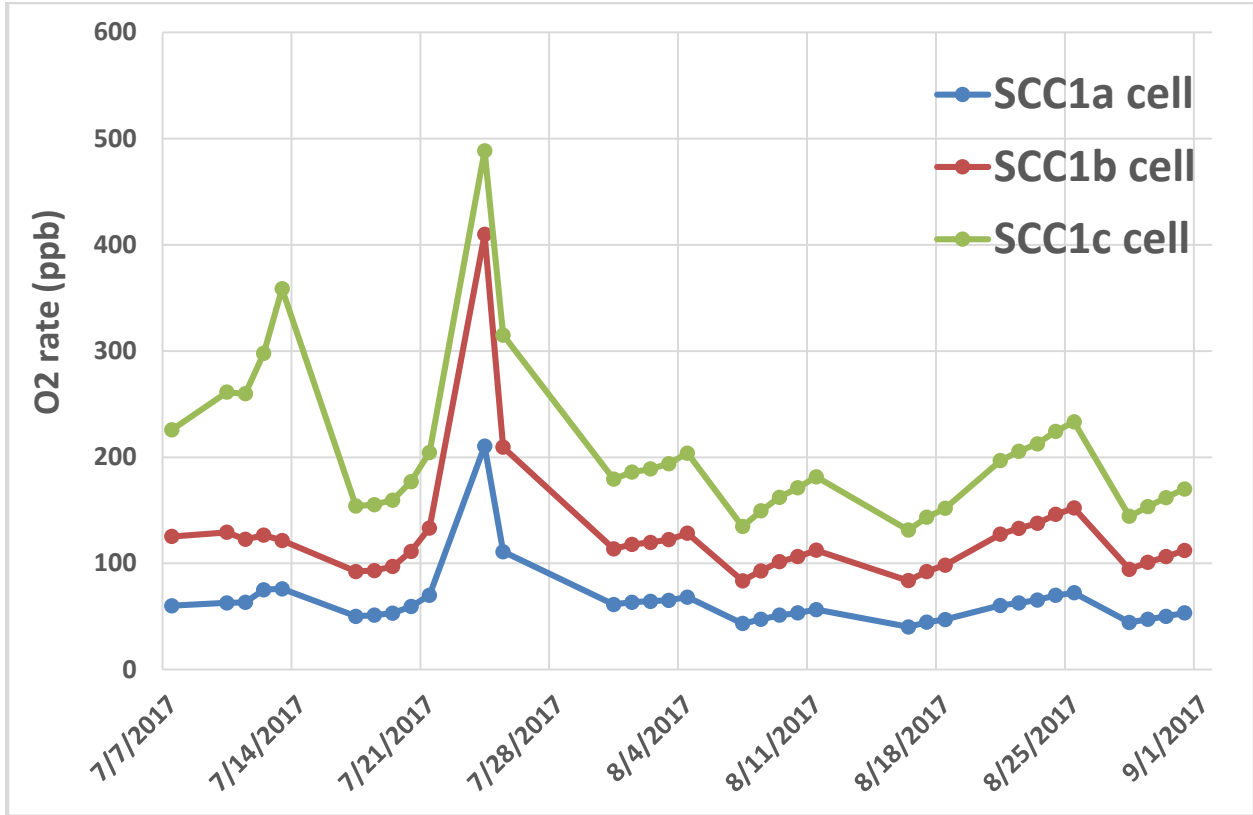


Figure 59: O₂ concentration during the gas pipeline condition test

Regarding oil pipeline condition test results, with UoA support, a new test protocol for gas pipelines loading conditions was established. The aim is to optimize test duration in order to perform the maximum number of cycles and to propagate the crack at the tip of the machined notches. It consists in several blocks with 100 minor load cycles (R=0.5) and 1 underload cycle (R=0.5). Moreover, the maximum pressure was increased from 67.7 bar to 86.8 bar. Loading conditions are presented in Figure 60 and in Table 36.

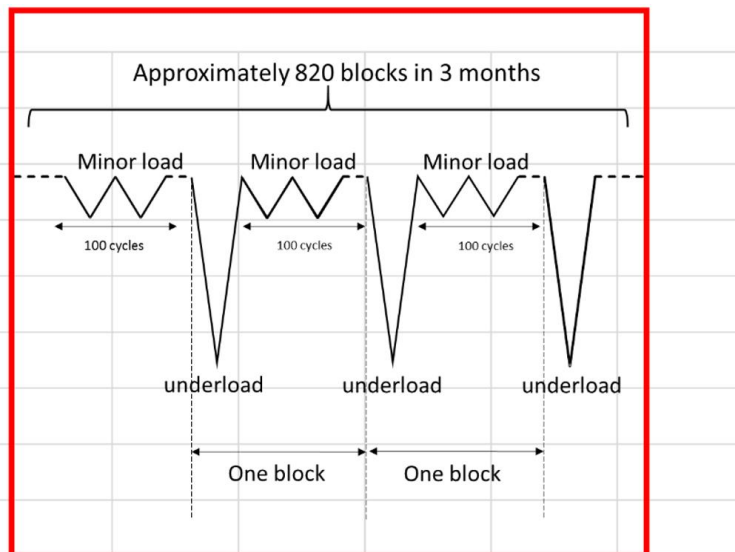


Figure 60: Loading conditions for gas pipeline condition test

Table 36: Conditions of loading for one cyclic block as defined in Figure 60

Under load cycle parameters		Minor load cycle parameters	
Maximum pressure (bar)	86.8	Maximum pressure (bar)	86.8
Minimum pressure (bar)	43.4	Minimum pressure (bar)	78.12
R-ratio	0.5	R-ratio	0.9
Pressure increase lasts (second)	338.5	Pressure increase lasts (second)	67.7
Pressure decrease lasts (second)	112.8	Pressure decrease lasts (second)	22.6
Total time per cycle	451.3	Total time per cycle	90.3
Number of cycle per one block	1	Number of cycle per one block	100

The three vessels containing the defects were submitted to 505.6 blocks, i.e. 50,560 cycles. As during the oil pipelines condition test, results of MPI show that no crack coalescence occurred in the real SCC colony on pipe SCC1a during the 50,560 cycles. At the end of the test, all the defects were destructively characterized in order to measure crack depth at the tip of the machined notch. Results are presented in Table 37.

Table 37: Crack depth measurements after gas pipeline condition test

Notch	Initial measured depth (mm)	Crack propagation (μm)
SCC-1a-10-13	1.32	140
SCC-1a-10-15	1.59	150
SCC-1a-11-13	1.29	490
SCC-1a-12-13	1.38	110
SCC-1a-5-15	1.45	320
SCC-1a-5-20	1.99	60
SCC-1a-6-15	1.54	150
SCC-1a-6-17	1.67	90
SCC-1a-7-15	1.48	130
SCC-1a-7-17	1.69	440
SCC-1a-8-15	1.59	100
SCC-1a-8-17	1.83	200
SCC-1a-9-15	1.39	360
SCC-1a-9-17	1.73	580
SCC-1b-11-15	1.56	230
SCC-1b-13-13a	1.43	180
SCC-1b-13-13bis	1.45	230
SCC-1b-13-15a	1.56	150
SCC-1b-13-15b	1.52	140
SCC-1b-13-15bis	1.7	180
SCC-1b-14-13bis	1.4	140
SCC-1b-16-12a	1.3	90
SCC-1b-16-12b	1.25	130
SCC-1b-17-12	1.18	200
SCC-1b-19-12a	1.27	140
SCC-1b-19-12b	1.29	50
SCC-1b-20-12	1.27	160
SCC-1b-22-12a	1.25	180
SCC-1c-14-15	1.61	280
SCC-1c-14-15bis	1.58	220
SCC-1c-15-15	1.57	280
SCC-1c-16-15a	1.59	230
SCC-1c-16-15b	1.54	230
SCC-1c-17-15	1.56	290
SCC-1c-18-15	1.49	240
SCC-1c-19-15a	1.48	170
SCC-1c-19-15b	1.57	260
SCC-1c-20-13	1.41	180
SCC-1c-21-13	1.52	230
SCC-1c-22-13a	1.38	200
SCC-1c-22-13b	1.27	130
SCC-1c-23-12	1.28	115
SCC-1c-23-13	1.29	140
SCC-1c-24-12	1.18	185
SCC-1c-24-12bis	1.34	220
SCC-1c-24-13	1.38	100
SCC-1c-24-13bis	1.39	170
SCC-1c-25-12	1.23	200
SCC-1c-25-12bis	1.34	110
SCC-1c-25-13	1.35	160
SCC-1c-25-13bis	1.41	240

Results show little crack propagation. One result shows the comparison between notches inside and outside the electrochemical cell which have the same initial size. These notches are located on pipe SCC1c and are named SCC1c-XX-YYbis. As shown in Figure 61, the results of the effect of the electrochemical cell are not clear cut. Indeed, crack propagation is larger for two notches located in the electrochemical cell than for two equivalent notches located outside of the electrochemical cell, and lower for the 3 other notch pairs. An explanation is that overall measured crack growth values are low, so even local material properties' scatter can interfere with crack growth rates. So, the discrepancies could be due to local microstructure fluctuations.

While these observations cover only six crack pairs, Table 37 shows a crack growth up to 580 μm , with most of the crack growth amounts being in the range of 150 – 300 μm . These are moderate crack growth values for more than 50,000 cycles.

It is difficult to interpret with the currently available tools the crack growth data from such complex loading patterns because the defects were submitted to several loading regimes with different R-ratios and underloads. The UofA tools (those not publicly available) might allow to achieve such an interpretation.

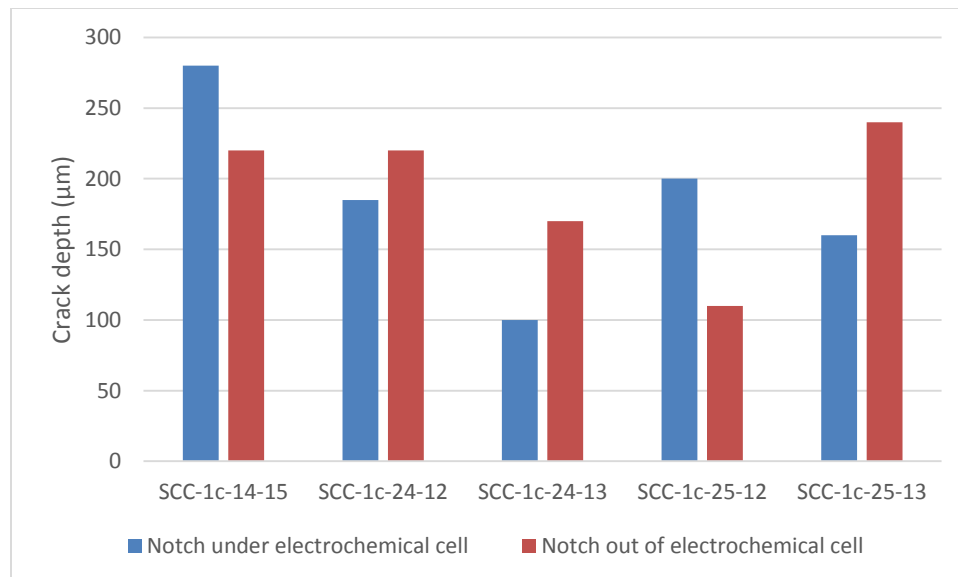


Figure 61: Comparison between crack size at the tip of notches located under or out of the electrochemical cell

6.5 Conclusions

The two fatigue tests (one with oil pipeline loading condition - $R=0.5$ and another with gas pipeline loading condition - $R=0.9$) performed on pipes with 58 machined EDM notches allowed characterization of crack depth propagation. The length of machined notches ranged from 5 mm to 25 mm and their depths ranged between 1.2 mm to 2 mm. These cracks are typical of shallow cracks found in service, which may or may not evolve during the pipeline's lifetime.

The first fatigue test performed with the “oil pipeline condition” loading pattern was compared to the only other existing, previous full scale tests, confirmed the identified trend. The results also add more data in areas that were not well covered by previous work, thus filling some existing experimental gaps.

The second fatigue test performed with the “gas pipeline condition” loading pattern showed that the crack growth of notches exposed to an electrochemical environment may not be significantly larger than crack

growth of the same initial size notches not exposed. For this notch set, it appears that they may be at the limit between a mechanical fatigue regime and a SCC mechanism.

To obtain additional results concerning the crack growth rate in an electrochemical environment, it would be interesting to enlarge the notch size range in order to reach higher combined factor values as defined by UoA. Such work would address more severe cracks, and would also allow comparison of full scale results with crack growth rates obtained on samples by UoA. This would further advance the full scale test validation of UoA's model on a wider range of cracks.

7 Finite Element Analysis of Longitudinal Strain (Task 7)

7.1 Background

Mechanical damage in a pipeline changes the response of the pipe to internal pressure and external loads and can significantly reduce the fatigue life a pipeline segment. However, the effect of an axial load on the fatigue life of a pipe containing mechanical damage has not been demonstrated. In principle if an axial load changes the shape of pipe containing mechanical damage it can affect its fatigue life.

Compressive strain due to axial load, bending, or combined axial and bending loads reduces the pipe load carrying capacity. Pipes can also buckle under the application of external pressure in deep-water (offshore) applications. Examples of sources of compressive axial load/bending are loads due to ground movement that can apply lateral or axial loading to the pipe, upheaval buckling of buried pipes (e.g., subsea applications) due to thermal expansion, and formation of wrinkle bends in pipes. Both geometric and material imperfections can affect the mode of pipe buckling.

7.1.1 Axial Load and Bending Moment Capacity of Pipes

Imperfections, such as material and geometric, can cause a round pipe to buckle under the application of compressive load (strain). In real world applications, the compressive strain limit of steel pipes can be a function of various parameters including pipe ovality, pipe local wall thickness reduction, pipe material stress-strain curve, geometric and material imperfections, cracks, and welds¹³.

Dents in pipe can promote pipe buckling by introducing a geometric imperfection in the pipe. The dent formation process introduces large plastic strains at the dent region, which can be considered a material imperfection in the pipe. In general, axial load and bending capacity of a dented pipe is lower compared to that of a round pipe.

The fatigue life of a dented pipe due to internal pressure fluctuation is lower than that of a perfectly round pipe. Dents in field are often subject to axial compressive/tensile loads and their behavior under internal pressure fluctuation is different from the dents without the axial load. Therefore, it is desirable to understand the effect of axial load on the fatigue life behavior of dented pipes.

7.1.2 Task Objective

The objective of the present study is to investigate the effect of axial load or bending on the fatigue life behavior of dented pipes.

FE models were developed to investigate the effect of a variety of dent shapes and dent restraint conditions on the fatigue life of the dented pipes under the application of a constant axial or bending loads. Additional information related to the buckling resistance of a dented pipe segment was investigated in support of the fatigue life assessment to understand the limits of axial loading before gross changes in the pipe cross section commence (i.e. buckling).

7.2 Finite Element Modeling

FE modeling was used to investigate the effect of axial load on the fatigue life behavior of plain dents. The validated BMT FE tool for modeling dents was used for generating results^{3,4,5}. Both restrained and unrestrained dent conditions with different depths and shapes were considered. Table 38 summarizes the FE modeling matrix.

ANSYS® 8-node quadrilateral curved shell element (Shell 281) was used to model the pipe¹⁴. This element is capable of capturing both material and geometry nonlinearities. A rigid elliptical indenter was used for

¹³ Yong Bai, "Limit state design of pipelines & risers", IBC training course, May 1999

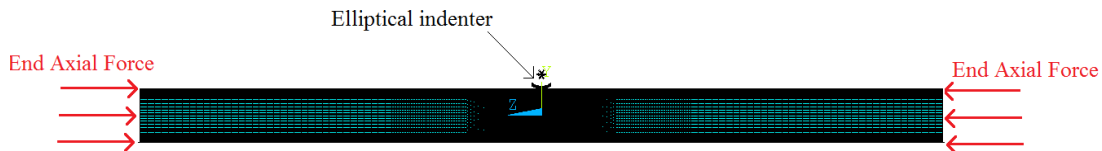
¹⁴ ANSYS Mechanical, Release 17.0, 2015

the indentation process forming the pipe dent. The indentation force was transmitted to the pipe using ANSYS® 3D surface to surface contact elements TARGE170 and CONTA174. To reduce the number of elements and computational time, reflective symmetry of the model with respect to two planes was used and only a quarter of the pipe was modeled. Figure 62 shows a typical FE model of the pipe and an enlarged view of the indenter.

Table 38: The FE Modeling Matrix

Parameter	Condition
Dent restraint condition	Restrained/Unrestrained
Indentation depth (%OD)	5 and 10 for unrestrained dent 1,2,3 and 4 for restrained dents
Pipe internal pressure (%PSMYS)	0, 30, 60 for axial load/bending 0,10, 20, 30, 40, 50, 60, 70 for developing load capacity equation
Indenter	4 inch and 12 inch elliptical indenter for axial load 4 inch and 24 inch elliptical indenter for bending
Axial load	Tension/compression (various magnitudes) Bending (various magnitudes)
Pipe OD (inch)	18, 24, 30 for axial load 24 for bending
Pipe wall thickness (inch)	0.25
Cyclic pressure (%PSMYS)	10 to 70
Pipe Grade	X52 and X70 for axial load, X52 for bending

The rigid indenter was moved downward to indent the pipe. After the indentation, the pipe was pressurized to 80% specified minimum yield strength (PSMYS) and 90% PSMYS pressure for the unrestrained and restrained dents, respectively. All dents were cycled between 10% PSMYS to 70% PSMYS cyclic pressure without the application of any axial end load. Subsequently, the axial load/bending was applied to the pipe and the pipe was cyclically pressurized to the same pressure level mentioned above while the end axial or bending load was maintained.



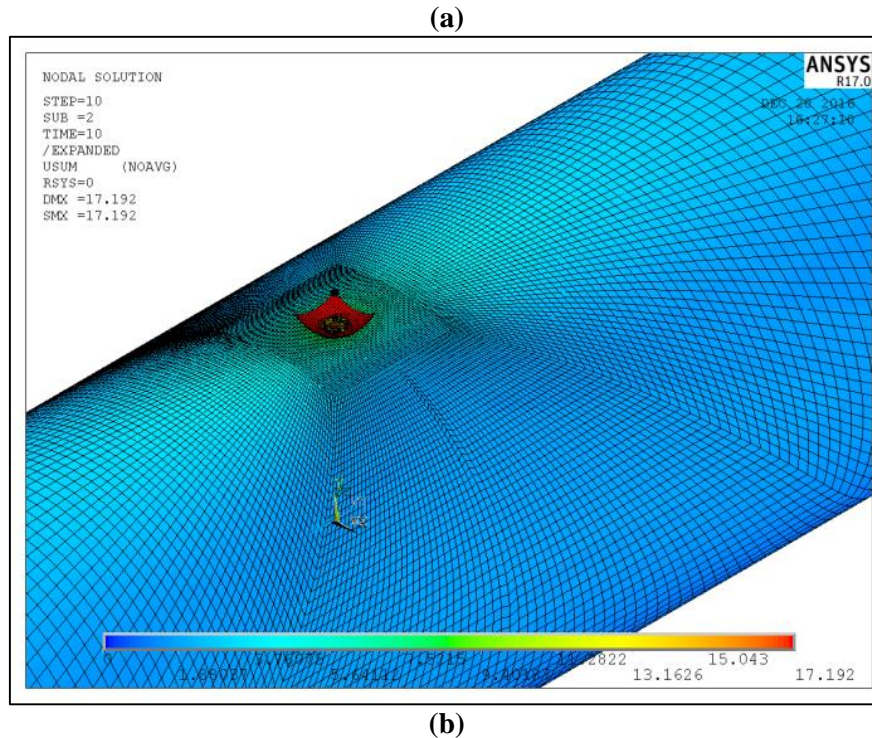


Figure 62: Typical FE Model of the Dent with Axial End Load (a) Side View of the Whole FE Model (b) Close up of the Dent Area

7.3 Results

7.3.1 Dent under compressive or tensile axial load

Depending on the load carrying capacity of the pipe, various compressive load levels were applied to the pipe up to the buckling point to investigate the effect of compression on the fatigue life of the dent. The post-buckling fatigue behavior of the dented pipes was also examined by applying compressive displacement loading. Similarly, different tensile load was applied to the pipe to investigate the effect of tension on the fatigue life of the dent. The following scenarios were observed depending on the magnitude and direction of the applied load.

- The magnitude of the applied load (either compressive or tensile) is below the load carrying capacity of the dented pipe; therefore, the dent under axial load remains stable and does not buckle (Figure 63a and Figure 64a).
- The magnitude of the applied compressive load is above the load carrying capacity of the dented pipe; therefore, the dent under axial load becomes unstable. Restrained dents become unrestrained due to buckling (Figure 63b).
- The magnitude of the applied tensile load is high and causes pipe thinning. A restrained dent becomes unrestrained due to the pipe circumferential contraction under the applied tensile load (Figure 64b).

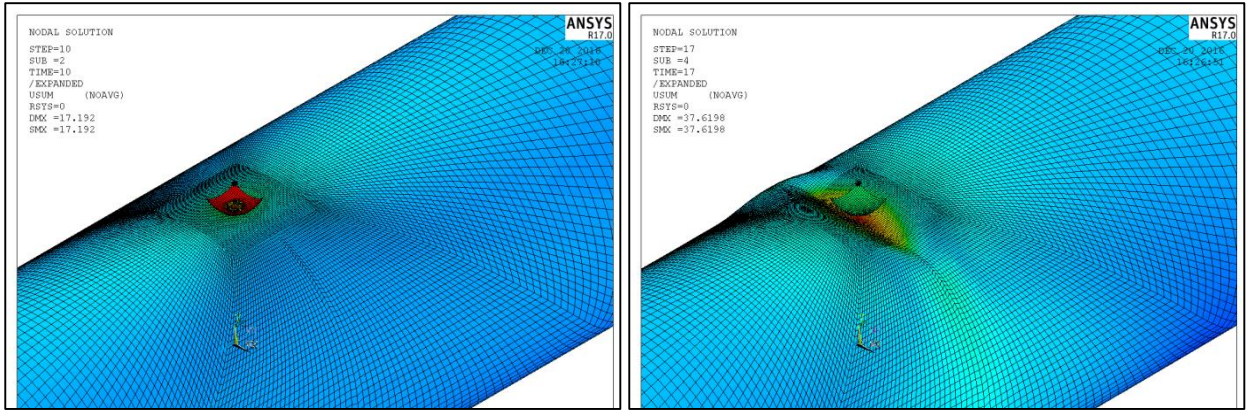


Figure 63: Buckling of a Restrained Dent due to Compression (a) Before Buckling (b) After Buckling

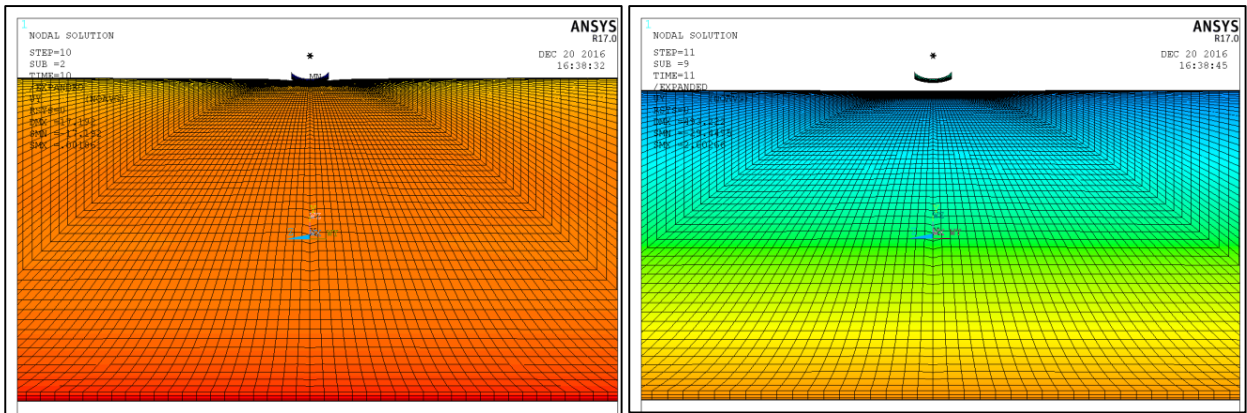


Figure 64: Restrained Dent Under a 1350 kips Tensile Force (a) Before Thinning (b) After Thinning

7.3.2 Dent under applied bending

Different bending moments were applied to the dented pipe segment. Depending on the magnitude of applied bending moment, the dent may remain in the stable regime (prior to buckling) or it may buckle. Figure 65 shows a restrained dent prior to the application of bending. Figure 66 shows the same dent after the application of bending. The magnitude of the applied bending load is below the load carrying capacity of the pipe, and therefore, the dent is in the stable regime. Figure 67 shows the same dent where the applied bending rotation was increased beyond the load carrying capacity of the pipe and caused the dent to buckle. It is clear from this figure that the restrained dent becomes unrestrained due to buckling.

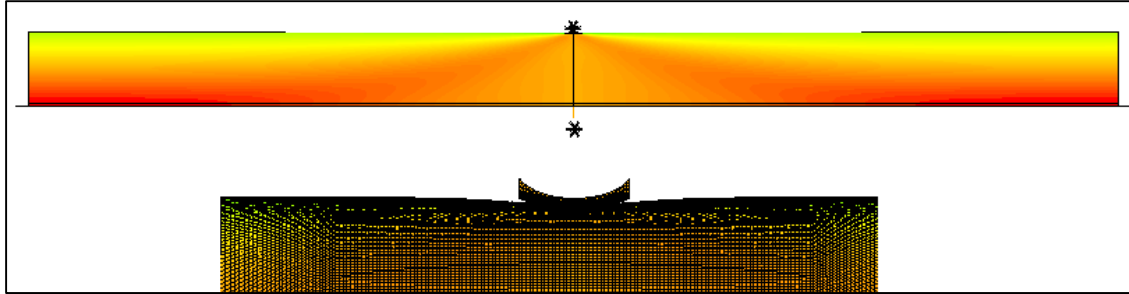


Figure 65: A Typical Restrained Dent Prior to the Application of Bending – True Scale

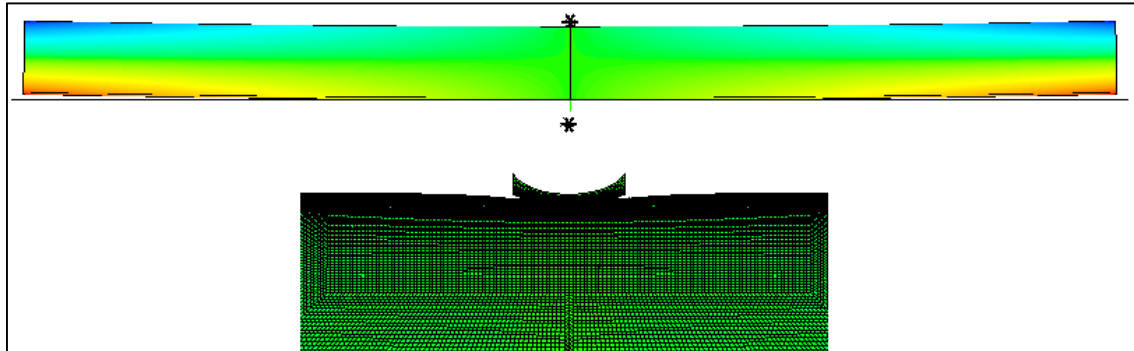


Figure 66: A Typical Restrained Dent under Bending, Before Reaching the Buckling Point – True Scale

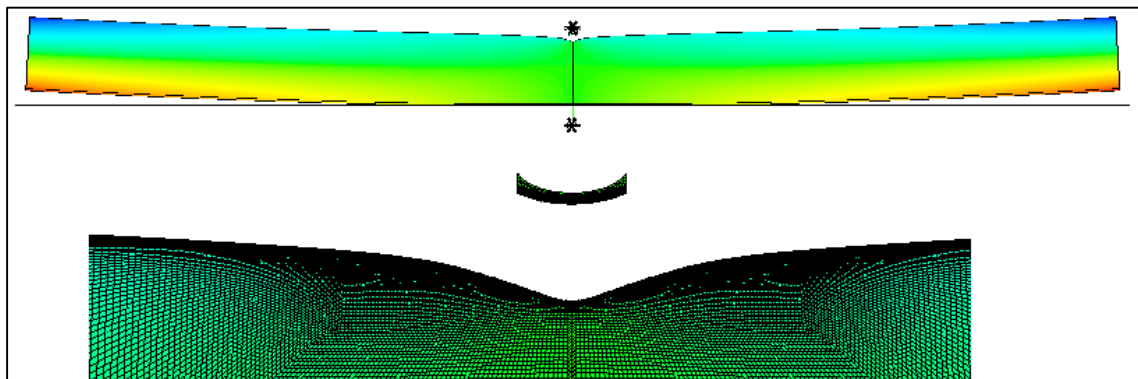


Figure 67: A Typical Restrained Dent under Bending, Beyond the Buckling Point – True Scale

7.3.3 Effect of axial load on Fatigue life

To investigate the effect of axial load on the fatigue life behavior of dents, pipes with three different outer diameter to wall thickness (OD/WT) ratios (i.e. 72 (18/0.25), 96 (24/0.25), and 120 (30/0.25)) and two different grades (i.e. X52 and X70 grades) were considered. The pipes were indented using two rigid elliptical indenters (i.e. 4 inch diameter and 12 inch diameter) to various dent depths. Both dent restrained and unrestrained conditions were included in the present study. First, for the pressure cycle of 10% to 70% PSMYS, fatigue lives of plain dents without any axial load were calculated. Then, different magnitudes of axial load were applied to the dented pipe and same cyclic pressure was applied to calculate the fatigue lives of the dents under the applied axial load.

A change in the fatigue life is inferred from the change in the dent stress range. A higher stress range for the same applied cyclic loading would result in lower fatigue life. The ratio of the dent stress range to the

stress range in a plain pipe is termed the stress magnification factor, K_M . Figure 68 shows the effect of applied axial load on the stress magnification factor of dents for the pressure cycle of 10% to 70% PSMYS.

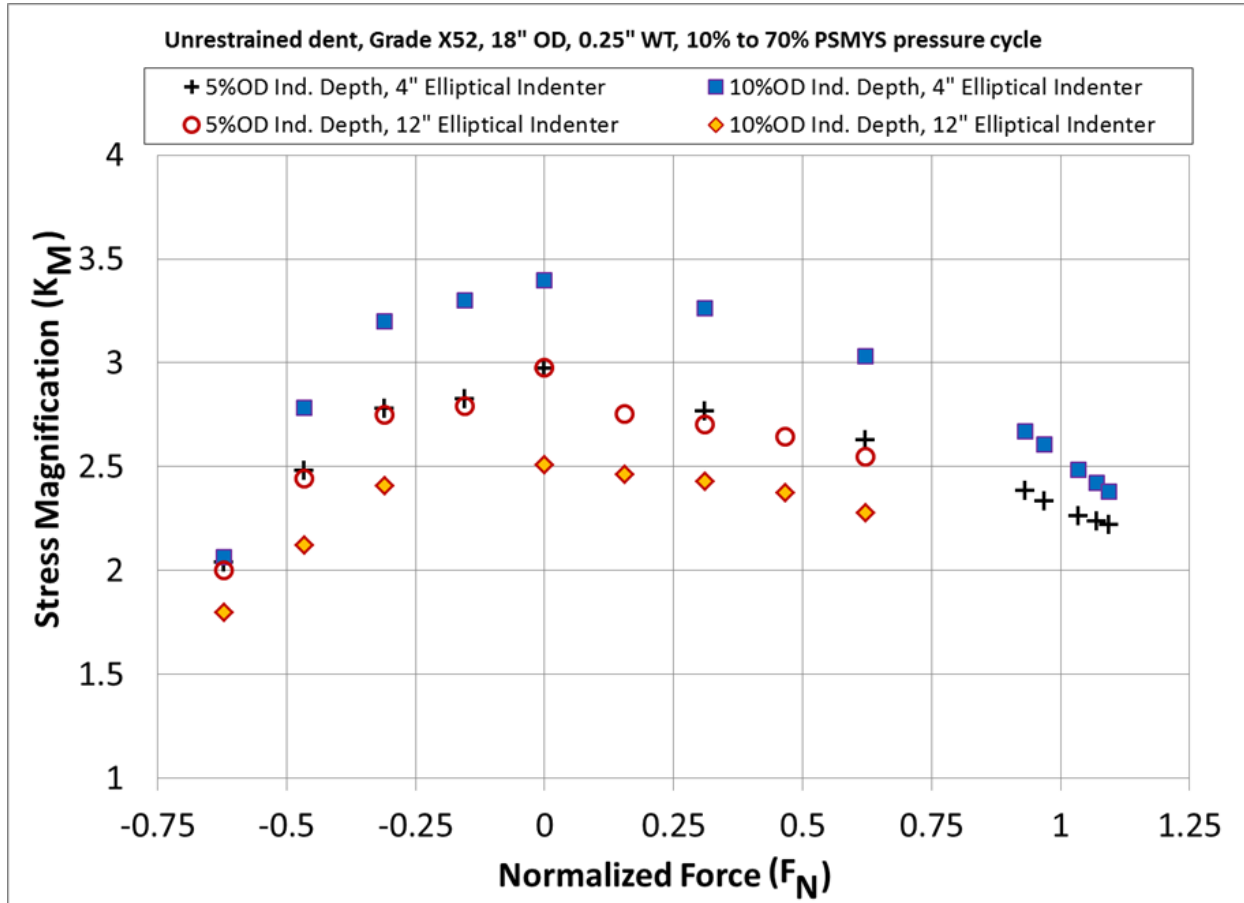


Figure 68: Stress Magnification Factor of Unrestrained Dents with Axial Force

Figure 68 plots the normalized force (F_N) is defined as:

$$F_N = \frac{\text{Applied Axial Force}}{F_{SMYS}}$$

where

$$F_{SMYS} = SMYS * A$$

and A is the round pipe cross section area and $SMYS$ is the material specified minimum yield strength. In Figure 68, $F_N = 0$ represents dents without any applied axial force. A positive normalized force corresponds to the application of tension to the dented pipe segment and a negative normalized force corresponds to the application of compression. The stress magnification factor (K_M) is defined as follows:

$$K_M = \frac{\Delta S_C}{\Delta S_{Nominal}}$$

where

$$\Delta S_{Nominal} = \frac{\Delta P \cdot OD}{2 \cdot WT}$$

$\Delta S_{\text{Nominal}}$ is the pipe nominal stress range, ΔP is the pipe internal pressure range, and ΔS_C is the dent critical stress range. The dent critical stress range is the maximum stress range in the dent region. Figure 68 shows that the applied axial load does not increase the dent stress magnification factor as compared to the stress magnification factor of dents without any applied axial load. As a result, the applied axial load does not adversely affect the fatigue life of the dents. These results suggest that an axial load stabilizes the dent feature and prolongs its fatigue life. While numerically this result is correct, the primary observation is that the axial loading on this scenario does not reduce the fatigue life of the dent.

It is worth mentioning that the results presented in Figure 68 are for the cases where the applied compressive axial force does not cause any global instability of the dented pipe. To assess the effect of axial load beyond the axial load capacity of the dented pipe, an axial displacement was applied to the same pipe and dents. Figure 69 shows the stress magnification factor versus the applied axial displacement.

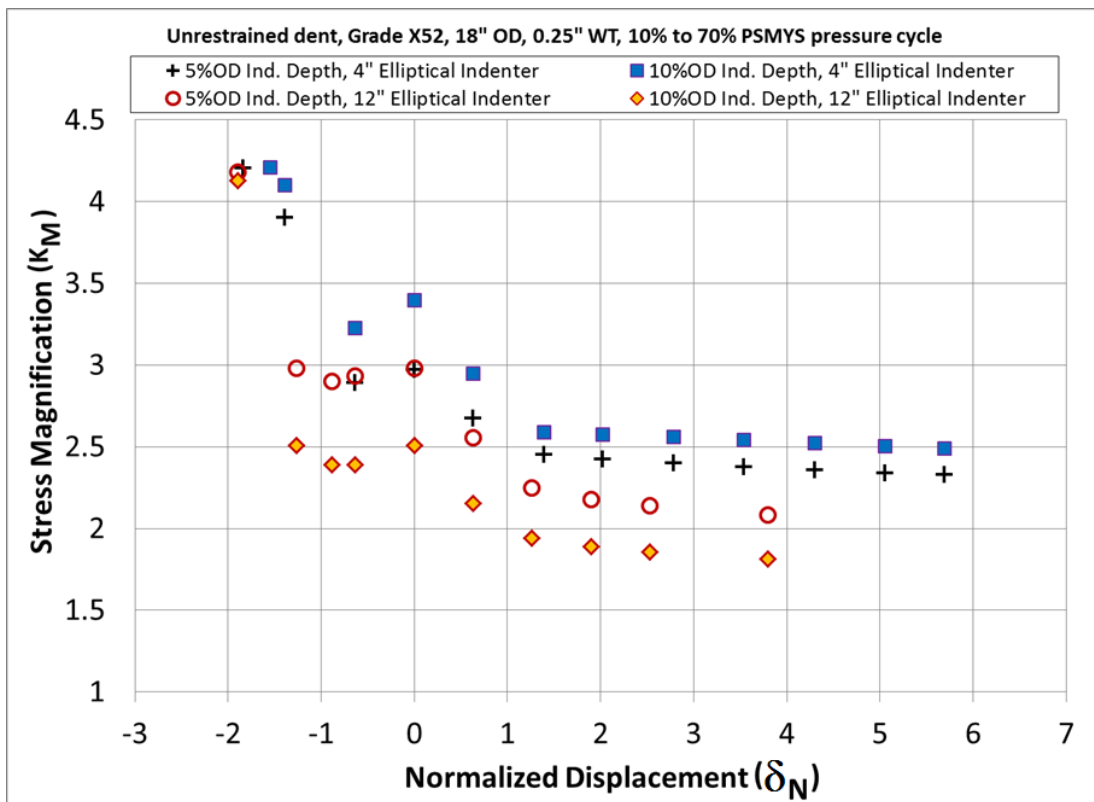


Figure 69: Stress Magnification Factor of Unrestrained Dents with Axial Displacement

In Figure 69, the normalized displacement is defined as

$$\delta_N = \frac{\text{Applied displacement}}{\delta_C}$$

where

$$\delta_C = \frac{SMYS * L}{E}$$

L is the pipe length, and E is the pipe elastic modulus. In Figure 69, $\delta_N = 0$ corresponds to dents without any applied axial displacement. A positive normalized displacement value represented stretching the pipe segment and a negative normalized displacement is compression of the pipe segment. Figure 69 shows that

for compressive axial displacement beyond the capacity of the dented pipe (i.e. for compressive $\delta_N < -1$) the dented pipe buckles and the stress magnification factor increases as compared to that of the corresponding dent without any applied axial displacement.

Analyses were completed for both the restrained and unrestrained dents in 18, 24 and 30 inch OD, X52 and X70 pipes. Detailed results for each individual pipe, grade, and dent condition, are given in Annex H. The results presented in Annex H suggest that for all pipe geometries, pipe grades, and unrestrained dents where the normalized displacement and the normalized force are within the range of $-1 \leq \delta_N \leq 1$ and $-1 \leq F_N \leq 1$, the dent stress magnification factor does not increase (as compared to that of the corresponding dent without applied axial load). This indicates that axial loading does not adversely affect unrestrained dent fatigue life.

The analysis results presented in Annex H indicates that for restrained dents, the stress magnification may increase up to 10% for a limited number of cases. These changes in stress magnification factors are observed for lower axial load magnitudes only. These results suggest that the fatigue life of restrained dents subjected to axial loads could be reduced as compared to dents without axial loads.

For dents with higher magnitudes of δ_N and F_N , promoting gross dent formation (i.e. buckling), the stress magnification factors increase and the dent fatigue life is adversely affected.

7.3.4 Effect of bending load on fatigue life

Similar to the case of axial load discussed in Section 7.3.3, a bending load was applied to dented pipes to investigate the effect of bending on the fatigue life behavior of dents. Figure 70 and Figure 71 show the effect of bending on the dent stress magnification factor for restrained dents with a 4 inch elliptical indenter and unrestrained dents with a 24 inch elliptical indenter, respectively.

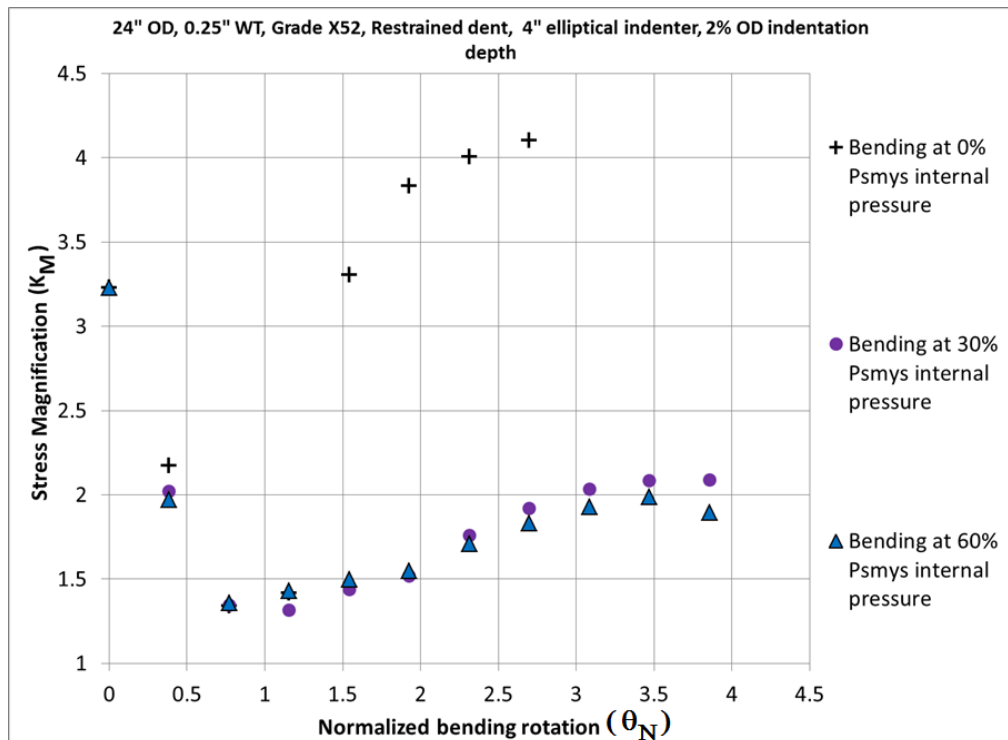


Figure 70: Stress Magnification Factor of Restrained Dents under bending

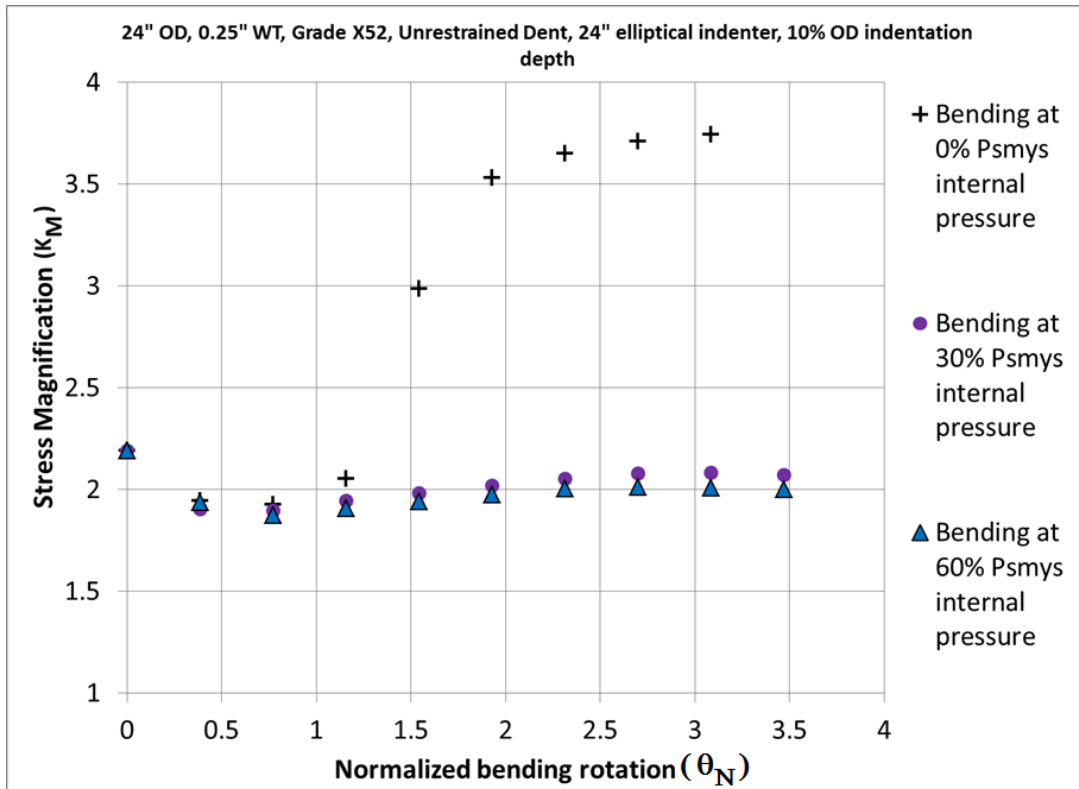


Figure 71: Stress Magnification Factor of Unrestrained Dents under bending

In Figure 70 and Figure 71, the normalized rotation θ_N is defined by

$$\theta_N = \frac{\text{Applied rotational bending}}{\theta_C},$$

where

$$\theta_C = \frac{SMYS \cdot L}{OD \cdot E},$$

and L is the pipe length. The case of $\theta_N = 0$ in these two figures corresponds to dents without the application of bending. As the results also show, the fatigue life of the dent is not adversely affected by the applied bending if it does not cause global instability of the dented pipe. For pipe with zero internal pressure the instability starts to happen around $\theta_N = 1.5$ while for pressurized pipe the instability is delayed and happens at a higher value of θ_N . Similar results are observed for all the cases considered in this study. Detailed results for dents with bending are given in Annex H.

7.3.5 Effect on other Limit States

The results presented in Sections 7.3.3 and 7.3.4 indicate that dents can reduce the force or moment capacity of the pipe subjected to axial load or bending. Figure 72 shows the effect of the dent and internal pressure on the axial force capacity of an 18 inch OD grade X52.

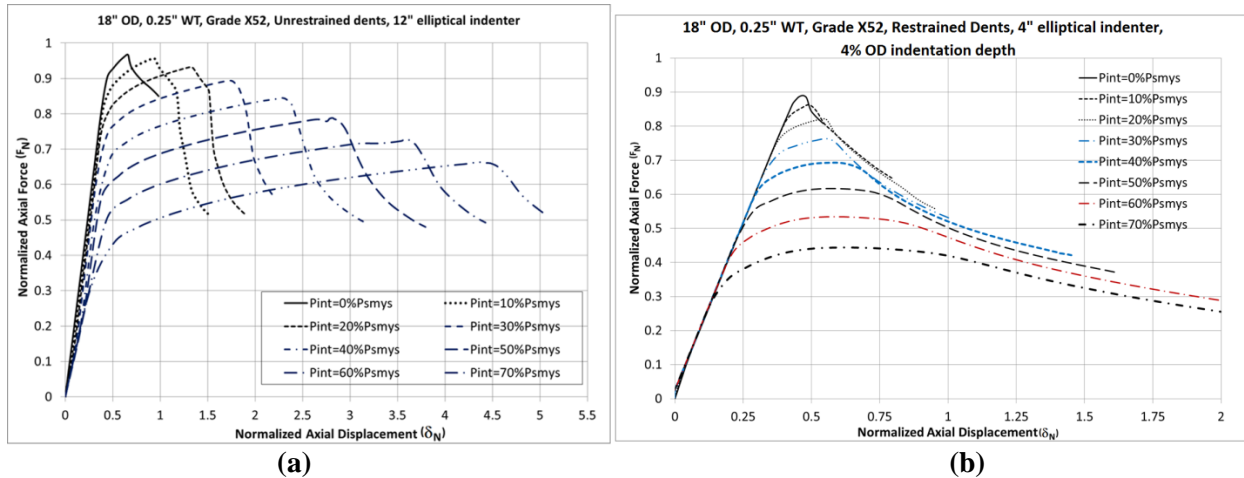


Figure 72: Variation of Axial Force Capacity with Internal Pressure: (a) Unrestrained Dents (b) Restrained Dents

Figure 72 suggest that presence of dents in a pipe can adversely affect the axial load capacity of the pipe. It is therefore desirable to know the effect of a dent on the load carrying capacity of a pipe.

As shown in Figure 72 the pipe axial load capacity decreases with increasing pipe internal pressure. This is in contrast to the buckling behavior of a pressurized round pipe where the buckling load increases with increasing pipe internal pressure. To better understand the differences, one has to consider that presence of dent introduces geometric and material imperfections in a dented pipe which differs from the imperfections that typically exist in a round pipe. In addition, a dented pipe with internal pressure tends to either bend or pushed the dent outward depending on the dent restraint condition which results in additional axial or bending loads. This additional load can promote the pipe buckling at a lower axial load as compared to the buckling of a round pipe.

Figure 73a shows a schematic of a dent with internal pressure and axial compressive end load. Considering that the dent shape changes with the pipe internal pressure, the effect of axial load would be different for the same dent if it is axially loaded at zero pressure or at an internal pressure. Therefore, for a given dent geometry, i.e. dent depth, indenter shape, etc., the buckling behavior would be different if the dent is axially loaded at different pipe internal pressure levels. In addition, internal pressure in the dent region introduces additional bending moment and axial force which is due to internal pressure and tends to bend the dent inward. This means that a lower axial force is required for the pipe to buckle. Figure 73b and Figure 73c show a buckled pipe under the application of end axial load with zero and 70% PSYMS pipe internal pressures, respectively. It is clear that the pipe internal pressure affects the buckled model shape of the dent.

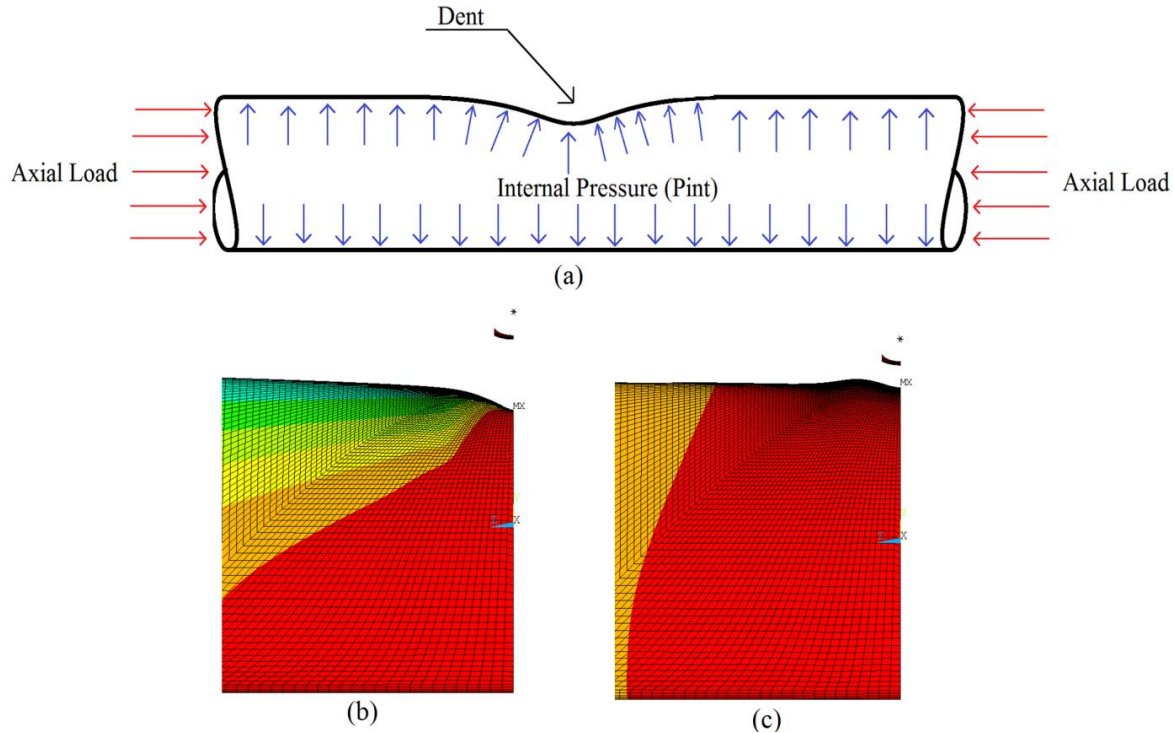


Figure 73: (a) Schematic of a dent under internal pressure and axial load, (b) buckling of dent with zero internal pressure, (c) buckling of dent with 70% PSMYS internal pressure

7.3.6 Preliminary Understanding of the Axial Load Capacity of Dented Pipes

As Figure 74a through Figure 74d suggest, the axial compressive limit load of a dent is affected by the ratio of the OD to wall thickness, material grade, pipe internal pressure, and the dent shape and dent restraint condition. Therefore, the following equation can be assumed to estimate the axial force capacity of a dented pipe.

$$F_N = \frac{F_{buckling}}{F_{SMYS}} = F(P_N, \beta, G_i)$$

where

$$P_N = 1 - \frac{P_{int}}{P_{SMYS}},$$

$$\beta = \left(\frac{WT}{OD}\right) \left(\frac{358}{\text{Pipe Grade in MPa}}\right),$$

P_{int} is the pipe internal pressure at which the axial load is applied, and G_i 's are the dent characteristic shape factors.

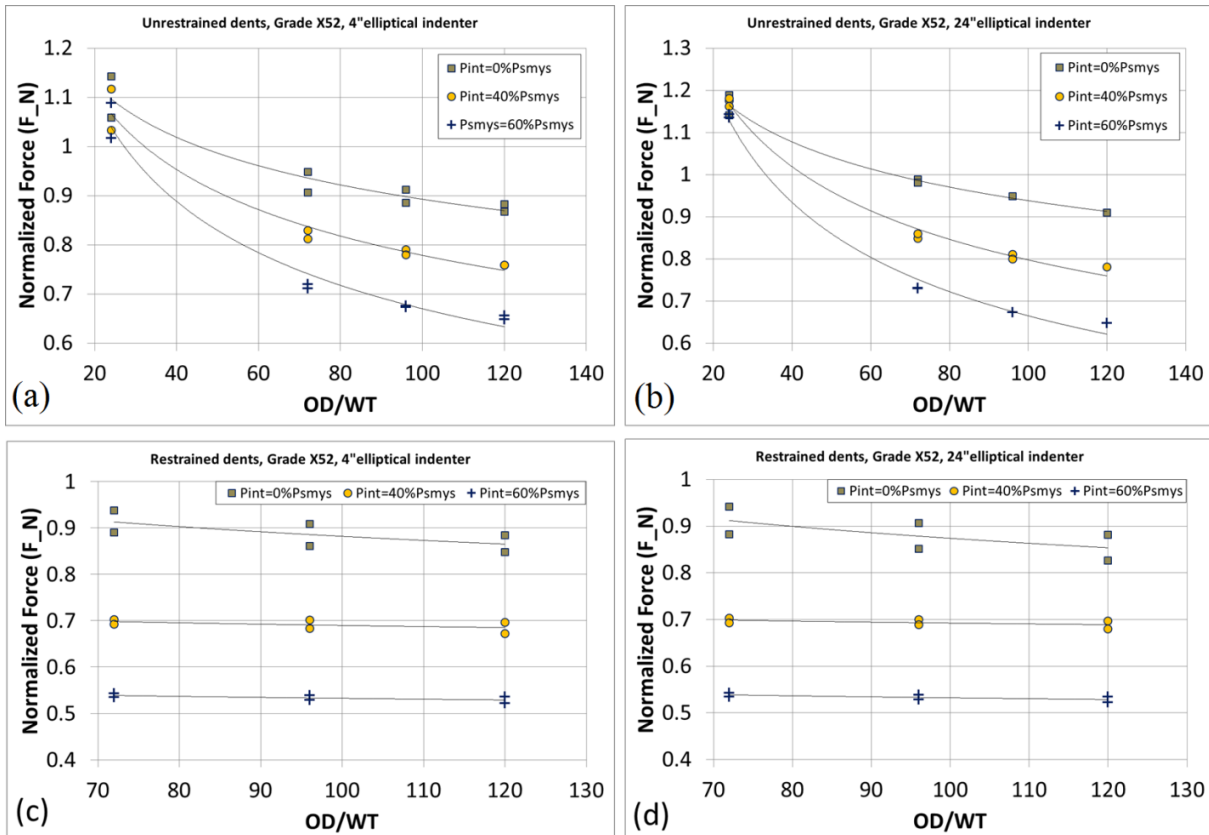


Figure 74: Effect of various parameters on the axial load capacity, (a) and (b) unrestrained dents, (c) and (d) restrained dents

Motivated by the trends observed in Figure 74a through Figure 74d, a series of regression analysis were performed using the FE analysis data for both the unrestrained and restrained dents.

Table 39 summarizes the FE case data used for the unrestrained and restrained dents to develop and test the regression equation. Figure 75 and Figure 76 show a comparison between the actual FE results for the dented pipes and the predicted results from the regression equation for the unrestrained and restrained dents, respectively.

Table 39: FE Data Used for Developing and Testing the Unrestrained Dent Regression Equation

Parameter	Value
OD	12 in, 18 in, 24 in, 30 in
WT	0.25 in, 0.5 in
Grade	X52, X70
Indenter Shape	4", 12", 24" elliptical shape, 4 in diameter transverse bar
Indentation Depth	5% and 10% OD for unrestrained 1% to 4% OD for restrained dents
Internal Pressure	Pmax: 50% and 80% PSMYS Internal Pressure: 0, 20, 40, 60% PSMYS for 80% PSMYS Pmax and 20%, 40% for 50% PSMYS Pmax

The unity plots presented in Figure 75 and Figure 76 suggest that the buckling capacity of pipe segments with dents subjected to axial loads can be reasonably predicted using a closed form equation. The equation is not presented at this time because it needs to be generalized to consider:

- Greater range of dent shapes,
- Greater range of materials,
- Effect of bending and
- Greater range of pipe geometries.

Despite the preliminary nature of this result, it indicates that there is a reasonable potential to develop a limit state equation to support the assessment of buckling of dented pipe segments.

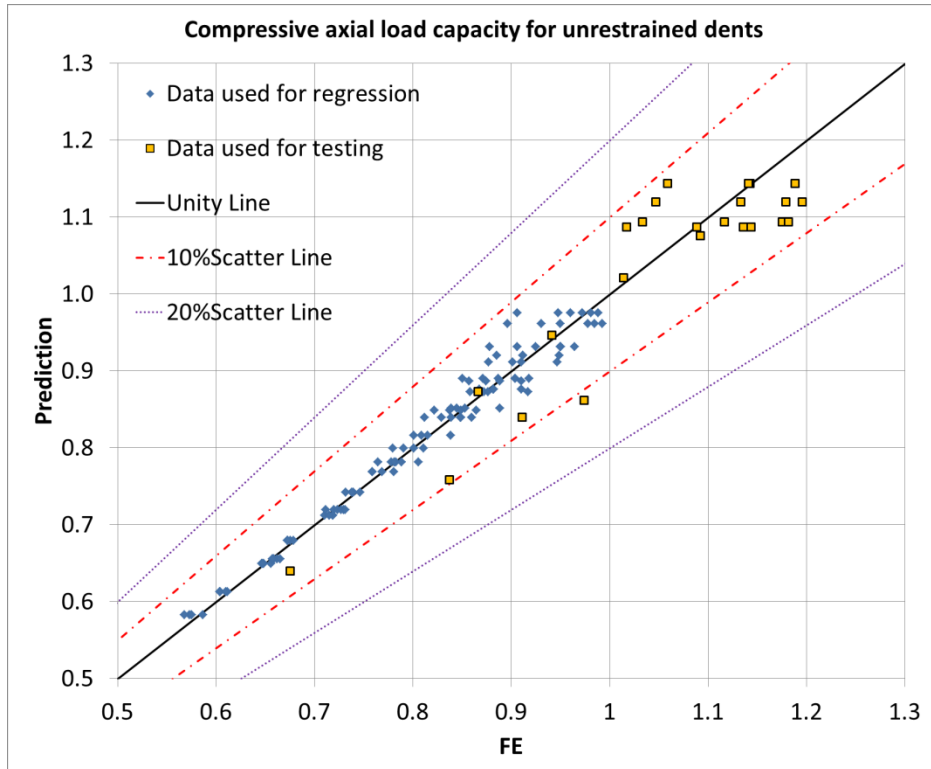


Figure 75: Unity Plot for the Unrestrained Dents Buckling Equation



Figure 76: Unity Plot for the Restrained Dents Buckling Equation

7.4 Conclusions

The BMT FE modeling tools that have been developed and validated against full scale trials to simulate the behavior of dents and estimation of their fatigue lives has been applied to the assessment of dents with applied axial and bending loads and cyclic internal pressure. This analysis was applied in a sensitivity study to understand the impact of the axial loading on the fatigue life of dented pipe segments. This analysis demonstrated that axial loads did not adversely affect unrestrained dent fatigue life. In restrained dents, reduction in fatigue life was observed for a limited number of cases. This result was demonstrated for:

- Differing pipe material grades X52 and X70,
- Three pipe geometries, D/t ratios (i.e. 72, 96 and 120),
- Restrained and unrestrained dents,
- Axial loads derived from applied axial forces and applied bending moments, and
- A number of indenter geometries and dent depths.

This analysis also demonstrated that when the axial loading (i.e. axial force, bending, axial displacement or rotation) causes the dented pipe segment to buckle or yield, the fatigue response of the dented and buckled pipe segment is lower than the dented pipe segment.

Axial loading was shown to not have a significant impact on the fatigue life of the dents, however, axial loading of dents affected other modes of failure, i.e. buckling. Preliminary results shown in the current program demonstrated that an analytical solution can be developed to predict the buckling capacity of the dented pipeline. It is recommended to carry out detailed FE modeling incorporating different dent sizes and shapes, pipe geometry, axial and bending load condition and mean pressure to investigate the effect of axial loading and bending on other limit states such as buckling for dented pipes.

8 Lessons learned

The follow section discusses what has been learned during this project.

8.1 *Full Scale Testing of Dents*

- The detailed material property data are required as input data for existing models and for any newly developed models to ensure that local material response and failure mechanisms are incorporated accurately. The team recommends that future similar experimental programs include a detailed material characterization phase as a significant contribution of the robustness of the database.
- Acquiring the appropriate vintage pipe and/or in-service pipe with features of interest can take a significant amount of time, and recommends that future projects that use vintage pipe identify them prior to the start of the program and/or have appropriate amount of time built in the schedule to avoid project delays.
- It is recommended to have accurate continuous monitoring of the essential test parameters including cyclic pressures, indentation loads on contact, and displacements where the indenter is removed (unrestrained conditions).
- The continued use of strain gauging on all experimental specimens provides valuable information with regards to the detailed local behavior of the pipe wall.
- To date, all the dents for the dent fatigue test program have been created in the laboratory using artificial indenters. It is recommended to carry out full scale fatigue tests on dents removed from the field and obtain fatigue life data on realistic dent shapes. The fatigue lives of field dents can then be compared against laboratory created dents and the applicability of the current standardized curve (BS7608 Class D) can be further validated.
- Dents created with round bar in the transverse orientation to the pipe longitudinal axis in the present program looked similar to buckles and had lower fatigue lives compared with other dent shapes. It is recommended to carry out additional full scale fatigue tests on dents created with transverse bars of different sizes to generate additional transverse dent shapes and corresponding fatigue life data to develop a separate fatigue life curve that will be more applicable to transverse dent that look similar in shape to buckles.
- To date, all the full scale dent fatigue tests have been carried out on dents that are either fully restrained or in unrestrained condition. There are possible scenarios where a dent in a pipeline can be partially restraint and/or the restraint condition of the dent may change depending upon the mean pressure of the pipeline. It is recommended to carry out additional full scale fatigue tests where dent is partially restraint or its restraint condition changes during the cyclic pressure loading. The work would also involve carrying out detailed FE modeling to assist in experimental design. The fatigue life data generated for the partially restrained dent will be compared against the restrained and unrestrained dent fatigue tests carried out previously and applicability of the current standardized curve (BS7608 Class D) can be further validated.
- The full scale dent fatigue tests involving dent interaction with secondary features (welds and corrosion features) focused on positioning secondary features at the critical locations in order to obtain the maximum reduction in fatigue life due to interacting features. It is recommended to carry out additional full scale tests to identify the minimum distance a feature has to be from the dent peak where it would not affect the dent fatigue life. This will enable to better define when a dent is considered to be interacting with a secondary feature and therefore requires repair/remediation. This study was completed numerically for welds. It is recommended to complete this numerical evaluation for metal loss and complete full scale trials for welds and metal loss to validate these results.

8.2 *Dent and Gouge*

- Analysis of test results evidenced the added value of the current work on Dent and Gouge defects, both realistically created, and retrieved from service. The experimental approach consisted in

covering a wide range of threat interaction cases, each time trying to compare the baseline burst and fatigue resistance with corresponding burst and fatigue resistance of the combined threats.

- The findings of this work show that based on defect geometry, the additional interacting threats can either play a significant role for already severe or very defects that are thus brought closer to failure, like cathodic overprotection or close geometric interaction, or for less severe defects, not influence significantly their burst and / or fatigue resistance.
- This approach requires therefore additional investigation on better defining the Dent and Gouge severity limits for those defects that become sensitive to other interacting threats.
- Based on current experimental findings, defect severity is a key factor when it comes to adding cathodic overprotection or close defect interaction. These aspects require clearly more work to define the key parameters in terms of defect severity that would make such defects more sensitive to these threat interactions. To perform this work, a combined experimental and FE modeling approach seems to be the most appropriate.
- Concerning superimposed axial loads, while axially oriented defects haven't seen their burst and fatigue strength significantly affected by axial loads generated with four-point bending, circumferentially oriented Dent and Gouge defects or such defects oriented at an angle with the pipe axis may be more sensitive to this interacting threat, and therefore require additional investigation.
- In the area of axial loads, soil-pipe interaction also plays a role, and the experimental part of this investigation could be performed in a soil box, thus accounting for soil restraint effects when applying the four-point bending conditions. In addition, other diameters and defect shapes are also of interest to enhance the representativeness of Dent and Gouge defects with respect to operational conditions.
- Dent and Gouge defects removed from service would need to undergo a similar procedure for comparison purposes. While finding systematically similar defects to be able to compare burst and fatigue strength for similar defects, as those created on purpose cannot be guaranteed, they should be looked for.

8.3 *Stress Corrosion Cracking (SCC) Colonies*

- The first test under near neutral pH SCC conditions typical of an oil pipeline fatigue loading ($R=0.5$) has provided new full scale SCC crack propagation results that could be added to the only full scale test results already existing in the literature, and performed by GRI. The new results align well with the existing trend, adding some points to areas with existing data, and fill in gaps in the current data.
- The second test under near neutral pH SCC conditions typical of a gas pipeline fatigue loading ($R=0.9$) lead to limited crack growth for the large set of EDM notches typical of shallow SCC that can be found in the field, therefore remaining somehow around the limit between mechanical fatigue and crack growth acceleration due to SCC.
- Additional testing of more severe defects would provide better coverage of the UoA near neutral pH SCC crack growth rate prediction model. Advanced interpretation of test results is still underway with UoA.

8.4 *Finite Element Analysis of Longitudinal Strain*

- Axial loads did not adversely affect unrestrained dent fatigue life. In restrained dents, reduction in fatigue life was observed for a limited number of cases.
- The analysis demonstrated that when the axial loading (i.e. axial force, bending, axial displacement or rotation) causes the dented pipe segment to buckle or yield, the fatigue response of the dented and buckled pipe segment is lower than the dented pipe segment.
- Axial loading was shown to not have a significant impact on the fatigue life of the dents, however, axial loading of dents affected other modes of failure, i.e. buckling. Preliminary results shown in the current program demonstrated that an analytical solution can be developed to predict the

buckling capacity of the dented pipeline. It is recommended to carry out detailed FE modeling incorporating different dent sizes and shapes, pipe geometry, axial and bending load condition and mean pressure to investigate the effect of axial loading and bending on other limit states such as buckling for dented pipes.

8.4.1 Other Recommendations

- Field Dent Shape Validation - Dent depths are not good indicators of their fatigue life performance. Under PRCI research program dent shape parameters were developed and correlated with their fatigue life performance. The dent shape parameters were developed using FE modelling, validated using full scale dent fatigue test data, based on the hypothetical dent shapes created using different shape and size indenters. It is recommended to incorporate realistic dent shapes using field dent data in the dent shape parameter fatigue life calculations. In line inspection (ILI) data of field dents will be used for detailed FE modeling, as well as, to calculate dent shape parameters. The fatigue lives based on FE modeling will then be compared against the fatigue lives estimated based on the dent shape parameter. The analysis should be carried out for around 300-500 dents incorporating different depths and shapes, pipe geometry and pressure loading conditions.
- Dent Strain Criteria Evaluation - Dent strain and dent depth criteria are used to assess dent fatigue life and/or for dent integrity management. Dent strain criteria are based on dent curvature or shape and which are static characterizations of the dent shape at a given loading condition. However, experimental trials and numerical modelling have clearly demonstrated that dent shape and depth change with pipe internal pressure. These changes in shape due to cyclic pressure loading give rise to changes in the pipe wall stress or strain state that promote fatigue damage accumulation. It is proposed to calculate dent strain values for all the dents created in the full scale test program and correlate it to the corresponding fatigue lives to evaluate whether there is any correlation between dent strain and dent fatigue life. The work can be extended to field dents that have leaked and there is enough information available about their shapes. This work will demonstrate the ability of dent strain criteria to be used in dent integrity management.
- Dent Remedial Action - Once a dent is identified and it is determined that remedial action is required, industry applies a variety of practices including, but not limited to:
 - tight fitting steel A or B sleeves (i.e. reinforcing or pressure retaining) with and without filling the annulus,
 - Steel over sleeve (i.e. wedding bands with over sleeves)
 - clamp/bolt on sleeves
 - composite reinforcing wraps with a range of pipe to composite filler materials,
 - cut out and replacement of the pipe segment

It would support effective remedial action to complete a literature review and numerical modelling studies to demonstrate the characteristics of a remedial actions that effectively address dent fatigue for the long-term. This investigation could address the requirements and characteristics of sleeve to pipe annulus fill requirements and characteristics for this remedial action. The minimum length of a cut out and recommendations related to maximum ovality that should be accepted in this repair scenario. This investigation could also be used to further investigate mechanical damage safe excavation practice¹⁵ to ensure that daylighting the pipe does not promote pipeline failure.

- Pressure Cycle Attenuation – Previous work has demonstrated that the fatigue life of a dent is a function of the severity of pipeline operational pressure fluctuation. Related research has developed a spectrum severity indicator that characterizes the severity of pipeline operating pressure fluctuation. The severity of this operation pressure fluctuation (i.e. amplitude and frequency) attenuates with distance from pump stations in liquid pipelines. Industry statistics have been

¹⁵ Fredj, A., Dinovitzer, A., Vignal, G., Tiku, S., “Pipeline Mechanical Damage Process Review and Recommendations”, International Pipeline Conference 2014, Paper IPC2014-33618

assembled for Canadian liquid pipelines and a predictive tool¹⁶ has been developed to define cyclic operational severity at any location between stations. It is recommended that this study be expanded to consider US liquid pipelines to develop tools to better support integrity management of features that respond to internal pressure fluctuations including dents, cracks and wrinkles.

¹⁶ Semiga, V., “Location Specific Pipeline Cyclic Pressure” 30424.DFR (Rev.01), Final Report Submitted to Canadian Energy Pipeline Association” Dec 2016

9 Dissemination of Results

In addition to discussions with the Technical Advisory Board and parallel project with Kiefner and Associates¹⁷, the project status and results were presented at the following:

- 2017 PRCI Research Exchange Meeting held in Feb 21-22 2017 in Houston, Texas
- “Dent Fatigue From Research To Integrity Management” 2016 API Pipeline Conference and Cybernetics Symposium, April 5-7, 2016, Carlsbad, California
- From Mechanical Damage Testing to Assessment Techniques, 7th Biennial Inspection Summit, API, Jan 30-Feb 02, 2017, Galveston Island, Texas

¹⁷ .S. Department of Transportation Pipeline and Hazardous Materials Safety Administration "Improving Models to Consider Complex Loadings, Operational Considerations, and Interactive Threats" (Agreement DTPH56-14-H-00004)

10 Annex

The annex is provided as a **separate** document from the main report and includes detailed results, photos, and analysis.

- A. Laser Scan Images and Photographs of Corrosion Features Tested in the Current Test Program
- B. Dent Axial Profiles Measurements
- C. Experimental Indentation and Cyclic Strains (Micro-Strains)
- D. Magnetic Particle Inspection (MPI)
- E. Cross Section Metallography
- F. Fracture Surface for each test specimen
- G. Typical Scanning Electron Microscope Fractographs
- H. Dent Stress Magnification Factor
- I. SCC Colonies